Report on the Unexpected Emissions of CFC-11

Ozone Research and Monitoring

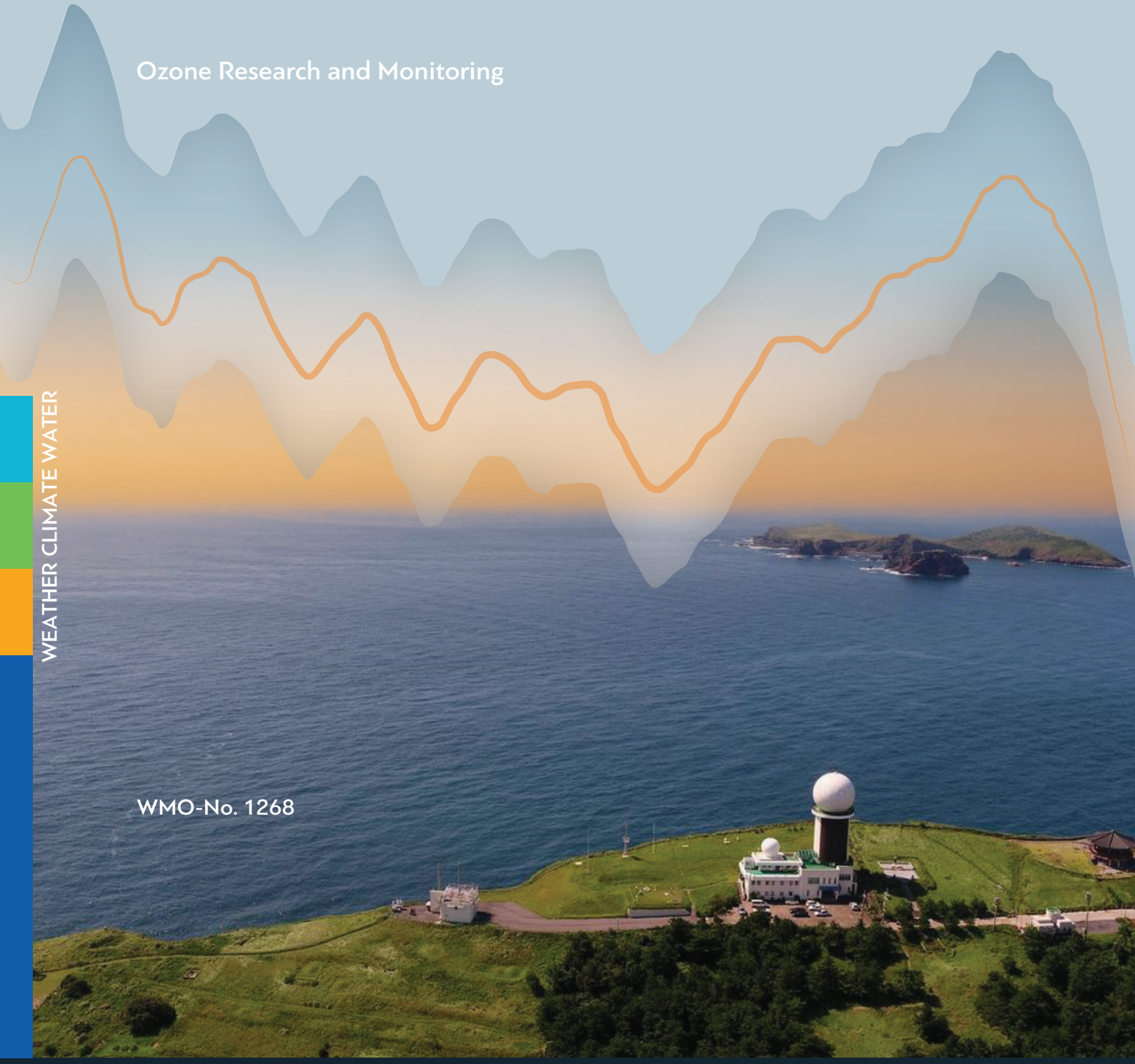

WEATHER CLIMATE WATER

WMO-No. 1268

WORLD METEOROLOGICAL ORGANIZATION

NASA

NOAA

UN environment programme

REPORT ON UNEXPECTED EMISSIONS OF CFC-11

A Report of the Scientific Assessment Panel of the Montreal Protocol on Substances that Deplete the Ozone Layer

Advisory Group

David W. Fahey
Paul J.B. Fraser
Neil R.P. Harris
Jianxin Hu
Paul A. Newman
John A. Pyle
Bonfils Safari
Michelle L. Santee

Authors

Martyn P. Chipperfield
Michaela I. Hegglin
Stephen A. Montzka
Paul A. Newman
Sunyoung Park
Stefan Reimann
Matthew Rigby
Andreas Stohl
Guus J.M. Velders
Helen Walter-Terrinoni
Bo Yao

Contributors

Peter F. Bernath
Martin Dameris
Sandip S. Dhomse
Geoffrey S. Dutton
Eric L. Fleming
Paul J.B. Fraser
Bradley D. Hall
Lei Hu
Patrick Jöckel
James Keeble
Megan Lickley
Emmanuel Mahieu
Alistair J. Manning
J. David Nance
Matthias Nützel
Eric A. Ray
Helen K. Tope
Cathy M. Trudinger
Isaac Vimont
Luke M. Western

Report Coordinator

Sarah J. Doherty

Editorial, Graphics, and Reference Support

Susan K. McFadden
Amy K. Moran
Chelsea R. Thompson
Kathy A. Thompson

Cover illustration: The Gosan GAW Regional Station (Global Atmosphere Watch Programme of the World Meteorological Organization), on the south-western tip of Jeju Island (Republic of Korea), facing the East China Sea

WMO-No. 1268

Chair, Publications Board
World Meteorological Organization (WMO)
7 bis, avenue de la Paix
P.O. Box 2300
CH-1211 Geneva 2, Switzerland

Tel.: +41 (0) 22 730 84 03
Fax: +41 (0) 22 730 81 17
Email: publications@wmo.int

ISBN 978-92-63-11268-2

CONTENTS

PREFACE

This report has been written in response to Decision XXX/3: Unexpected emissions of trichlorofluoromethane (CFC-11) of the Montreal Protocol, agreed upon in November 2018. CFC-11 (CCl_3F) was reportedly fully controlled under the Montreal Protocol since 2010. This report augments and updates the Scientific Assessment Panel's 2018 ozone assessment with new and expanded scientific detail of CFC-11 emissions with respect to atmospheric monitoring and modelling, and underlying assumptions in emission quantification. The Scientific Assessment Panel convened a team of experts to write this report and arranged for two separate peer reviews by independent scientists. The report was originally scheduled for publication in late 2020 (as mandated in Decision XXX/3). However, it was delayed into early 2021 to allow for the inclusion of updated measurements and analysis provided in two scientific publications released in February 2021 on CFC-11 emissions.

The report addresses: current and past observations of CFC-11 atmospheric abundances; information on the CFC-11 global and regional emission increase and subsequent decrease; changes derived for emissions of dichlorodifluoromethane (CFC-12, CCl_2F_2) and carbon tetrachloride (CCl_4); estimates of CFC-11 banks (CFC-11 that has been produced but has not yet been emitted); scenarios of future emissions and atmospheric concentrations; and the impact on the stratospheric ozone layer of the anomalous enhancement in CFC-11 emissions.

EXECUTIVE SUMMARY

Global CFC-11 emissions were expected to decrease steadily after 2010 because of the full phaseout of production and consumption (see Figure ES.1, blue shading). Surprisingly, however, CFC-11 emissions began to increase in 2013 and were high from 2014 to 2018 (Figure ES.1, purple line). After the publication of this emission increase in 2018, emissions were substantially lower in 2019. A large fraction of the emission increase was attributed to Eastern China based on regional emission estimates. These regional emissions also declined substantially from 2017 to 2019. The increase in global CFC-11 emissions was not a result of increased bank releases. The amounts of CFC-11 in banks and the release rates from the banks remain highly uncertain (see Figure ES.1, blue shading). The increases in emissions observed to date are small enough not to have a major impact on CFC-11 atmospheric abundances, so they will not have a major impact on the expected stratospheric ozone recovery. However, the increases in banks and how they might augment future emissions have large uncertainties.

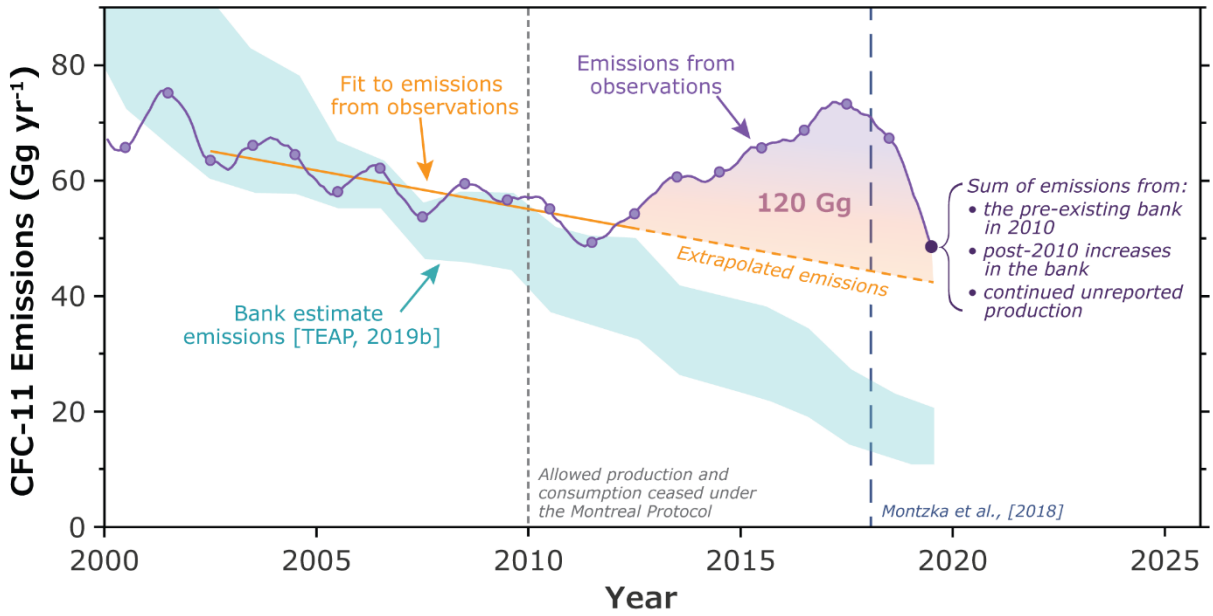

Figure ES.1. Annual averaged global CFC-11 emissions derived from National Oceanic and Atmospheric Administration (NOAA) and Advanced Global Atmospheric Gases Experiment (AGAGE) observations (purple line and points). Expected bank emissions from a range of bottom-up inventory analyses of past uses, sales, and emission release functions (blue shading). Linear fit of emissions to observations over the 2002–2012 period (orange solid line). Extrapolation of this linear fit to the 2013–2019 period (orange dashed line). The purple-orange shaded area between the observations (purple) and extrapolation (orange dashes) shows the lower limit of total emissions of 120 Gg (gigagrams) over the 2012–2019 period. Larger estimates for total unexpected emissions for 2012–2019 (440 Gg) are derived by comparing observed emissions with the expectations of the Technology and Economic Assessment Panel (TEAP) from bank-related emissions (blue shading). See section 3 in the main body for additional details.

ES.1 KEY FINDINGS

ES.1.1 CFC-11 emissions

- **The unexpected increase in global CFC-11 emissions first emerged in 2013 and continued until 2018; emissions then declined to pre-2013 levels in 2019 (Figure ES.1).** These emission changes are derived from atmospheric observations that enable estimates of globally averaged abundances and their changes inter-annually. The data are provided by the AGAGE and the NOAA global networks, which

continually monitor the atmospheric abundances of CFC-11 and other ozone-depleting substances at remote sites across the globe (see section 3).

- The unexpected increase in global CFC-11 emissions emerged in 2013 and was first reported publicly in 2018. By 2019, emissions had decreased to values consistent with those observed during the 2008–2012 period (see section 3).

- The unexpected emissions were first detected as a slowing of the long-term decline in global CFC-11 abundances from 0.8% yr^{-1} (2002–2012) to 0.5% yr^{-1} (2014–2018) and as a concurrent increase in the hemispheric concentration difference (see sections 2 and 3).

- Global CFC-11 emissions as derived on an annual basis from observations and highlight the important changes that occurred over the last decade (see Figure ES.1, section 3):

  - In the initial publication announcing unexpected emissions, the mean value for 2014–2016 (67 ± 3 Gg yr^{-1}) was estimated to be 13 ± 5 Gg yr^{-1} larger than for 2002–2012 (Gg = gigagram, 1 Gg = 1 kiloton = 10^9 g).

  - In 2018, emissions were 70 ± 10 Gg yr^{-1}, which were similar to the 2014–2017 mean.

  - Emissions declined markedly in 2019 by 18 ± 6 Gg yr^{-1}, which is 26 ± 9% lower than the mean values for 2018 and for 2014–2017.

- Observations of interhemispheric differences in CFC-11 abundances strongly suggest that the sources of unexpected emissions from 2012 to 2018 were predominantly in the northern hemisphere (see section 2).

- CFC-11 atmospheric concentrations declined by 0.8% yr^{-1} (2002–2012), then they declined more slowly, by approximately 0.5% yr^{-1} (2014–2018), then more rapidly again, by 0.7% yr^{-1} (2018–2019) (see section 2).

- **A large proportion of the increase in unexpected global CFC-11 emissions during 2014–2017 is attributed to Eastern China. These emissions decreased substantially between the 2014–2017 period and 2019.** Regional emissions of trace gases can be derived from observations at sites located immediately downwind of source regions. The distribution and magnitude of sources are derived from concentration enhancements measured in pollution plumes. Relatively few regions of the world currently characterize emissions in this way (see section 4).

  - Regional CFC-11 emissions estimated in this way show a significant increase in emissions from Eastern China of 7 ± 4 Gg yr^{-1} between the 2008–2012 and 2014–2017 periods). This increase explains 60 ± 40% of the global increase in CFC-11 emissions between these periods (see section 4).

  - Emissions of CFC-11 from Eastern China declined by 10 ± 3 Gg yr^{-1} between the 2014–2017 period and 2019. This decrease accounts for 60 ± 30% of the global decline during the same period (see section 4).

  - Multiple lines of evidence suggest that the CFC-11 emissions increase from Eastern China was due to new production and use, not from an increase in emissions from pre-existing CFC-11 banks (see sections 3 and 5, TEAP [2019*b*]).

ES.1.2 Banks

- **Current and future CFC-11 emissions are dependent on bank magnitudes and release rates. Estimates of the CFC-11 bank magnitudes are highly uncertain**

and it is difficult to assess the release rates from these banks and how they vary with time. Global CFC-11 emissions from the existing bank were expected to continually decrease after 2010 thanks to compliance with Montreal Protocol control measures. Non-compliance and unreported production since 2010 led to new emissions directly into the atmosphere and a likely enhancement of the bank. Although precise quantification of the bank enhancement is not possible at present, some estimates have been made (see sections 3 and 5).

  - A bottom-up analysis estimates a global CFC-11 bank as high as 1 475 Gg for 2018, while an analysis that uses both top-down and bottom-up information shows a bank range of 900–2 300 Gg for 2018 (neither analysis considered unreported production). Both analyses suggest that the elevated emissions during 2014–2018 are unlikely to be from enhanced emissive losses from the pre-existing 2010 bank (see section 5).

  - Estimates based on top-down regional emissions suggest that the net increase in the bank size in 2019 for Eastern China was as large as 112 Gg (upper 95% uncertainty interval) due to new production between 2013 and 2018 (see section 4).

- **Quantifying unreported CFC-11 production in the last decade and its future impact on emissions more precisely requires an improved understanding of present-day bank emissions from pre-2010 production and the likely enhancement from unreported production since 2010.**

  - The extent to which emissions in 2019 (Figure ES.1, orange purple shading) remain elevated above projected emissions from the 2010 bank (Figure ES.1, blue shading) is highly uncertain (1 to 50 Gg yr^{-1}). This value is poorly constrained because of large emission uncertainties associated with pre-2010 production and how banks might have changed from 2010 to 2019 (Figure ES.1) (see section 3).

  - Relative to the global emission decline expected from the projected decrease in the global CFC-11 bank after 2010, a cumulative global emission enhancement of 120 to 440 Gg is estimated up to 2019 due to unreported production (see Figure ES.1) (see section 3).

ES.1.3 CFC-12 AND CARBON TETRACHLORIDE EMISSIONS

- **Global CFC-12 (CCl_2F_2) emissions have declined since the mid-1990s, but the rate of decline was slower in the 2010–2017 period than in the 2000–2009 period. There was a significant reduction in emissions after 2017.** Unexpected CFC-12 emissions were a possibility together with the unexpected CFC-11 emissions increase, because CFC-12 is typically (but not necessarily) co-produced during the manufacture of CFC-11. Like CFC-11, CFC-12 is a primary ozone-depleting substance (ODS) and a powerful greenhouse gas (GHG). Reported CFC-12 production ceased by 2010 under the Montreal Protocol, except for essential small-quantity exemptions to manufacture metered-dose inhalers (which were curtailed in 2015) (see section 3).

  - While global CFC-12 emissions decreased at 12 ± 2% yr^{-1} during 2000–2009, the mean decline slowed to only around 5 ± 2% yr^{-1} during 2010–2017 (see section 3).

  - Global CFC-12 emissions in 2019 were 21 ± 7 Gg yr^{-1}, which is 38 ± 15% lower than estimated for 2018, indicating a significant reduction in global CFC-12 emissions at a similar time to the decline in global CFC-11 emissions (see section 3).

- Regional CFC-12 emissions declined suddenly in around 2016 in Eastern China (see section 4).

- **Global carbon tetrachloride (CCl_4) emissions did not decline in the 2010–2019 period. Inverse analysis suggests that CCl_4 emissions from Eastern China increased after 2012 and subsequently decreased in around 2017.** CCl_4, CFC-11, and CFC-12 can be co-emitted during CFC-11 production since CCl_4 is a feedstock for CFC-11 and CFC-12 (see section 3).

    - Global CCl_4 emissions did not significantly decline during the 2010–2019 period (0.1 ± 0.2 Gg yr^{-1}), but they declined steadily in the previous 2000–2009 period (1.6 ± 0.3 Gg yr^{-1}). Interannual changes in global emissions of CCl_4 are not well correlated with changes in global emissions of CFC-11 after 2012, although year-to-year changes in CCl_4 emissions have substantial uncertainties and are not consistently determined by the two networks. CCl_4 emissions have remained above expectations for many years (see section 3).

    - Regional emissions of CCl_4 from Eastern China increased from 6.0 ± 1.4 Gg yr^{-1} for 2011–2012 to 10 ± 2 Gg yr^{-1} for 2014–2017, then declined in 2017–2019 to values consistent with the 2011–2012 average (see section 4).

ES.1.4 Impacts of Recent CFC-11 Emissions

- **The anticipated recovery from stratospheric ozone depletion will not be substantially delayed by these enhanced CFC-11 emissions, because they were significantly elevated only for a brief period (2014–2019).** If elevated emissions had persisted, they could have significantly delayed the recovery of the Antarctic ozone hole and the return of stratospheric chlorine (Cl) abundances to 1980 values. In light of the new results for 2019, a substantial ozone impact is no longer expected, assuming future compliance with the Montreal Protocol phaseout of CFC-11 production (see section 6).

    - The cumulative unexpected emissions of CFC-11 during 2012–2019 were 120–440 Gg, which will increase stratospheric chlorine loading in future years by 15–57 parts per trillion Cl and will have only a small impact on stratospheric ozone. The maximum future decrease in mean global column ozone is less than 0.3 Dobson units (DU) or 0.1% and the additional September Antarctic ozone loss is less than 2.5 DU (1%). Ozone recovery, measured as a return to 1980 levels, is delayed by only 0.4–1.3 years globally and by 0.5–3.1 years for the Antarctic ozone hole (see section 6).

    - The additional CFC-12 and CCl_4 emissions, possibly associated with the enhanced CFC-11 production, will lead to small additional impacts on future ozone depletion, delayed ozone recovery, and greater climate forcing (see sections 5 and 6).

- **The anticipated recovery of stratospheric ozone will also be delayed if substantial amounts of the unreported CFC-11 production were added to foam banks after 2010.** TEAP analyses showed that the mostly likely use of the unreported CFC-11 production was for insulating foams. If true, this would result in additional CFC-11 in foam banks that would continue to augment future CFC-11 emissions above expectations (see sections 5 and 6).

    - Uncertainty in bank estimates and future emissions of CFC-11 (and potentially CFC-12) from these banks leads to a lack of precision in estimates of future ozone depletion associated with the unexpected CFC-11 emissions (see section 5).

    - Sustained CFC-11 emissions at the elevated 2014–2017 levels would have caused additional stratospheric ozone loss and led to an ozone recovery delay. The impact

varies with region and is proportional to the total additional CFC-11 emissions. Globally, column ozone is 0.4–0.7 DU lower and 1980 return dates are delayed by 3 years per 1 000 Gg of cumulative CFC-11 emissions. For the Antarctic, models show a near-linear decrease of 5 DU in springtime column ozone and a delay of 4–7 years for September 1980 return dates per 1 000 Gg of cumulative CFC-11 emissions (see section 6).

- **CFC-11 atmospheric abundances are projected to continue to decline in emission scenarios that assume future compliance with the Montreal Protocol.** These scenarios also assume decreasing CFC-11 emissions from banks (see section 5).

  - The projected global cumulative CFC-11 emissions for 2020–2060 are 580–780 Gg (3–4 cumulative Gt of CO_2 equivalent), based upon CFC-11 scenarios from previous assessments. The unexpected CFC-11 emissions after 2012 are projected to add an additional 60–200 Gg (0.3–1.0 cumulative Gt of CO_2 equivalent) of emissions for 2020–2060, depending on the assumed rate of release from the banks (Gt = gigatonne, 1 Gt = 10^9 tons = 10^{15} g) (see section 5).

1. INTRODUCTION

Trichlorofluoromethane (CFC-11, CCl_3F) is an ozone-depleting substance (ODS) controlled under the 1987 Montreal Protocol, with atmospheric levels that have been declining since the mid-1990s (WMO, 2018). However, Montzka et al. (2018) showed that the recent observed CFC-11 decline rate was slower than expected – if developed and developing countries were fully adhering to Montreal Protocol chlorofluorocarbon (CFC) consumption controls. This is a summary report on this increase in CFC-11 emissions, which slowed the rate of decline of atmospheric CFC-11 concentrations. The report further discusses the recent apparent return to lower emission rates.

CFC-11 is primarily destroyed in the stratosphere by solar ultraviolet (UV) photolysis. The majority (98%) is photolysed in the 190–230 nm wavelength range in the lower stratosphere (15–30 km altitude). Approximately 2% is destroyed in a reaction with atomic oxygen ($O(^1D)$) atoms in the troposphere (Burkholder and Mellouki, 2013). These loss processes result in a 52-year CFC-11 atmospheric lifetime, with an uncertainty range of 43–67 years (SPARC, 2013). Once CFC-11 emissions become negligible, atmospheric concentrations should decrease at about 2% yr^{-1} and decline by 95% in 130–200 years (3 times the lifetime).

A "bottom-up" emissions inventory analysis shows that CFC-11 emissions increased steadily from close to zero in the 1940s to about 350 Gg (Gg = gigagram, 1 Gg = 1 kiloton = 10^9 g) per year (yr^{-1}) in 1974 (see Figure 6.4 in TEAP/UNEP, 2019*b*). These "bottom-up" emission models typically include CFC-11 production emissions, usage emissions from products incorporating CFC-11, and end-of-life emissions. Following the publication of a scientific paper in 1974 highlighting the ozone-destroying nature of CFCs (Molina and Roland, 1974), there was a significant decrease in emissions, largely due to a ban in the United States of America and several European countries on using CFC-11 as an aerosol propellant. Emissions fell below 300 Gg yr^{-1} in the 1979–1982 period. However, emissions subsequently increased again, peaking in 1987 at about 350 Gg yr^{-1} due to growth in foam and refrigerant CFC-11 uses (see Figure 6.4 in TEAP/UNEP, 2019*b*). The Montreal Protocol caused a steep decline in emissions, beginning in 1987. Bottom-up analysis suggests that CFC-11 emissions should have steadily declined from about 2000 onwards to less than 20 Gg yr^{-1} in 2019 (see Figure ES.1) (TEAP/UNEP, 2019*b*).

The Montreal Protocol controls CFC-11 production and consumption, not emissions. Initially the Protocol froze consumption and production at 1986 levels. Subsequent amendments led to a 100% phaseout of production by 1 January 1996 for non-Article 5 ("developed") countries and by 1 January 2010 for Article 5 ("developing") countries. Atmospheric CFC-11 concentrations derived from the NOAA and the AGAGE networks showed that atmospheric concentrations peaked in 1993–1994 (Montzka et al., 1996; Cunnold et al., 1997) and have declined ever since (Engel et al., 2018).

Montzka et al. (2018) showed that, after 2012, the rate of decline of the observed CFC-11 concentration became slower than expected, assuming developed and developing countries were fully adhering to Montreal Protocol controls. This decline slowdown was contrary to CFC-11 concentration projections by both WMO (2011) and WMO (2014). Using atmospheric observations from the NOAA global network, the authors showed that the CFC-11 decline rate slowed by approximately 50% after 2012. Their derived global emissions showed a 13 Gg yr^{-1} enhancement during 2014–2016 relative to the preceding decade (2002–2012) (see Figure ES.1). They further showed that the likely source of some portion of this emission increase was East Asia. This unexpected CFC-11 emission increase was not easily explained by increased escape from banks[1] or changes in atmospheric processes, and was therefore probably the result of new production.

[1] Hereafter, a bank is defined as CFC-11 that has been produced but has not yet been emitted, that is, the total amount of CFC-11 existing in products such as foam, equipment, stockpiles and landfills that will eventually escape to the atmosphere (most CFC-11 in landfills will not escape to the atmosphere (Scheutz et al. 2010; Hodson et al., 2010; Liu et al., 2017)).

The WMO (2018) assessment concluded that global 2014–2016 CFC-11 emissions were higher than the relatively constant 2002–2012 emissions by about 10 Gg yr^{-1}, or around 15% (Engel and Rigby, 2018). This assessment included AGAGE observations of CFC-11 (Prinn et al., 2018), which confirmed the conclusions in Montzka et al. (2018), but revised the emission increase downward slightly. Carpenter et al. (2018) also found that if total CFC-11 emissions continued at 2002–2016 levels (67 Gg yr^{-1}), the recovery of mid-latitude and polar equivalent effective stratospheric chlorine (EESC) to their 1980 levels would be delayed by about 7 years and 20 years, respectively.

The Parties to the Montreal Protocol responded to the findings of Montzka et al. (2018) with Decision XXX/3: Unexpected emissions of trichlorofluoromethane (CFC-11). This decision requested "the Scientific Assessment Panel to provide to the Parties a summary report on the unexpected increase of CFC-11 emissions, which would supplement the information in the quadrennial assessment, including additional information regarding atmospheric monitoring and modelling, including underlying assumptions, with respect to such emissions; a preliminary summary report should be provided to the Open-ended Working Group at its forty-first meeting, a further update to the Thirty-First Meeting of the Parties and a final report to the Thirty-Second Meeting of the Parties".

The Montreal Protocol's Scientific Assessment Panel convened a team of experts to write this report, which examines current research and adds information on these unexpected CFC-11 emissions. In 2020, two new papers documenting a CFC-11 emission decrease were submitted for publication (Montzka et al., 2021; Park et al., 2021). In order to include these new results, the report authors asked the Parties to delay delivery of the final version of this report until early 2021. The first version of this report was peer-reviewed in early 2020 and a second review took place in early 2021.

This report is divided into six sections:

1. The introduction, with basic information and the background;

2. Current and past observations of CFC-11 atmospheric abundances along with a description of networks and observational techniques;

3. Global emissions derived from the network of observations at remote sites, with discussion of the transport process that could modify global emission estimates;

4. Regional emissions derived from observations at sites close to source regions and the analysis techniques, most specifically for East Asia;

5. Scenarios of CFC-11 emissions and surface concentrations, including descriptions of methodologies for estimating banks and determining future projections;

6. The modelled impacts of these unexpected emissions using state-of-the-art models that include chemical, radiative, and dynamical effects.

2. OBSERVATIONS

Main points:

- Globally representative networks have been essential in showing the benefit of the Montreal Protocol and its Amendments, which led to a decrease in tropospheric CFC-11 mixing ratios from ~265 ppt[2] in around 1994 to ~226 ppt in 2019.

- The annual decline in the global growth rate remained relatively close to 2.0 ppt (0.8%) yr^{-1} between 2002 and 2012 before slowing down to approximately 1.1 ppt (0.5%) yr^{-1} between 2014 and 2018, then accelerating again between 2018 and 2019 to 1.6 ppt (0.7%) yr^{-1}.

- The CFC-11 interhemispheric difference (IHD) in concentration increased from 1.8 ppt in 2012 to 2.9 ppt during 2014–2017, indicating increased emissions in the northern hemisphere during this period. These increases then slowed substantially in 2019 and the first part of 2020, when the interhemispheric difference returned more or less to its 2012 value.

- Pulses with elevated mixing ratios at regional atmospheric measurement sites indicate nearby anthropogenic emissions. The long-term behaviour of these pollution events can be used to assess trends of regional emissions on the continental scale. Elevated mixing ratios in pollution events measured at European and North American sites decreased or remained stable after the CFC-11 ban. At the Gosan station offshore of East Asia, measured distributions of elevated CFC-11 mixing ratios also remained unchanged from 2008 to 2012, then increased from 2013 to 2017 before decreasing in 2018 and 2019.

- Measurements of the oldest firn[3] air collected to date, from periods preceding anthropogenic CFC-11 emissions, show mixing ratios that are not significantly different from zero. This excludes the possibility of natural sources (e.g., volcanoes) having an influence on current CFC-11 mixing ratios.

This section provides an overview of the temporal and spatial evolution of CFC-11 over the past five decades. The period covered extends from the period of unhindered production and consumption to the introduction of a total ban on CFC-11 and up to the present day, including the period of unexpected emissions. After the first, intermittent measurements of long-lived halocarbons in the early 1970s, NOAA and AGAGE established globally representative continuous measurement networks. These networks have been essential in establishing that evolving ODS levels are influenced by stratospheric ozone depletion. Measurements are ongoing and have been expanded: they no longer take place only at background sites, but also at locations that are at least periodically under the influence of important source regions.

Measurement networks for ODSs span the globe (see Table 2.1 and Figure 2.1). In addition to long-term in situ measurements within the surface-based NOAA and AGAGE networks, aeroplane and balloon campaigns are used and remote sensing measurements are taken from the ground and from satellites, adding a vertical dimension to measurements and producing a more complete picture in terms of the breakdown of CFC-11 in the stratosphere (see Figure 2.2). Additional measurements from Europe, the United States and East Asia are available for assessing the influence of Montreal Protocol restrictions on emissions from these regions (see Figure 2.3).

[2] The mixing ratio is the dry air mole fraction and the unit ppt refers to parts per trillion (parts in 10^{12}).
[3] Ice that is at an intermediate stage between snow and glacial ice. Firn ice contains air in layers that can be used to estimate CFC-11 concentrations in the past.

Table 2.1. Ground-based atmospheric observations of CFC-11 (see the map in Figure 2.1). AGAGE and affiliated stations are in red and NOAA observations in blue. Station instrument sampling intervals are: C – continuous observation on-site; D – daily sampling using canisters and subsequent analysis in a central laboratory; and W – weekly sampling using canisters.

Global in situ networks (NOAA/AGAGE)			
#	*Station*	*Position, height* [a]	*Sampling interval*
1	Alert, Canada	82.5°N, 62.3°W, 195 m	W
2	Zeppelin, Svalbard, Norway	78.9°N, 11.9°E, 475 m	C
3	Summit, Greenland, Denmark	72.60°N, 38.50°W, 3 217 m	W
4	Barrow, AK, United States	71.3°N, 156.6°W, 27 m	C/W
5	Mace Head, Ireland	53.3°N, 9.9°W, 18 m	C/W
6	Jungfraujoch, Switzerland	46.5°N, 8.0°E, 3 580 m	C
7	Monte Cimone, Italy	44.2°N, 10.7°E, 2 165 m	C
8	Cape Ochiishi, Japan	43.2°N, 145.5°E, 49 m	C [b]
9	Trinidad Head, CA, United States	41.1°N, 124.2°W, 120 m	C/W
10	Shangdianzi, China	40.7°N, 117.2°E, 393 m	C [b]
11	Niwot Ridge, United States	40.1°N, 105.6°W, 3 523 m	C/W
12	Gosan, Jeju Island, Republic of Korea	33.3°N, 126.2°E, 71 m	C
13	Hateruma Island, Japan	24.1°N, 123.8°E, 10 m	C [b]
14	Mauna Loa, HI, United States	19.5°N, 155.6°W, 3 433 m	C/W
15	Cape Kumukahi, HI, United States	19.5°N, 154.8°W, 39 m	W
16	Ragged Point, Barbados	13.2°N, 59.4°W, 42 m	C
17	Cape Matatula, American Samoa, United States	14.2°S, 170.6°W, 77 m	C/C/W
18	Cape Grim, Australia	40.7°S, 144.7°E, 164 m	C/W
19	Palmer Station, Antarctica	64.8°S, 64.1°W, 15 m	W
20	South Pole, Antarctica	90.0°S, 2 866 m	C/W
Regional in situ networks			
	USA-based daily sampling	19 sites	D
	China-based weekly sampling	7 sites	W [c]
Global remote sensing network (NDAAC)			
R1	Peterhof, St. Petersburg, Russia	59.9°N, 29.8°E, 20 m	
R2	Jungfraujoch, Switzerland	46.6°N, 8.0°E, 3 580 m	
R3	Maïdo, La Réunion, France	21.1°S, 55.4°E, 2 155 m	

[a] Position information from http://www.gawsis.meteoswiss.ch/ and http://www.ndacc.org/
[b] AGAGE and AGAGE affiliated stations with data not available on public data centres
[c] AGAGE technique-based analysis instrumentation

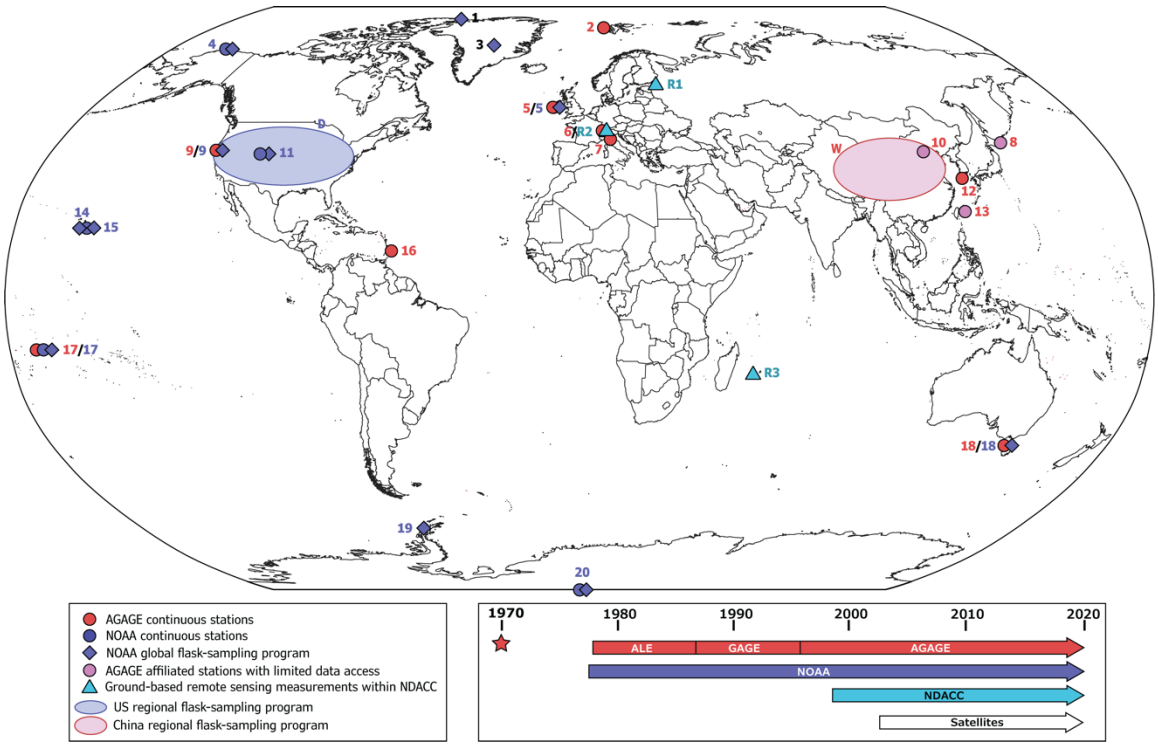

Figure 2.1. Map of global ground-based CFC-11 observations: AGAGE and NOAA continuous measurements (red and blue filled circles, respectively), NOAA flask measurements (blue diamonds). AGAGE and AGAGE affiliated stations with data not available on public data centres: magenta circles; NOAA United States regional flask-sampling programme: blue shaded area (D: daily samples at 19 sites); China regional flask-sampling programme, pink shaded area (W: weekly samples); NDACC (Network for the Detection of Atmospheric Composition Change) ground-based remote sensing measurements (triangles).

2.1 OVERVIEW OF GLOBAL MEASUREMENT CAPABILITIES

2.1.1 Ground-based in situ networks

The first CFC-11 measurements were performed in the summers of 1970 and 1971 at Adrigole, Ireland, using gas chromatography-electron capture detection (GC-ECD) (Lovelock, 1971, 1972). After early campaigns and cruises (see Appendix A), the Commonwealth Scientific and Industrial Research Organisation (CSIRO) began to perform continuous in situ measurements (4 times per day) of CFC-11 and other ODSs in late 1976 at Cape Grim, Australia (Fraser et al., 1983). In 1977, NOAA began analysing weekly flask samples from five sites (Barrow, Alaska, US; Niwot Ridge, Colorado, US; Mauna Loa, Hawaii, US; Cape Matatula, American Samoa; South Pole, Antarctica) (Elkins et al., 1993). This was followed in mid-1978 by the establishment of the ALE (Atmospheric Lifetime Experiment) programme, in which CFC-11 and other ODSs were continuously analysed 4 times per day at five sites (Adrigole, Ireland; Cape Meares, United States; Ragged Point, Barbados; Cape Matatula, American Samoa; Cape Grim, Australia) (Prinn et al., 1983).

The observations used for emission estimates are from the NOAA and AGAGE networks. These networks have been steadily developed and are currently analysing CFC-11 and other halogenated compounds using GC-ECD and/or GC-mass spectrometry (GC-MS) at globally and regionally representative sites (see Table 2.1 and Figure 2.1). These techniques, used for ambient air analysis, were also used to analyse firn air samples (air trapped in the intermediate stage between snow and glacial ice), yielding CFC-11 mixing ratios that go back to the 1930s, prior to industrial-scale CFC-11 production. The earliest measured concentrations in these samples were not statistically different from zero, which means there

cannot be any major natural sources of CFC-11 (e.g., volcanoes). This is supported by recent studies that found there were virtually no natural emissions of CFC-11 (see Appendix A).

The current NOAA global network (used in Montzka et al. (2018)) derives globally representative averages with results from on-site instrumentation (5 sites, hourly frequency) and flask sampling (12 sites, weekly frequency). This is further supported by a United States flask-sampling network, in which samples are collected daily from tall towers (19 sites) and approximately every 2-4 weeks from aircraft profiles (up to 8 km above sea level, at 15 sites) (Hu et al., 2017). This flask sampling has enabled emission location mapping and emission magnitude estimates across regions in the United States using inverse modelling techniques. While daily flask sampling may reduce the resolution of information derivable around any one site when compared with what is derivable from continuous in situ observations, multiple flask collection sites combined with a single analysis instrument can provide broader geographic coverage.

The ALE programme (1978–1981) evolved into GAGE (Global Atmospheric Gases Experiment, 1982–1992) and then AGAGE (1993–present). The current AGAGE network consists of nine stations with identical gas chromatograph-mass spectrometers (GC-MS-Medusa; Miller et al., 2008; Arnold et al., 2012) and three affiliated sites with similar measurement technologies (Prinn et al., 2018).

Since 2010, CFC-11 has been measured in a regional flask network in China on a weekly basis, also using the GC-MS-Medusa technology (Zhang et al., 2017). In addition, the University of California, Irvine (UCI) has flask measurements of CFC-11 mixing ratios and other trace gases in remote locations in the Pacific Basin dating back to 1979. CFC–11 data from the NOAA, AGAGE and UCI networks CFC-are reported in Engel et al. (2018).

The NOAA and AGAGE networks perform regular inter-comparison exercises (Hall et al., 2014), and conversion factors are well established for CFC-11, with minor differences between them, in the range of 1 ppt (or 0.5%) from 2000 until the present. These data are further discussed in section 2.2.

Apart from these long-term measurements, many campaigns have been performed in specific regions of the world and at different altitudes of the atmosphere. A short overview of the history of these activities is given in Appendix B1. Since a focal point of this report is newly occurring emissions and their attribution to activities in Asia, Appendix B2 provides a comprehensive overview of campaigns from this region of the world.

2.1.2 Measurements by remote sensing

In addition to in situ measurements, observations of the CFC-11 abundance within the atmospheric column are possible using remote-sensing infrared spectroscopy techniques from the ground and from space (see Figure 2.1).

The first CFC-11 ground-based remote-sensing retrievals were performed using Fourier transform infrared (FTIR) at Jungfraujoch (Switzerland) (Zander et al., 2005), and these retrievals are regularly updated (Engel et al., 2018). In addition, data from La Réunion island (Zhou et al., 2016) and St. Petersburg (Polyakov et al., 2018) have recently been published. All three sites belong to the global NDACC. Long-term satellite observations of CFC-11 column abundances are available from the MIPAS (Michelson Interferometer for Passive Atmospheric Sounding) instrument from 2002 to 2012 (Kellmann et al., 2012; Eckert et al., 2016). The Atmospheric Chemistry Experiment Fourier Transform Spectrometer (ACE-FTS) satellite instrument has provided mixing ratio observations of the stratosphere since 2004 (Steffen et al., 2019). Infrared observations from the Atmospheric Infrared Sounder (AIRS) satellite instrument also provide mid-troposphere CFC-11 observations (Chen et al., 2020). For a discussion of both ground-based and space-based remote-sensing measurement data, see section 2.2.

2.2 RECENT BEHAVIOUR OF CFC-11 IN THE GLOBAL ATMOSPHERE

The CFC-11 globally averaged mixing ratio, its IHD in concentration, and its global concentration growth rate (GR) were derived using concentration data from the AGAGE and NOAA networks (see Figure 2.2(a)).

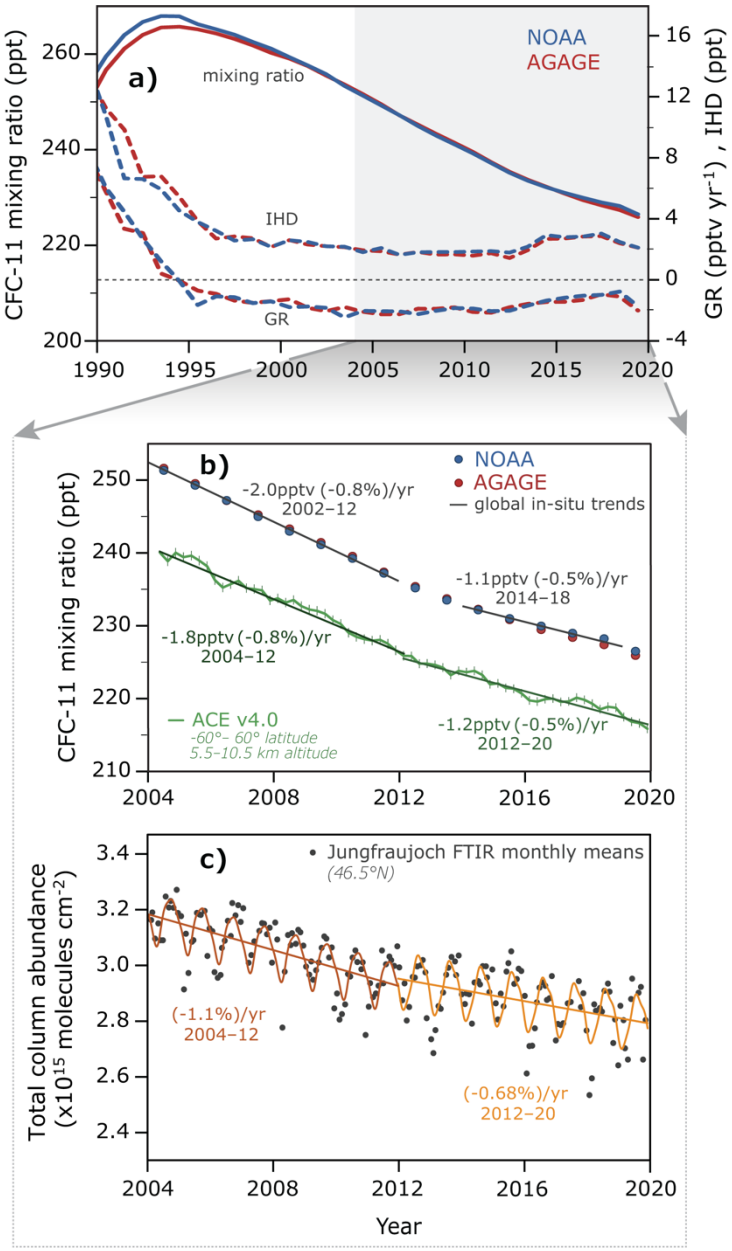

Figure 2.2. (a) CFC-11 mixing ratios, global GRs and the IHD from the NOAA (blue) and AGAGE (red) networks, for 1990–2019, adapted from Engel et al. (2018); (b) CFC-11 global volume mixing ratios and trends for 2004–2020, as retrieved from the ACE-FTS satellite instrument (v4.0, (green, adapted from Bernath et al., 2020)) compared with in situ measurements from panel (a), above; (c) northern hemispheric CFC-11 column abundances, based on surface-based remote sensing measurements at Jungfraujoch (update of Zander et al., 2005).

Results from both networks indicate that tropospheric CFC-11 mixing ratios peaked at ~265 ppt in around 1994 and have continuously declined since then, reaching ~229 ppt in 2017 (Engel et al., 2018) and ~226 ppt in 2019 (Montzka et al., 2021). The decline in the CFC-11 annual mixing ratio remained relatively close to 2.0 ppt (0.8%) yr^{-1} between 2002 and 2012. However, due to new emissions, mainly from East Asia (Montzka et al., 2018; Rigby et

al., 2019), the decline slowed to approximately 1.1 ppt yr^{-1} (0.5% yr^{-1}) for 2014–2018. A recent study by Montzka et al. (2021) shows that the decline accelerated to 1.6 ppt (0.7%) yr^{-1} between 2018 and 2019, then to 2.3 ppt (1.0%) yr^{-1} by late 2019 and early 2020. This is the lowest annual rate since measurements began in the 1970s, and is therefore a strong indicator of the decline in emissions since 2018 (see also section 3). During the 2014–2018 emissions increase, the CFC-11 IHD widened from 1.8 ppt in 2012 to 2.9 ppt in 2014–2017, suggesting that new emissions originated from northern-hemisphere sources during this period (Montzka et al., 2018). In 2019, the IHD shrank back to 2.1 ppt, providing further evidence of a return to lower emissions in the northern hemisphere.

Since 2004, the ACE-FTS satellite instrument has shown a relative decrease in CFC-11 concentrations of 1.2% yr^{-1}. That decrease has been substantially slower since 2012, at around 0.5% yr^{-1} (see Figure 2.2(b)) (Bernath et al., 2020). ACE-FTS uses spectral information to derive CFC-11 mixing ratios at altitudes of 5.5–10.5 km. Absolute mixing ratios derived from ACE-FTS are lower than those from global in situ networks, but the relative changes are very similar.

Northern hemispheric CFC-11 total column abundances measured using ground-based FTIR spectroscopy (Jungfraujoch, Switzerland) also show a slowdown in the decline of abundances in recent years, with a trend of −1.1% between 2004 and 2012 and −0.7% in the following years (see Figure 2.2(c); update from Zander et al., 2005; Engel et al., 2018). These observations are concurrent with the globally representative data shown in Figures 2.2(a) and 2.2(b). Although these measurements cover the whole atmospheric height in the northern hemisphere mid-latitudes, the decline rates are similar to those from in situ measurements and satellites.

2.3 REGIONAL MEASUREMENTS USED TO DETECT SPATIALLY RESOLVED EMISSIONS

Measurements close to source regions contain information on the behaviour of emissions from specific regions before and after the CFC-11 phaseout date (see also section 4.2). Concentrations measured at a given site are a combination of CFC-11 background concentrations, the amount and location of emissions in the region, and the transport of those emissions to the measurement site. CFC-11 emissions can come directly from production sites (before the phaseout of production), places of usage (i.e. foam-blowing industries) and banks. Mixing ratios above the background level are indicative of regional emissions within the range of the monitoring site. These enhanced mixing ratios can be used to quantify emissions by combining them with atmospheric transport models and statistical "inverse" techniques or through interspecies correlation with a concurrently measured substance with known regional emissions.

Time series of CFC-11 mixing ratios at a given site reveal the evolution of background concentrations as well as spikes in concentrations from regional pollution events. This is shown in Figure 2.3 for sites in Europe (Mace Head, Ireland), North America (several sites) and East Asia (Gosan, Jeju Island, Republic of Korea; Shangdianzi, China). To enhance the visibility of the temporal behaviour of pollution events against background measurements at the different sites, the data are also shown in annually separated box-and-whisker plots for 2007–2019 (see Figure 2.3).

After the CFC-11 phaseout in non-Article 5 (developed) countries in 1996, mixing ratio "spikes" above the background measured at the European Mace Head site decreased quickly from a maximum of around 80 ppt in the early 1990s to around 10 ppt in 1995, one year before the phaseout (Simmonds et al., 1996). Occasional pollution events are still detected at Mace Head, although with very low enhancements above the baseline concentration. In North America, CFC-11 measurements from a flask network programme (see section 2.1) show occasional concentrations considerably elevated above background levels from 2008 to 2014 and decreasing pollution events afterwards (update of Hu et al., 2017). The difference

between these two sites is the proximity of the North American sites to urban environments, which have significant CFC-11 banks and emissions that decrease only slowly.

In East Asia, observed elevated CFC-11 mixing ratios in pollution events did not change at Gosan from 2008 to 2012 or at Shangdianzi from 2007 to 2010. Shangdianzi measurements are unavailable from mid-2011 due to local contamination. At Gosan, mixing ratios of CFC-11 during pollution events increased between 2013 and 2017, with episodic enhancements as large as 50–70 ppt. These elevated concentrations have been attributed to an increase in CFC-11 emissions from China during this period (Rigby et al., 2019). From 2018 onwards, elevated CFC-11 mixing ratios decreased and were comparable to those in 2012. This suggests a decline in emissions from Chinese sources, to which Gosan measurements are sensitive (Park et al., 2021). Emissions derived from the measurements at these regionally influenced sites are described in more detail in section 4.3.

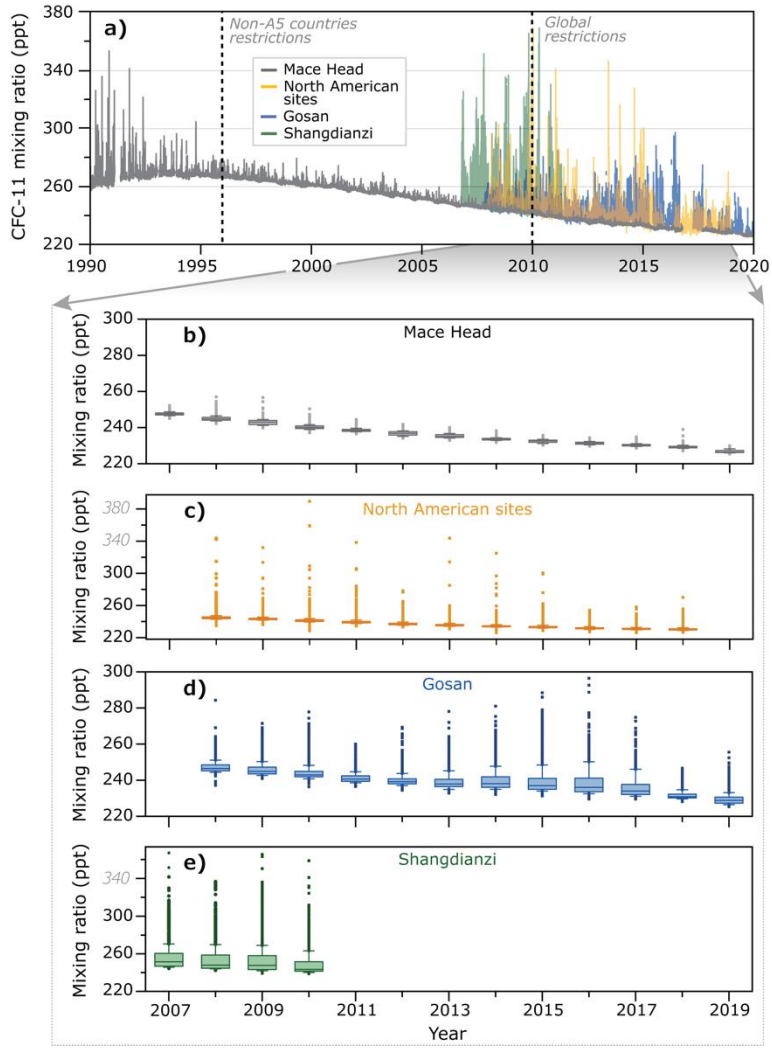

Figure 2.3. CFC-11 mixing ratios observed using in situ measurements at Mace Head, Ireland (update of Simmonds et al., 1996); Gosan, Republic of Korea (Park et al., 2021); Shangdianzi, China (update of F. Zhang et al., 2010); and from flask measurements at multiple stations in North America (update of Hu et al., 2017). (a): Mixing ratios for all four regional sites. (b)–(e): Box-and-whisker plots. Boxes indicate the 25th and 75th percentile of the individual measurement data, with the median shown as a horizontal orange line within each box. The whiskers above and below the boxes show the 10th and 90th percentiles. The dots indicate events outside this range.

3. GLOBAL EMISSIONS

Main points:

Global-scale total emissions are derived from regular measurements of atmospheric mole fractions of CFC-11 at remote sites around the world, combined with an understanding of atmospheric removals (lifetime). The resulting derived emissions indicate that:

- Global emissions of CFC-11 unexpectedly increased by 13 ± 7 Gg yr^{-1} beginning in 2013, from a mean value of 56 ± 10 Gg yr^{-1} during 2008–2012 to a mean of 69 ± 10 Gg yr^{-1} during 2014–2017.
    - Estimates of this increase vary depending on the measurement network: 11 ± 3 Gg yr^{-1} is derived from AGAGE measurements, and 17 ± 3 Gg yr^{-1} is derived from NOAA measurements.
- Updated observations show a substantial drop in global emissions by 2019:
    - Global emissions in 2019 were 52 ± 10 Gg yr^{-1}, which is 18 ± 6 Gg yr^{-1} (26 ± 9%) lower than global emissions in 2018.
    - Global emissions in 2019 were comparable to mean emissions during 2008–2012 (56 ± 10 Gg yr^{-1}), before the observed anomalous emission increase.
    - Global emissions in 2018 (70 ± 10 Gg yr^{-1}) were not different from the mean emissions derived for 2014–2017.

In the absence of unreported production, global CFC-11 emissions from banks were expected to decrease after 2010, so the full impact of unreported production and renewed use of CFC-11 since 2010 on future stratospheric ozone is more accurately estimated from the enhancement of observed emissions above those expectations.

- The extent to which 2019 emissions remain elevated above expectations is highly uncertain and could be anywhere from 1 to 50 Gg yr^{-1}. This value is poorly constrained because of the large uncertainties in how rapidly emissions from banks created from pre-2010 production declined between 2010 and 2019.
    - If these bank emissions had continued to decline slowly after 2010 at the same rate that global emissions dropped during 2002–2012, the estimated emission enhancement remaining in 2019 from unreported production would be 7 ± 6 Gg yr^{-1}, that is, at the low end of the 1 to 50 Gg yr^{-1} range.
    - A more rapid decline in these bank emissions after 2010, as suggested by the Technology and Economic Assessment Panel inventory model, would suggest emissions well above expectations in 2019, at the upper end of the 1 to 50 Gg yr^{-1} range.
    - Emissions during 2012–2019 were 70 Gg yr^{-1} higher than the mean emission rate during 2008–2012; relative to the expected emission decline from banks after 2010, cumulative emissions were enhanced by 120–440 Gg.
- Inter-annual variations in atmospheric transport processes add uncertainty to global emission estimates, particularly over periods of one year; over longer periods (3–5 years), these uncertainties become smaller. An updated accounting of these influences suggests that emissions during 2014–2017 were 13 ± 7 Gg yr^{-1} higher than during 2008–2012; this estimate is comparable to the increase reported previously.

Furthermore, the 18 ± 6 Gg yr^{-1} (26 ± 9%) drop in CFC-11 emission between 2018 and 2019 is estimated taking dynamical influences into account, otherwise the drop would be similarly large.

- Global emissions of CFC-12 (which is typically, but not necessarily, co-produced with CFC-11) have declined since the mid-1990s. While global CFC-12 emissions decreased at approximately 12 ± 2% yr^{-1} during 2000–2009, they declined at only around 5 ± 2% yr^{-1} during 2010–2017. Emissions in 2019 were 21 ± 7 Gg yr^{-1}, which is significantly lower (by 38 ± 15%) than estimated emissions for 2018, suggesting a substantial drop in global CFC-12 emissions by 2019, as was observed for global CFC-11 emissions.

- Global CCl_4 emissions (a feedstock for CFC-11 production) declined from 2000 to 2009 at 1.6 ± 0.3 Gg yr^{-1}, but have not declined significantly since 2010 (approximately 0.1 ± 0.2 Gg yr^{-1} during 2010–2019). The uncertainties associated with annual estimates and year-to-year changes in global CCl_4 emissions preclude any robust assessment of global emission changes concurrent with those of CFC-11. Global CCl_4 emissions have remained elevated above expectations for many years.

- The slower decline in global CFC-12 and CCl_4 emissions during 2010–2017 may be related to the enhanced global production of CFC-11 inferred over this same period.

3.1 GLOBAL CFC-11 EMISSIONS

Ongoing concentration measurements of long-lived trace gases in the remote atmosphere can be used to derive global emissions when considered together with annual losses (see Box 3.1). In 2018, measurements at NOAA sites around the globe (see section 2.1.1) indicated that, beginning in 2013, global CFC-11 emissions had unexpectedly increased and had remained elevated until 2016, despite a reported phaseout of global production in 2010 (Montzka et al., 2018). These findings were assessed and confirmed by results from the AGAGE Network (see section 2.1.1) in Engel et al. (2018).

Updated global results in Rigby et al. (2019) indicated that emissions remained elevated until 2017 (Rigby et al., 2019). Average global emissions averaged from 2014 to 2017 were 80 ± 5 Gg yr^{-1} (NOAA) or 74 ± 5 Gg yr^{-1} (AGAGE) when derived with a 52-year lifetime (Figure 3.1).

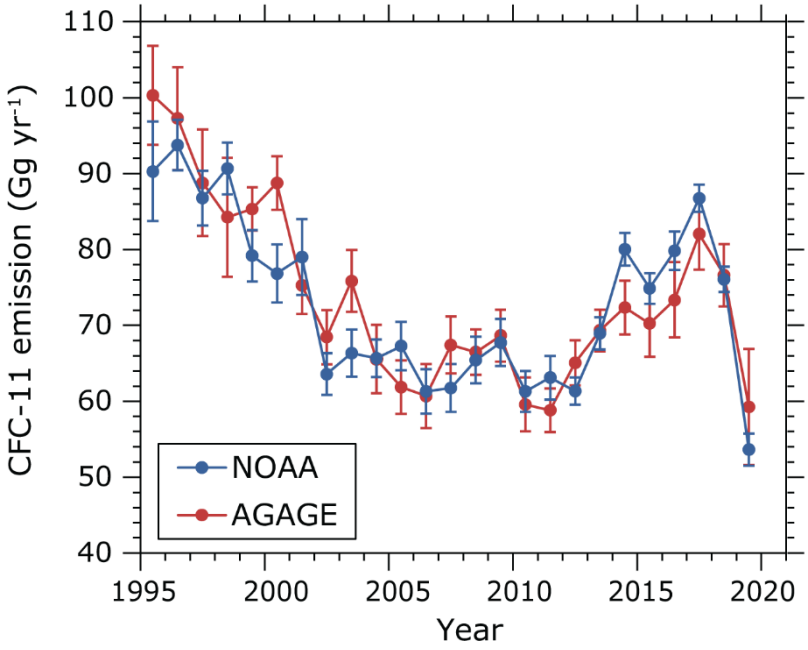

Figure 3.1. Annual CFC-11 global emissions derived from the NOAA (blue) and AGAGE (red) networks from 1995 to 2019. Emissions and their uncertainties were derived from measured atmospheric concentrations at remote sites and a three-box model with constant dynamics and a 52-year lifetime for CFC-11. The uncertainties indicated for annual mean values account for measurement precision, atmospheric variability and uncertainty in estimating global means from a limited number of measurement stations (see Box 3.1).

Uncertainties quoted here do not account for lifetime uncertainties but, if added, would increase stated 1-standard deviation uncertainties on these estimates to ±10 Gg yr^{-1} (Montzka et al., 2021). The 2014–2017 mean emissions were determined to be between 11 ± 3 Gg yr^{-1} (NOAA) and 17 ± 3 (AGAGE) Gg yr^{-1} larger than average global emissions during 2008–2012. These values are comparable to the 13 ± 5 Gg yr^{-1} emission increase derived by Montzka et al. (2018) for a slightly different period (which gave the 2014–2016 average relative to the 2002–2012 average; all uncertainties are 1 standard deviation).

Measurement records from both networks and derived global emissions have now been updated until early 2020 (see Figure 2.2) and indicate global changes following initial efforts to mitigate recent increases in CFC-11 emissions (section 2). While there are differences in results derived from the two networks for certain years, results from both networks confirm that there was a significant drop in emissions in 2019 relative to 2018 and that emissions in 2018 were comparable to the elevated values during 2014–2017 (see Figure 3.1).

A detailed analysis of observations until early 2020 was performed with a combined observational record derived from both NOAA and AGAGE. It also included a slightly longer CFC-11 lifetime (54 or 56 years) to ensure consistency with mean lifetimes innate to the three-dimensional (3-D; longitude, latitude, altitude) models that were used to estimate biases arising from inter-annual changes in air transport and mixing (see Figure 3.2 and Box 3.1) (Montzka et al., 2021). Use of these longer lifetimes and the removal of transport-related biases leads to global CFC-11 emission estimates for 2008–2012 (56 ± 5 Gg yr^{-1}) and 2014–2017 (69 ± 6 Gg yr^{-1}) that are slightly smaller than reported previously (Rigby et al., 2019) (uncertainty is ± 10 Gg yr^{-1} for both estimates if lifetime uncertainties are included). The emission difference of 13 ± 7 Gg yr^{-1} between the two periods is similar to a previously reported increase that did not explicitly account for transport-related biases. Thanks to this new result, the suggestion in a previous study (Montzka et al., 2018) that "as much as 40 to 60%" of this derived emission increase was from transport-related biases is unlikely.

The new analysis confirms that there was a substantial decline in global emissions by 2019, which approximately coincided with the mitigation efforts spearheaded by the Parties to the Montreal Protocol, China, and other interested groups (Montzka et al., 2021; Park et al., 2021). In 2019, global CFC-11 emissions were 18 ± 6 Gg yr^{-1} (26 ± 9%) lower than in 2018; whereas emissions in 2018 (70 ± 4 Gg yr^{-1}, or ± 10 Gg yr^{-1} if lifetime uncertainties are included) were equivalent to mean emissions for 2014–2017. The substantial drop in global emissions by 2019 derived using the combined NOAA and AGAGE records or using either records alone is consistent with the reduced hemispheric difference measured by both networks in 2019 (see Figure 2.2(a)) and is not appreciably altered by variability in atmospheric transport processes and CFC-11 loss estimated from 3-D models (see Box 3.1). Furthermore, the emission reduction in 2019 was not a result of reduced economic activity associated with the global SARS-CoV-2 pandemic, since that impact became substantial only after 2019.

The global CFC-11 emission in 2019 of 52 ± 5 Gg yr^{-1} (± 10 Gg yr^{-1} including lifetime uncertainties) is similar to the 56 ± 5 Gg yr^{-1} mean emission derived during 2008–2012, which was before emissions had unexpectedly increased. While this similarity confirms the mitigation of a substantial amount of the unexpected CFC-11 emission enhancement, it does not necessarily imply that the problem of unreported production and renewed use has been completely mitigated. This is because emissions were expected to decrease after the 2010 reported production phaseout, rather than to remain constant over time (TEAP/UNEP, 2019*a*; Harris et al., 2014; Carpenter et al., 2018; Lickley et al., 2020).

Expectations of how global CFC-11 emissions would have declined in the absence of unreported production after 2010 are poorly constrained owing to uncertainties in bank sizes, release rates, and how they might have changed over time. A projection of emission changes from the 2002–2012 period to 2019 is one straightforward means of deriving expectations. If the emission decline observed during 2002–2012 had continued until 2019, the derived emission enhancement in 2019 would be small (7 ± 6 Gg yr^{-1}) compared with the emission enhancements in the preceding five years (see Figure 3.2) (Montzka et al., 2021). Relative to this simple linear extrapolation, global emissions derived from observations during 2012–2019 were elevated by a cumulative total of 120 Gg, which is significantly larger than the cumulative emission enhancement during 2012–2019 of 70 Gg relative to the 2008–2012 emission mean. Similar quantities are derived from the assumption of a constant release fraction of CFC-11 from banks after 2010 at constant value (~3% yr^{-1}, depending on the bank size considered).

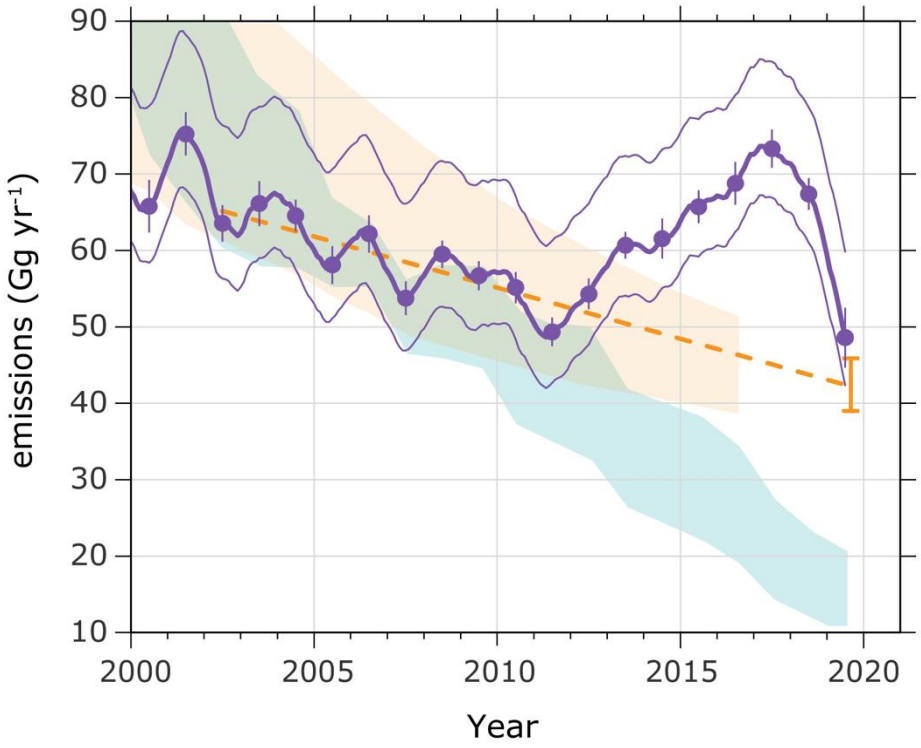

Figure 3.2. Observationally derived and expected global CFC-11 emissions. A single, observationally derived emission record was derived by simultaneously using NOAA and AGAGE data in a three-box model with a 56-year lifetime (thick purple line and points), after accounting for biases related to inter-annual variations in dynamics (biases were estimated from a 3-D model analysis; annual bias corrections from WACCM (Whole Atmosphere Community Climate Model) average 5 ± 4 Gg yr^{-1}). Details on how the NOAA and AGAGE data were combined to create this single emission history are described in Montzka et al. (2021). The influence of lifetime uncertainties is shown (thin purple lines) for lifetimes of 50 and 60 years; this range encompasses the lifetime derived from most atmospheric models (SPARC 2013; Chipperfield et al., 2014) (see Box 3.1). Multiple estimates of expected emissions from banks are also presented and assume no unreported production following the 2010 reported phaseout in production. They include: 1) a linear extrapolation of emissions for 2002–2012 (orange dashed line, with an orange vertical bar indicating the range projected for 2019); 2) the range of four different scenarios from an inventory analysis of past uses, sales and emission release functions (blue shaded region; (TEAP/UNEP, 2019*b*)), and 3) a probabilistic analysis that incorporated inventory and atmospheric data (tan shaded area from Lickley et al., (2020)).

A separate probabilistic analysis of CFC-11 banks and emissions that incorporated inventory-based information and atmospheric measurements also provides an estimate of expected emissions from banks created from pre-2010 reported production (Lickley et al., 2020). Results from that analysis suggest emission expectations and, therefore, unexpected emission enhancements, that are similar to those derived from the simple linear extrapolation until 2016, the interval studied in that work (see Figure 3.2, tan shaded area).

Emission expectations have also been derived using an inventory-based model in which reported production is considered in multiple applications together with use practices and their historical evolution over time (TEAP/UNEP, 2019*b*) (see also section 5). The range of emissions encompassed by the four scenarios developed by TEAP in its report to the Parties (TEAP/UNEP, 2019*b*) (low, medium, high and most likely) is indicated by the blue shaded area in Figure 3.2. Considering that the comparison between inventory-based estimates of expected emissions and the observationally based estimate is sensitive to the true CFC-11 lifetime, the range of emissions in the TEAP-derived scenarios encompasses the observationally derived emission

values until 2005 (or 2011 if the true CFC-11 lifetime is 60 years instead of 52 years). After 2012, however, expected emissions diverge significantly to values lower than those derived from observed concentrations.

The steep decline after 2010 derived for bank emissions and fractional release rates from banks in the absence of unreported production in the TEAP inventory model stems in part from the cessation of fugitive emissions associated with new production. It also stems from assumptions related to the usable lifespan of CFC-11-containing products and the fate of CFC-11 in those products as they reach their end of life and are transitioned to landfill (see the Methods section in Montzka et al. (2021)). It has been shown that some reasonable alternative assumptions can substantially affect the model-derived emissions from banks and their decline during 2010–2020. For example, a longer mean lifetime of in-use chiller equipment results in modelled emissions during 2012–2017 that are comparable to those suggested from the linear extrapolation of emissions during 2002–2012 or from the Lickley et al. (2020) analysis (Montzka et al., 2021). The post-2010 emission declines inferred by the TEAP model could in theory be tested in regions not impacted by unreported production after 2010. However, regional estimates of emissions are available in only a few regions of the world and no consistent pattern has yet emerged in those regions that might support or refute the TEAP-derived emission trend after 2010; significant declines after 2010 are derived for CFC-11 emissions from the United States, while other regions show only small changes (see Figure 4.3).

Despite these uncertainties, the TEAP model represents an independent estimate of expected bank emissions over the past decade. The declines in bank emissions and fractional release rates from banks derived in the TEAP model after 2010 imply that the observationally derived CFC-11 emissions in 2019 could still be enhanced above expectations by as much as 23–50 Gg yr^{-1} (see Figure 3.2). These enhancements correspond to a cumulative emission above expectations during 2012–2019 of 175–440 Gg. The large range in this estimate is a result of two factors in equal measure: the uncertainty of the CFC-11 lifetime, and the range of emissions represented by the four TEAP scenarios (TEAP/UNEP, 2019*b*).

3.2 ON POTENTIAL FUTURE GLOBAL EMISSIONS OF CFC-11

Considering only the magnitude of global emission enhancement above the 2008–2012 mean (13 ± 7 Gg yr^{-1} from 2014 to 2018), the associated ozone depletion would likely be small (Dhomse et al., 2019; Dameris et al., 2019; Keeble et al., 2020) (see also sections 5 and 6). Two considerations suggest, however, that cumulative CFC-11 emission and ozone impacts could be larger than implied from the 13 Gg yr^{-1} for these five years (or 65 Gg for 2014–2018; 70 Gg if including 2013). First, as discussed above, based on the expectation of decreasing bank emissions after 2010–2012 (Harris et al., 2014; Carpenter et al., 2018; Lickley et al., 2020; TEAP/UNEP, 2019*b*), a cumulative emission enhancement for 2012–2019 of 120–440 Gg is estimated (this range reflects the expectations discussed in section 3.1), which is ~2–6 times larger than the cumulative emission enhancement above the 2008–2012 mean. Second, the CFC-11 emissions increase may represent only a fraction of the cumulative unreported production in recent years, particularly because the new CFC production is likely associated with manufacturing closed cell foams (TEAP/UNEP, 2019*b*). The emissions associated with CFC-11 production and from the production and installation of insulating foams are estimated to amount to only 25%–45% of the total production quantities; the remainder of the produced CFC-11 is retained in the installed foams (TEAP/UNEP, 2019*b*; Montzka et al., 2021). This suggests total CFC-11 production magnitudes that are ~2–4 times larger than derived emission enhancements, increases in CFC-11-containing foam banks, and sustained elevations in CFC-11 emissions from those banks for many years to come (see section 5).

The linear extrapolation analysis in Figure 3.2 suggests 2019 emissions are enhanced by 7 ± 6 Gg yr^{-1}, or 15% (2%–30%), above expectations. This relative magnitude may represent an upper limit for the increase in CFC-11 foam banks and for emission enhancements in the future related to the newly created banks, although substantially larger additions to banks and future emission enhancements cannot be ruled out given the inventory model expectations.

The updated observations, covering the period up to 2019, indicate a substantial reduction in renewed production and use of CFC-11 since the 2010 reported phaseout, and they place limits on increases in CFC-11 banks and, therefore, enhanced emissions in the future. Currently, however, the limited understanding of emission expectations (emissions from banks owing to reported production) and actual production magnitudes make it difficult to more accurately quantify the impact that the renewed production and use will have on future CFC-11 emissions and the ozone layer.

3.3 CFC-12 GLOBAL EMISSIONS

CFC-12 (CCl_2F_2) is an ozone-depleting chemical controlled by the Montreal Protocol that was used primarily in refrigeration and air-conditioning applications. CFC-11 and CFC-12 are typically both produced with significant yield during the anhydrous fluorination of CCl_4, although if only CFC-11 is desired, methodologies exist that prevent significant co-production of CFC-12 (TEAP/UNEP, 2019*b*). As a result, changes in regional or global emissions of CFC-12 could provide further evidence for unreported CFC production (Engel et al., 2018; Rigby et al., 2019; Lickley et al., 2020). From 2000 to 2009, global CFC-12 emissions declined by approximately 12 ± 2% yr^{-1} (see Figure 3.3). From 2010 to 2017, however, this decline slowed to only 5 ± 2% yr^{-1}. Global emissions in 2019 totalled 21 ± 7 Gg yr^{-1} and were 38 ± 15% lower than the 2018 value. This change is significantly larger than typical inter-annual variability derived for global CFC-12 emissions (1 standard deviation of 13%–17%, depending on the network), and appears to suggest a substantial drop in global CFC-12 emissions by 2019, as was observed for global CFC-11 emissions.

Given the substantial uncertainties regarding the expected decline in global CFC-12 emissions in recent years, any assessment of observationally derived emission changes relative to expectations are difficult. For example, the CFC-12 emission inventory analysis did "not provide an accurate representation of the historic use and expected emissions of CFC-12 and cannot describe atmospherically derived emissions" (TEAP/UNEP, 2019*b*). Furthermore, in the "Summary for Policymakers" chapter in the Scientific Assessment Panel's most recent quadrennial report, the available information allowed for the possibility that CFC-12 in banks may already have been entirely depleted (Carpenter et al., 2018), although this conclusion is sensitive to the CFC-12 lifetime assumed in that analysis. If true, CFC-12 emissions should currently be indistinguishable from zero, but ongoing global atmospheric measurements indicate otherwise, given the best-estimate lifetime for CFC-12 of 102 years (see Figure 3.3). While ongoing CFC-12 emissions could be associated with renewed CFC-11 production, they might also stem primarily from underlying inconsistencies and uncertainties in our understanding of CFC-12 emissions from banks. The probabilistic analysis in Lickley et al. (2020) concluded that the continued CFC-12 emissions and their changes since 2012 do not fall outside the expectations provided in their analysis, given the uncertainties involved, although their expectations do not encompass the observationally derived emissions during the preceding 10–15 years.

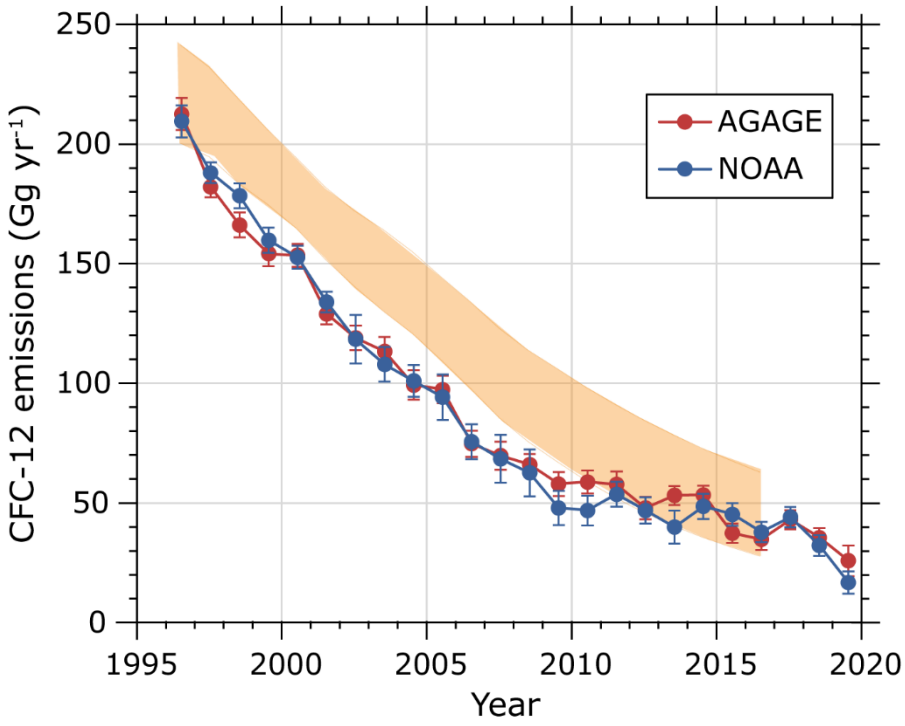

Figure 3.3. As per Figure 3.1, but for annual CFC-12 global emissions for 1995–2019 derived from global-scale measurements from two independent networks and a lifetime of 102 years. Uncertainties were estimated using the same methods as described for CFC-11 in the caption to Figure 3.1. Emission expectations are also shown from a probabilistic analysis of reported CFC-12 production, banks and emissions that incorporated inventory-based and atmospheric data (tan shaded area representing the 5%–95% likelihood range from Lickley et al. (2020)).

3.4 GLOBAL EMISSIONS OF CCl_4

Carbon tetrachloride (CCl_4) is the chemical feedstock that was used most commonly in the production of CFCs, including CFC-11 (TEAP/UNEP, 2019*b*). As is the case with CFC-12, however, there are substantial gaps in our understanding of CCl_4 emissions in recent years (SPARC, 2016). CCl_4 production for emissive use was phased out worldwide in 2010 under the Montreal Protocol. Following the phaseout in 1996 of CFC production in Parties not operating under Article 5 of the Protocol (non-A5 countries), emissions of CCl_4 arising from losses during production and other associated processes have decreased over time (see Figure 3.4). Global CCl_4 emissions declined at approximately 1.6 ± 0.3 Gg yr^{-1} from 2000 to 2009, but have not declined significantly since 2010 (the average for 2010–2019 was 0.1 ± 0.2 Gg yr^{-1}). Emissions in 2014–2019 averaged 39 ± 4 Gg yr^{-1}. The uncertainties and variability associated with annual estimates and year-to-year changes, however, preclude any robust assessment of global emission changes concurrent with CFC-11, although a relationship between CFC-11 and CCl_4 emissions from East Asia has been noted (Lunt et al., 2018).

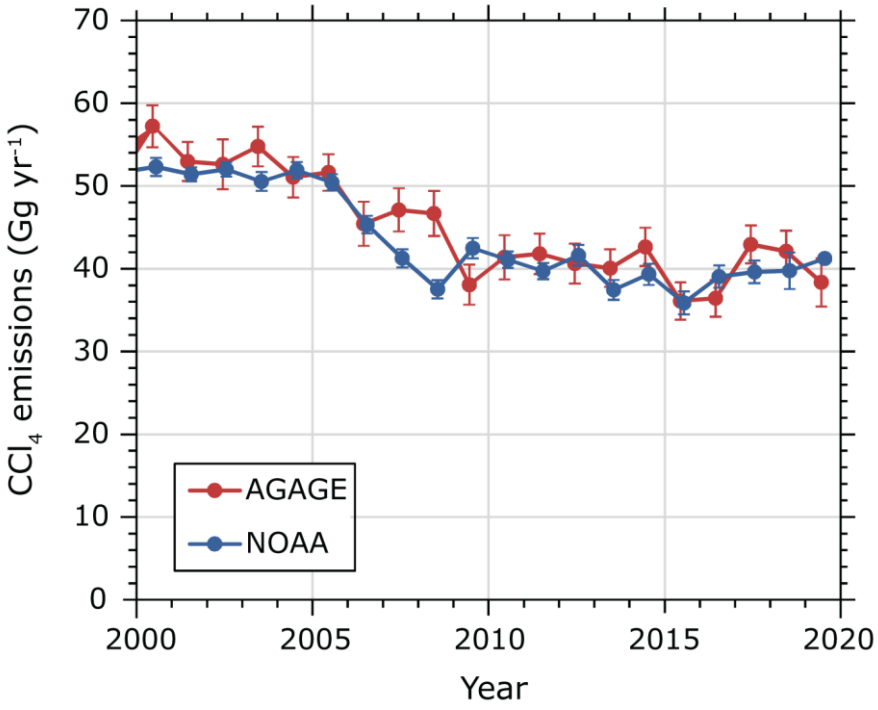

Figure 3.4. As per Figure 3.1, but for annual CCl_4 global emissions derived from surface measurements from two independent networks using a lifetime of 32 years. Uncertainties do not reflect those associated with lifetime and were estimated using the same methods as described for CFC-11 in the caption to Figure 3.1.

Global CCl_4 emissions remain elevated above expected levels for reasons that are not fully understood (SPARC, 2016 and previous WMO ozone assessment reports). One potential contributor to sustained CCl_4 emissions is the continued production and consumption of CCl_4 for non-dispersive use as a chemical feedstock and as a process agent. This production totalled 203 Gg in 2014 (Sherry et al., 2018). A recent SPARC (2016) report and the 2018 Scientific Assessment of Ozone Depletion (Engel et al., 2018) updated our understanding of the CCl_4 budget, showing a considerable narrowing of the gap between bottom-up and top-down emission estimates, but with the new bottom-up value still lower than atmosphere-derived global emissions, even with the large remaining uncertainties.

Because these gaps in our understanding have persisted for many years, it seems unlikely that unreported CFC-11 production is the primary cause of the unexpectedly high CCl_4 emissions. While it is possible that the slower decline in global CCl_4 emissions after 2010 was partly due to unreported CFC production, the 5 Gg decline in CCl_4 emissions by East Asia from 2016 to 2019 (Park et al., 2021) is not apparent in global estimates (see Figure 3.4). This apparent inconsistency may be the result of the offsetting of emission increases in other regions, but also may reflect the inability of global networks to reliably determine emission changes of this magnitude for CCl_4, considering the variations and inconsistencies in CCl_4 global emissions derived from the two networks in the past.

For the 40–70 Gg yr^{-1} of CFC-11 production estimated by TEAP to account for the observed increase of CFC-11 emissions after 2012, CCl_4 production of 45–120 Gg yr^{-1} would be required (TEAP/UNEP, 2019*b*). For CCl_4 emissions CFC-of 0.3%–5% during CFC-11 production, depending on CFC-11 production scale and operation conditions (TEAP/UNEP, 2019*b*) the related CCl_4 emission could account for less than half (< 6 Gg yr^{-1}) of the emission gap, and probably only in the most recent years. The potential for higher levels of CFC-11 production (see section 3.2) would imply higher levels of CCl_4 production and emissions, thereby accounting for more of the emission gap for CCl_4, but only for those recent years.

Box 3.1. Methodology for deriving global emissions from atmospheric abundance measurements

Atmospheric trace-gas abundance is typically measured and reported as a mole fraction, which represents the number of moles (or molecules) of a trace gas per moles (or molecules) of air. For ODSs, mole fractions are very small, on the order of a few molecules per trillion molecules of air, so are expressed as parts per trillion (ppt) after multiplying by 1×10^{12}. In this report, the terms mole fraction and concentration are used interchangeably to represent trace gas atmospheric abundance.

The link between global atmospheric mole fractions and global emissions

A trace-gas release to the atmosphere (expressed as moles yr^{-1} or grams yr^{-1}) changes the averaged global trace-gas mole fraction by an amount related to the total number of moles of air in the atmosphere (1.8×10^{20}). For example, an instantaneous emission of 100 Gg (100,000 tonnes) of CFC-11 (which is equivalent to 0.73 Gmol of CFC-11, calculated as 100×10^9 g ÷ 137 g mol^{-1} CFC-11) would increase the average global atmospheric mole fraction of CFC-11 by 4.3 ppt ($7.3 \times 10^8 \div 1.8 \times 10^{20}$). Atmospheric measurements would readily pick up this change in the measured mole fraction if that emission were distributed uniformly throughout the entire atmosphere. A 4.3 ppt increase in CFC-11 would add 1.9% to its global atmospheric abundance and augment current equivalent Cl by 0.3%.

This example demonstrates how measurements of global mole fraction are sensitive to emissions. To derive quantitative estimates of global emissions from the mole fraction, however, it is important also to take into account that trace gases are constantly being destroyed and removed from the atmosphere by photolysis and oxidation. In other words, an estimated global emission is derived from a change in the global mole fraction plus an amount reflecting removals during that year, which is derived from the trace-gas lifetime. Simply expressed, the annual change in the measured global atmospheric burden of a trace gas reflects the difference between emissions and loss:

$$\frac{\mathrm{d}G}{dt} = Emission - Loss$$

or

$$Emission = \frac{\mathrm{d}G}{dt} - Loss$$

where G = global mass, t = time (years), and *Loss* is estimated by G multiplied by a pseudo first-order loss frequency (yr^{-1}), which is approximately equal to the reciprocal of the chemical's global lifetime (yr^{-1}).

Global-scale sampling programmes (see section 2.1.1) provide an estimate of G and dG/dt. While these estimates are typically derived only from surface-based measurements from flask samples or on-site instrumentation at a limited number of sites, in the case of CFC-11 they have low uncertainty because the remote troposphere is well mixed vertically and accounts for >80% of the mass of the atmosphere, and because concentration gradients on the Earth's surface are relatively small (the pole-to pole gradient for CFC-11 is currently ~1%). This is especially true for long-lived trace gases like CFC-11 that lack tropospheric sinks, and also because the measurements are made at sites far removed from sources, so they provide results that are more representative of broad regions of the troposphere.

Models are used for deriving global emissions from atmospheric mole fraction measurements for two main reasons. First, models enable an estimate of the global mass of trace gases and change to that mass over time that is consistent with measured mole fractions only at the Earth's surface. Simple box models (3 or 12 boxes) are typically used successfully for this purpose and give similar results for long-lived gases like CFC-11, provided they include similar lifetimes (Montzka et al., 2018). Second, they enable an improved estimate of loss by considering trace gas burdens in the relevant loss region (e.g., the stratosphere) as opposed to the entire atmosphere.

Box 3.1. Methodology for deriving global emissions from atmospheric abundance measurements (continued)

Knowledge about the average loss frequency (the inverse of which is called the chemical's lifetime) is also a key component to estimating global emissions in this way. Estimates for this loss-rate constant can be derived from numerous sources, such as from the analysis of mole fraction measurements in the stratosphere, or laboratory determinations of rate constants associated with photolytic destruction and oxidation (Chipperfield et al., 2014; SPARC, 2013). These photolytic rate constants are then incorporated into 2-D and 3-D models of the atmosphere that simulate fluxes of light and transport of air through the stratosphere (where loss occurs). As a result, CFC-11 lifetimes contain uncertainty arising from how the models represent both of these processes.

Uncertainty in the mean long-term lifetime of CFCs and CCl_4 implies that the magnitude of an entire emission history can be biased high or low. While this consideration is important for assessing differences between global concentration-based emission estimates and those from sales- and use-based inventory models, it does not strongly affect estimates of year-to-year changes in derived emissions or changes in mean emissions within a decade. For this reason, uncertainty in lifetime is not incorporated into the error bars on annual emissions shown in the figures in this section. Changes in mean lifetimes over periods longer than a decade are expected (Chipperfield et al., 2014), but are not discussed further here.

The region between the thin lines in Figure 3.2 shows the influence of assuming mean CFC-11 lifetimes of 50–60 years on the emissions derived from NOAA or AGAGE data . This range was chosen based on CFC-11 lifetimes estimated by multiple 3-D models and one 2-D model (Chipperfield et al., 2014; SPARC 2013). The best-estimate, steady-state lifetime from those models was 55 ± 4 (1 standard deviation) years, which is nearly identical to the value diagnosed for 2000–2006, the most recent period analysed; this lifetime is not projected to change substantially in the future (Chipperfield et al., 2014). Other methods, particularly those based on interpretations of surface-based or satellite observations, can be used to derive CFC-11 lifetimes and give values that are within this range (53 years ± 15% from inversions) or slightly lower (45 years ± 25% from satellites) (SPARC 2013).

While multiannual trends derived using NOAA or AGAGE data show similar patterns and changes, when year-to-year timescales are used, emissions estimated using NOAA or AGAGE data sometimes show larger-than-expected differences and inter-annual variability that are based on uncertainties in *G* and *dG/dt* alone (see Figure 3.1). Such differences may arise from measurement errors, as variations are not always consistently captured by the different network results. The inter-annual variability that is captured by both networks, however, may arise in part from variations in atmospheric transport and mixing processes (i.e. dynamics) between the troposphere and stratosphere that affect global surface concentrations (Elkins et al., 1993; Nevison et al., 2011; Ray et al., 2020). When left unaccounted for, these inter-annual variations in dynamics can skew estimates of annual emissions and their inter-annual changes. Given the cyclical nature of these variations, however, biases in emission estimates are reduced when emission estimates are averaged over 3–5 years. Montzka et al. (2018) estimated that unaccounted dynamics could have skewed the emission increase of 13 ± 5 Gg yr^{-1} estimated for CFC-11 after 2012 by up to 40%–60%. An updated analysis of this increase includes explicit estimates of biases on derived emissions related to dynamical variability (Montzka et al., 2021). These biases were derived from two different reanalyzed wind fields and two 3-D models in an attempt to understand their sensitivity to reanalyses and 3-D models, which contain substantial uncertainties. With the bias-corrected results, the mean emission enhancement during 2014–2017 (or 2014–2018) relative to 2008–2012 is estimated to be 13 ± 7 Gg yr^{-1} (Montzka et al., 2021). This updated result replaces the previous suggestion that dynamical influences may have accounted for up to 40%–60% of the 13 ± 5 Gg yr^{-1} emission enhancement (2014–2016 compared with 2002–2012) that was derived without an explicit consideration of dynamics-related biases (Montzka et al., 2018).

Ray et al., (2020) have estimated biases in derived inter-annual changes in CFC-11 emissions from quasi-biennial oscillation (QBO)-related dynamical variability to be ±6 Gg, on average, but found they can be as large as ±10 Gg. Two 3-D model analyses suggest mean biases of similar magnitude (Montzka et al., 2021). These values are larger than the statistical uncertainties associated with deriving emissions from the NOAA or AGAGE networks (see Figure 3.1). These studies, however, suggest that when annual emission magnitudes are averaged over three- to five-year periods, dynamics-related biases are minimized.

Box 3.1. Methodology for deriving global emissions from atmospheric abundance measurements (continued)

Despite the uncertainties of using 3-D models to estimate the influence of dynamical variability on surface CFC concentration and derived emissions, the substantial drop in emissions by 2019 is a robust feature of the observations, with or without considering dynamical changes.

Dynamical variability persisting over five years or longer is possible and can be similar in size to QBO-induced changes. Variability on these timescales is not as regular or as well understood as QBO-induced variability. A stratospheric circulation change following the year 2000, for example, persisted for ~6 years and was thought to be due to anomalous tropical sea surface temperatures (Randel et al., 2006; Rosenlof and Reid, 2008; Bönisch et al., 2011). This circulation change was not predicted by any climate model so our understanding of this event is limited, but it suggests that anomalies on this timescale are possible due to internal variability of the climate system. An increase in the stratospheric Brewer-Dobson circulation is predicted over multidecadal periods in response to enhanced greenhouse gas concentrations (e.g., Butchart, 2014). This would involve a slow change in stratospheric circulation (~2%–3% decade^{-1}) and potentially shorter CFC lifetimes, but has not yet been verified with observations (e.g., Engel et al., 2009; Ray et al., 2014).

4. REGIONAL EMISSIONS

Main points:

- There are a small number of regions of the world for which detailed regional atmospheric data-based inference of emissions is possible.
- Of these regions, thus far, an increase in CFC-11 emissions since 2012 has only been identified from Eastern China.
- CFC-11 emissions from Eastern China are estimated to have increased by 7 ± 4 Gg yr^{-1} between the periods 2008–2012 and 2014–2017, accounting for around 60 ± 40% of the global increase.
- Subsequently, CFC-11 emissions from Eastern China dropped, starting in around 2018, with emissions in 2019 falling by 10 ± 3 Gg yr^{-1} compared with 2014–2017. This fall accounted for 60 ± 30% of the concurrent global emissions decline.
- CCl_4 emissions from Eastern China increased after 2012, growing from 6.0 ± 1.4 Gg yr^{-1} for 2011–2012 to 10.9 ± 2.0 Gg yr^{-1} for 2014–2017. Around 2017, emissions from this region declined again, returning to 6.2 ± 1.4 Gg yr^{-1} in 2018–2019.
- CFC-12 emissions from Eastern China had not increased after 2012, remaining close to 3.0 ± 1.2 Gg yr^{-1} (the 2011–2012 mean) until 2016. CFC-12 emissions declined sharply after 2016, reaching levels indistinguishable from zero in the 2017–2019 period.

It is possible to infer CFC-11 emissions at regional scales (~100–1 000 km) in the vicinity of the monitoring sites, provided that measurements of atmospheric mole fraction exist in sufficient density in space and/or time (see section 2). This section briefly outlines the methodologies that have been employed for this purpose and assesses recent regional estimates of CFC-11 emissions.

4.1 METHODOLOGY

For long-lived trace gases, atmospheric mole fractions can broadly be separated into two components (see section 2): a "baseline" or "background" component, representing the mole fraction that would be observed in the "well-mixed" atmosphere, far from emission sources, and an enhancement due to the influence of any emission sources within the vicinity of the measurement station (see Figures 4.1 and 2.3). Global or regional 3-D atmospheric chemical transport models (CTMs) can be used to estimate the source of these signals in the data. The focus herein is on recent studies of CFC-11 emissions using regional modelling approaches.

Regional CTMs can be used to estimate the magnitude of above-baseline mole fractions based on an initial emission estimate by accounting for the advection (transport by the wind) and mixing (driven by atmospheric turbulence) that trace gases undergo in the atmosphere. For long-lived gases,[4] regional CTMs often ignore the influence of atmospheric chemistry, photolysis or deposition, which have little influence over the timescales considered for regional atmospheric transport. Regional CTMs are driven by meteorological variables, such as wind, temperature and pressure, which meteorological services provide using the global network of in situ and remotely sensed meteorological observations and data assimilation algorithms. For

[4] For ODSs, a long-lived atmospheric substance is generally considered one with a lifetime greater than six months.

regional CFC-11 studies, a particular type of CTM known as a Lagrangian particle dispersion model has been most widely used (e.g., Seibert and Frank, 2004). For each concentration measurement, a Lagrangian CTM can estimate how sensitive the above-baseline mole fraction enhancement at the measurement point is to a unit emission rate from a nearby source. The geographic representation of this source–receptor relationship is often referred to as an air history, an emission sensitivity, or the "footprint" of the measurement (see Figure 4.1). The annual mean footprint for the existing network of CFC-11 observations from AGAGE stations (Prinn et al., 2018) and NOAA's flask-sampling and high-frequency in situ networks (Hu et al., 2017) is shown in Figure 4.2 (see also section 2.1). The darker shading indicates areas where emission sources would contribute substantially to the observed mole fraction enhancements, and the lighter shading marks indicate regions with less influence. As shown in Figure 4.2, which uses a logarithmic scale, the footprint's magnitude decreases rapidly as the distance from the monitoring sites increases, because of advection and atmospheric mixing. Depending on the meteorology, observations are usually sufficiently sensitive to emissions to derive emissions magnitudes and distributions (of scales of 10s to 100s of km) within about 1 000 km of the monitoring sites. Thus, there are large areas of the globe where regional emissions cannot be well constrained by the current monitoring networks (e.g., South America, most of Africa and large parts of Asia).

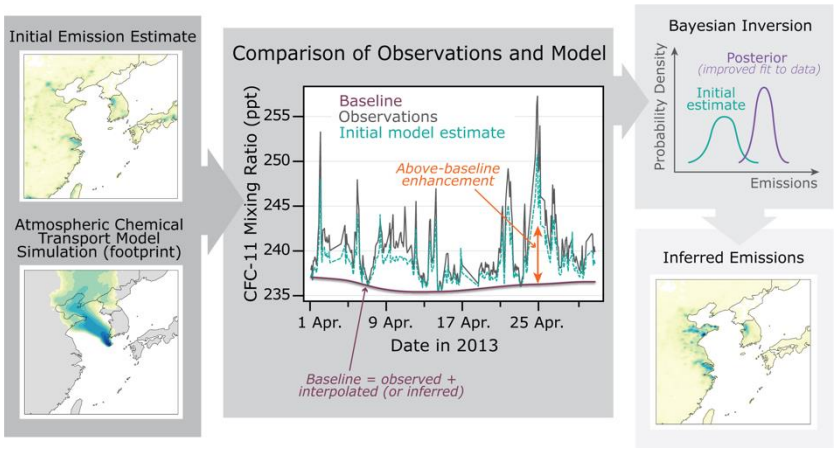

Figure 4.1. Schematic representation of the regional inverse modelling process. Initial estimates of mole fractions at a monitoring site are made based on an initial estimate of the emission field (top-left), atmospheric chemical transport model simulations (bottom-left), and an estimate of the regional baseline (purple line in the central figure). The baseline can either be inferred directly from observations or estimated as part of the inversion. Following this initial comparison between the model (turquoise in the central figure) and the data (synthetic data shown in black in the central figure), a Bayesian inverse modelling framework is usually employed to adjust the emissions (right-hand side) in order to make the modelled results consistent with the measurements, given the uncertainties in the initial emission estimate, the atmospheric CTM and the data.

The first consideration in regional inverse modelling of emissions (see Figure 4.1) is the ability to account for baseline mole fractions entering the domain of interest. Certain inverse modelling systems attempt to identify baseline points in the data and interpolate between them so that a continuous baseline contribution can be approximated (e.g., Manning et al., 2011; Hu et al., 2017). Other methods calculate baseline mole fractions as part of the overall estimation framework (e.g., Stohl et al. 2010; Henne et al., 2016) or take the baseline from a global model simulation, which itself may be constrained with observations (e.g., Thompson and Stohl, 2014; Lunt et al., 2016).

Once a baseline has been defined, a forward model simulation can be performed for a measurement site an estimate of the mole fraction contributions due to regional emission sources is added to the baseline. An initial regional emission estimate is required, which can be based on estimates of industrial activities, for example. These emissions can be propagated through the CTM to provide an initial comparison with the mole fraction data. Following this

initial comparison, inverse modelling frameworks adjust the regional emission field (and the estimated baseline, in some cases) to bring the simulated mole fractions into closer agreement with the observations. Bayesian statistical approaches are usually adopted, which attempt to find a solution that satisfies the prior emission estimate, the data and their CTM representation, given some estimate of the uncertainty in each term. The initial (a priori) emission estimate is needed to guide the framework to a meaningful final (a posteriori) solution, in particular to avoid the occurrence of spurious emission values in regions that are not well constrained by the observation network.

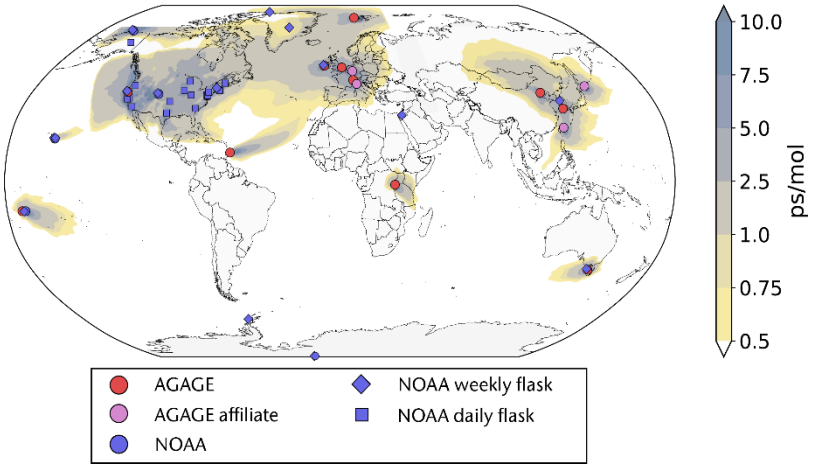

Figure 4.2. Mean footprints for the two global halocarbon measurement networks: AGAGE (red circles) and affiliated (pink circles) high-frequency monitoring stations, and NOAA high-frequency measurement sites (blue circles). Blue squares indicate NOAA sites that collect daily flask measurements, and blue diamonds indicate sites that collect weekly flask measurements for substances controlled by the Montreal Protocol. The footprint is a measure of the contribution to the above-baseline mole fraction made by a unit emission. No footprint is shown for the NOAA high-frequency site located at the South Pole, and the footprint for the NOAA site at Barrow, Alaska, is truncated to the north. Note that CFC-11 data are not currently available at all these sites (see section 2.1.1).

There are many approaches for solving this inverse problem (e.g., Stohl et al., 2010; Manning et al., 2011; Henne et al., 2016; Lunt et al., 2016; Arnold et al., 2018). A critical component of each method is the quantification of the initial emission uncertainties, the observations, and the emissions estimated from the CTM simulations. Usually, the observation uncertainty is almost negligible compared with the much larger – and poorly quantified – CTM uncertainty. Because of the difficulties associated with quantifying the CTM uncertainty, the authors of some studies have opted to base their conclusions on multiple CTMs and multiple inverse methods (e.g., Hu et al., 2017; Rigby et al., 2019). While such an approach cannot provide a comprehensive estimate of the uncertainty in a top-down emission estimate, it does provide a measure of the sensitivity of the results to key assumptions and model architectures.

4.2 REGIONAL CFC-11 EMISSIONS ESTIMATES 2008–2019

Measurements exist in sufficient density to estimate regional CFC-11 emissions (see section 2.1.1; Figure 4.2) in a small number of regions. The high-frequency measurement approach used by the AGAGE network, where mole fraction data are obtained every ~2 hours, allows emissions to be inferred in the vicinity of AGAGE and affiliated stations, which are located in, or near to, industrialized countries (for example, the Western United States, North-Western Europe, East Asia, Southern Australia). The NOAA North America network collects approximately daily flask samples and approximately fortnightly to monthly aircraft measurements, thus allowing emissions to be inferred for the United States. Infrequent flask sampling (such as weekly to monthly) from global networks does not provide data at sufficient density to infer regional emissions in detail.

Recent studies of CFC-11 measurements have derived emission time series for parts of East Asia, the United States, North-Western Europe and Southern Australia. A relatively dense aircraft-based sampling campaign over India has provided a snapshot of Indian CFC-11 emissions during the summer of 2016.

4.2.1 East Asia

In finding a global CFC-11 emissions increase beginning in 2013, Montzka et al. (2018) also identified an increase in the correlation between CFC-11 mole fraction enhancements and other substances emitted from anthropogenic sources (e.g., HCFC-22 (chlorodifluoromethane)) in air samples taken in Hawaii (United States). Air histories calculated using a CTM suggested that these enhancements were associated with air masses from East Asia, although neither the magnitude nor a more precise location of any increased CFC-11 emissions could be deduced.

In 2019, inverse modelling analysis was carried out using high-frequency (~hourly) measurements from the AGAGE Gosan station on Jeju Island, Republic of Korea, and the National Institute for Environmental Studies (NIES) station on Hateruma Island, Japan, to infer emissions from East Asia for the period 2008–2017 (Rigby et al., 2019) (see Figures 4.3 and 4.4). Owing to the uncertainties associated with CTMs and inverse methodologies (see section 4.1.1), two CTMs driven by two different meteorological data sets were used, together with four inverse modelling methods performed by four independent research groups. The inverse analysis focused only on regions to which the Gosan and Hateruma data were sensitive (Figure 4.2): Western Japan, the Korean Peninsula, and a part of China denoted by the authors as "Eastern China" (the measurements were not thought to be sensitive to other regions in China). This part of China encompasses the provinces of Anhui, Beijing, Hebei, Jiangsu, Liaoning, Shandong, Shanghai, Tianjin and Zhejiang, which collectively contain around 35% of the Chinese population. The study noted an increase in the magnitude of above-baseline enhancements in CFC-11 concentrations, particularly at Gosan (see Figure 2.3), beginning in 2013, indicating an increase in regional emissions. Inverse modelling by all four groups found that these increasing enhancements were due to a rise in emissions from Eastern China (see Figure 4.3). Within this area, the highest emission increase was found in or around Shandong and Hebei provinces (see Figure 4.4).

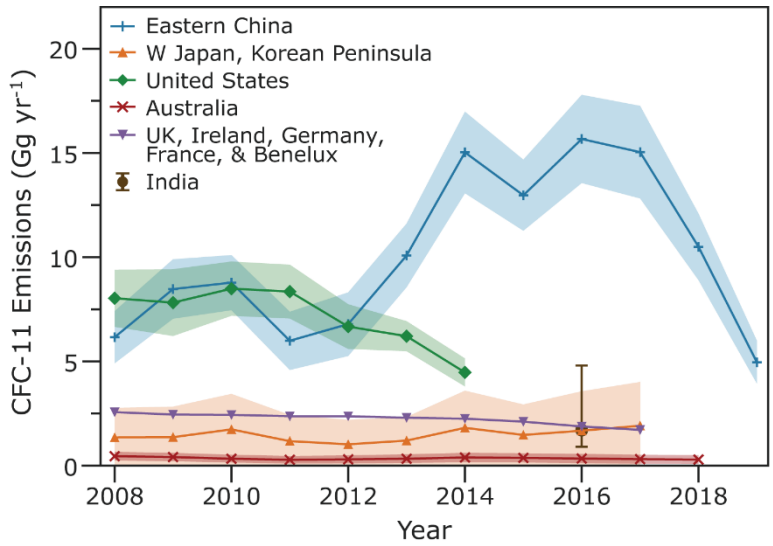

Figure 4.3. Top-down emission estimates and 1-standard deviation uncertainties (shading) for Eastern China (blue) (multi-inversion mean from Park et al., 2021), the United States (green) (Hu et al., 2017), Western Japan and the Korean Peninsula (orange) (multi-inversion mean from Rigby et al., 2019), Western Europe (purple), Australia (red) (Fraser et al., 2020), and a 2016 estimate for India (brown) (Say et al., 2019)

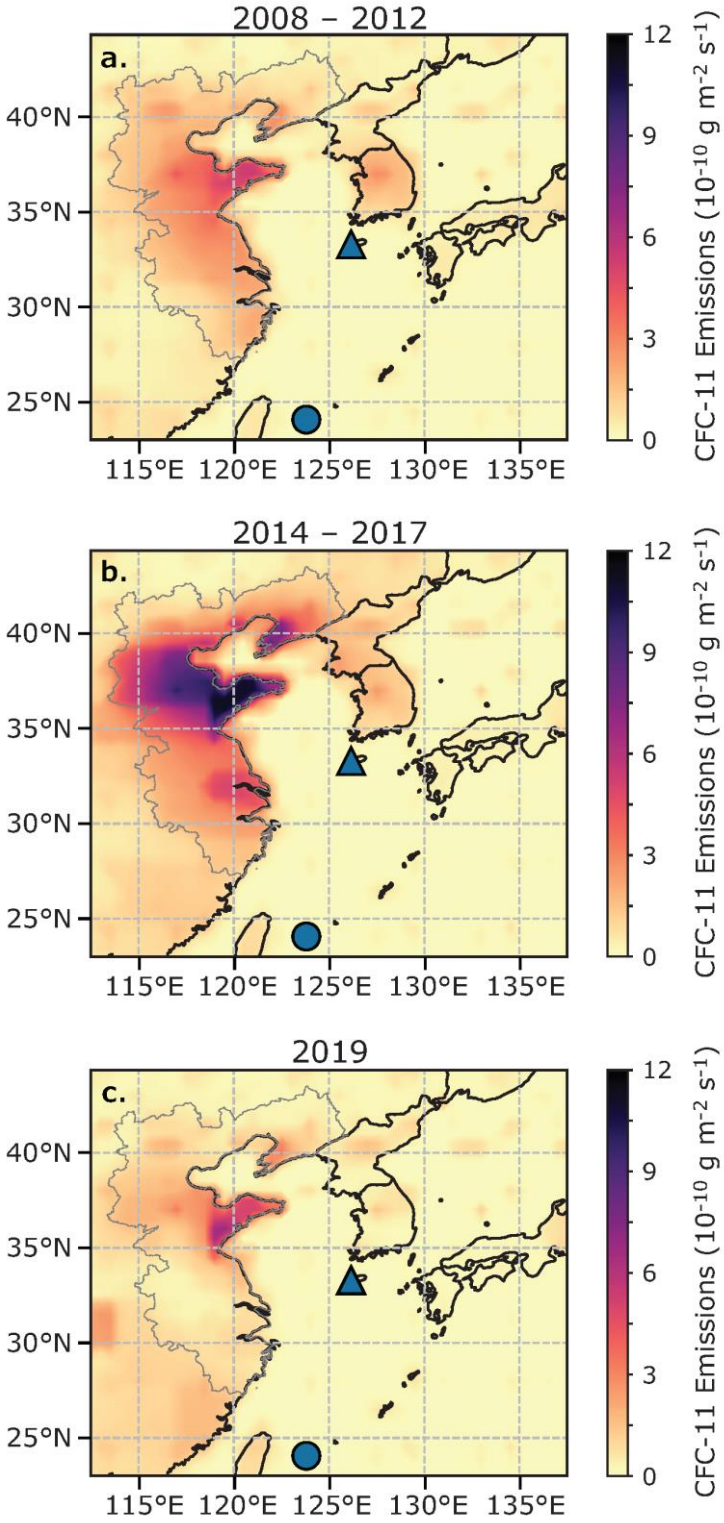

Figure 4.4. Emission distribution from East Asia for 2008– 2012 (a. top panel), 2014– 2017 (b. middle panel) and 2019 (c. lower panel) (Park et al., 2021). Gosan (blue filled triangle) and Hateruma (blue filled circle) station locations are shown. It was found that data from these stations were sensitive to a region referred to as Eastern China (grey line) and to the Korean Peninsula and Western Japan.

The emission increase for Eastern China between the periods 2008–2012 and 2014–2017 was estimated to be 7 ± 3 Gg yr^{-1}, which is 110% of the 2008–2012 Eastern China average (2013 was deemed a transition year and ignored, following Montzka et al. (2018)). Park et al. (2021)

subsequently revised this emission increase slightly to 7 ± 4 Gg yr^{-1}. These values represent the mean across the multiple regional emission inversions. No significant increases in CFC-11 emissions were identified from Western Japan or the Korean Peninsula (Figure 4.3). The rise in emissions from Eastern China was later supported by Adcock et al. (2020), who used independent data from Taiwan Province of China and an interspecies correlation method (in which emissions of a gas assumed to be better understood are scaled by the ratio of the gas's observed above-baseline enhancements to those of CFC-11) to infer an emission increase of 7 ± 5 Gg yr^{-1} for the slightly different period of 2014–2018 relative to the 2008–2011 average.

The rise in emissions from Eastern China was initially estimated to account for 40%–60% of the total global rise, which was inferred using independent data and models (Rigby et al. (2019); see section 3). However, there was evidence that the global inverse modelling approach used in Montzka et al. (2018) and Rigby et al. (2019), which did not consider inter-annual changes in meteorology, overestimated the global rise in emissions (see section 3), in which case a larger fraction of the global increase may be explained by the enhanced emissions from Eastern China (Ray et al., 2020). This proposal was supported by revised estimates of the global rise in emissions by Montzka et al. (2021), which implied a contribution from Eastern China of 60 ± 40% (Park et al., 2021). These findings suggest that additional emission increases probably occurred in regions to which the current global observing system is insensitive (see Figure 4.2).

The Eastern Asian regional inverse analysis was updated up to 2019 by Park et al. (2021). Using the same models, methods, and updated data as used in Rigby et al. (2019), they showed that CFC-11 emissions from Eastern China had declined in 2018, reaching 5.0 ± 1.0 Gg yr^{-1} in 2019. Allowing for uncertainties, this emission rate is consistent with the 2008–2012 mean (7.2 ± 1.5 Gg yr^{-1}). The magnitude of the decline in emissions between the 2014–2017 average and 2019 was 10 ± 3 Gg yr^{-1}, which was similar to the contribution to the rise, implying that the drop in emissions from Eastern China was responsible for 60 ± 30% of the coincident global emission decline reported by Montzka et al. (2021) (see section 3).

Several factors suggest that the post-2012 increase in CFC-11 emissions was due to new production, rather than to an increased rate of release from existing banks of CFC-11 (e.g., in insulating foams manufactured before the CFC-11 phaseout) (Rigby et al., 2019). First, the size of the 2013 CFC-11 bank for the whole of China (54 Gg), based on consumption reports and estimates of bank release rates (Fang et al., 2018), was similar to the cumulative emissions derived between 2014 and 2017 for Eastern China only (56 ± 7 Gg). This suggests that the 2013 bank was not large enough to support the inferred emissions in the subsequent years. Second, even if the 2013 bank size was substantially underestimated, the subsequent rise in emissions would have required an increase in the bank release rate of an order of magnitude over a five-year period (e.g., through a hypothetical rapid increase in the rate of demolition of old buildings or chillers that contained CFC-11). It was concluded that such a rise would be highly unlikely. Third, while the location of any unreported CFC-11 production and that of its emission to the atmosphere do not necessarily coincide, Park et al. (2021) found that Eastern China CFC-12 and CCl_4 emission trends, which are associated with CFC-11 production, showed some similarities to CFC-11 emission trends (see section 4.3).

Further analysis of the bank size and release rate by TEAP/UNEP (2019*b*) supports the suggestion that the emission rise identified in Rigby et al. (2019) could not be explained by the release of CFC-11 from existing banks, and that new production had likely occurred. Park et al. (2021) used estimates of the TEAP/UNEP (2019*b*) bank release fractions and cumulative emissions of CFC-11, CFC-12 and CCl_4 during the 2013–2018 period (assuming that unreported production had begun after 2012 and ceased by 2019) to infer unreported production of up to 165 Gg from Eastern China (upper 95% uncertainty interval, with a median of 118 Gg and a lower bound of 74 Gg). By 2019, the net increase in bank size for this region, as a result of the new production, was estimated to be up to 112 Gg (median of 75 Gg, lower bound 46 Gg).

4.2.2 United States of America

Estimates of United States emissions from several of the most abundant halocarbons were made by Hu et al. (2017) based on approximately daily flask samples from 22 surface-based sites in North America and approximately fortnightly samples from aircraft at a further 15 locations (see Figure 4.2). Two CTMs were employed along with a Bayesian inverse method to derive emission estimates for the period 2008–2014. It was found that emissions of CFC-11 from the United States declined throughout this period, reaching an annual average value of 4.5 ± 0.7 Gg yr^{-1} in 2014 (see Figure 4.3). Top-down estimates were found to be largely in agreement with bottom-up estimates from the United States Environmental Protection Agency (U.S. Environmental Protection Agency, 2016).

4.2.3 Australia

Data from the AGAGE high-frequency measurement station at Cape Grim, Tasmania, have been used to estimate emissions of CFC-11 for Southern Australia (Fraser et al., 2020) (see Figure 4.3). Emissions were inferred using a CTM and a Bayesian inverse method as well as an interspecies correlation method, where CFC-11 emissions were estimated based on an analysis of the ratio of enhancements in CFC-11 and carbon monoxide, whose emissions in Southern Australia were assumed to be well known. It was estimated that the Cape Grim data are sensitive to an area within which approximately 38% of Australia's population reside. The top-down values estimated using the Bayesian inverse method were scaled by population to estimate mean total Australian emissions of approximately 0.3 Gg yr^{-1} over the period 2004–2018, which generally agreed well with interspecies correlation-based estimates. No long-term trend was inferred from either method after 2010, although the interspecies correlation method suggests that emissions were higher on average in the late 1990s and early 2000s. It was proposed that emissions of CFC-11 were consistent with release primarily from above-ground banks (non-land-filled), thought to consist largely of closed cell foams in recent years.

4.2.4 India

During the summer of 2016, a two-month aircraft sampling campaign was carried out over Northern India (Say et al., 2019). In total, 175 whole air samples were collected and analysed in a laboratory using an AGAGE GC-MS-Medusa system (Miller et al., 2008; Arnold et al., 2012; Prinn et al., 2018). A regional CTM was used, along with a Bayesian inverse method, to infer emissions for India of 1.7 (0.8–3.1) Gg yr^{-1}. This value was thought to represent around 2.3% (1.1%–4.2%) of the global total. Although a longer time series of top-down emission estimates is not available for India, the authors concluded that the small magnitude of these emissions in 2016 suggests that India could not have been a primary contributor to the global emissions rise since 2013.

4.2.5 Europe

Rigby et al. (2019) noted that the magnitude of above-baseline events at the AGAGE station at Mace Head, Ireland, had declined consistently between 2008 and 2017 (see Figure 2.3). This finding suggested that emissions from North-Western Europe had fallen during this period. Inverse estimates using these data were presented, without uncertainty analysis, in TEAP/UNEP (2019*b*) (see Figure 4.3). It was estimated that emissions from the United Kingdom of Great Britain and Northern Ireland, Ireland, Germany, France, Belgium, Luxemburg and the Netherlands were approximately 2.2 Gg yr^{-1} (2008–2017 mean). The TEAP/UNEP (2019*b*) results support the qualitative finding by Rigby et al. (2019) of a gradual

emission decline. However, without uncertainty estimates, the statistical significance of this trend cannot be established.

4.3 REGIONAL EMISSION ESTIMATES FOR RELATED SPECIES

As noted in section 3.4, production of CFC-11 has been associated with the use of CCl_4 as a feedstock and the co-production of CFC-12. Changes in regional emissions of these substances therefore have the potential to provide further information on the processes responsible for the increase in CFC-11 emissions.

Based on data from Gosan, Republic of Korea, Park et al. (2021) inferred emissions of CCl_4 and CFC-12 from Eastern China. For CCl_4, their results supported an earlier finding by Lunt et al. (2018) that emissions from Eastern China had increased after 2012, growing from 6.0 ± 1.4 Gg yr^{-1} for 2011–2012 to 10.9 ± 2.0 Gg yr^{-1} for 2014–2017. While they caution that CCl_4 emissions are now known to originate from a wide range of industrial sources, making attribution to a single process difficult (e.g., Liang et al., 2016; Sherry et al., 2017), such an increase could indicate increased use of CCl_4 as a feedstock in CFC-11 production. In around 2017, emissions from this region declined again, returning to 6.2 ± 1.4 Gg yr^{-1} in 2018–2019.

For CFC-12, Park et al. (2021) supported earlier qualitative findings by Rigby et al. (2019) that emissions from Eastern China had not increased after 2012 and had in fact remained close to 3.0 ± 1.2 Gg yr^{-1} (2011–2012 mean) until 2016. However, Park et al. (2021) found that CFC-12 emissions had declined drastically after 2016, reaching levels indistinguishable from zero during the period 2017–2019 (0.8 ± 0.9 Gg yr^{-1}). The authors posited that these trends could be the result of increasing CFC-11 production–related emissions offsetting declining emissions from CFC-12 banks between 2012 and 2016. The subsequent decline could then have been a result of a drop in CFC-11 production in around 2016. Taken together, the trends of CFC-12 and CCl_4 emissions from Eastern China may be consistent with unreported CFC-11 production occurring in this region, with emissions of both substances increasing substantially after 2012, but then declining from 2016 (CFC-12) or 2017 (CCl_4), that is, 1–2 years before the CFC-11 emission decline.

Like for CFC-11, no substantial upward emission trend has been reported for regions outside of China for CCl_4 or CFC-12, though few studies are available for recent years. Graziosi et al. (2016) found gradually declining emissions of CCl_4 for Europe up to 2014, which they attributed primarily to industrial sources such as chlor-alkali plants (drawing similar conclusions to a study in the United States by Hu et al. (2016) that covered earlier years). Hu et al. (2017) found that CFC-12 emissions from the United States had declined between 2008 and 2014, similar to bottom-up estimates by the U.S. Environmental Protection Agency.

_____

5. CFC-11 SCENARIOS AND SENSITIVITY CASES

Future CFC-11 abundance and its effect on the ozone layer are determined by potential future CFC-11 production, the amount banked in equipment or landfills, and the recovery or destruction of CFC-11 from banks. The effects of these on the EESC, CO_2-equivalent (CO_2-eq) emissions and radiative forcing are discussed using scenarios and sensitivity analyses. The effects on stratospheric ozone of different scenarios are discussed in section 6.

Main points:

- Estimates of the amount of CFC-11 contained in banks (mainly in foams) are uncertain. A bottom-up estimate has an upper limit of 1 475 Gg (7.6 Gt CO_2-eq) for 2018 (TEAP/UNEP, 2019*b*), while an analysis that uses both top-down and bottom-up information shows a bank range of 878–2 264 Gt (4.5–11.7 Gt CO_2-eq) (95% confidence interval) for 2018 (Lickley et al., 2020). Both estimates exclude the effect on banks of any unexpected production starting in 2012.

- Importantly, there is a difference in measured emission rates from banked CFC-11 in foams during use and decommissioning compared with the observed atmospheric emissions globally and in regions where there is high confidence that production has not resumed. Scenarios that include decommissioning compensate for this incongruity temporarily, but they do not eliminate this inconsistency in the long term. Although the estimated timing of releases from decommissioning foams containing CFC-11 can be shifted, doing so does not address this difference in emission rates in the long term.

- The WMO (2018) CFC-11 baseline projection took into account the increased emissions up to 2016 and the subsequent drop in emissions in the years that followed. The increased CFC-11 emissions up to 2016 included direct emissions from production and products manufactured with CFC-11 and emissions from this new bank of unreported CFC-11. Montzka et al. (2021) reported a sharp decrease in emissions from 2018 to 2019. If this drop is taken into account in a scenario, the date at which EESC returns to 1980 values is close to the date under the WMO (2018) baseline scenario.

- In scenarios developed from emission models, assuming complete future compliance with the Montreal Protocol, CFC-11 atmospheric concentrations are projected to continue decreasing. However, if new production occurs after phaseout in the future, the date at which EESC returns to 1980 values could be delayed by a few years.

- CFC-11 contributes up to 3–4 cumulative Gt CO_2-eq emissions between 2020 and 2060. Depending on the assumed rate of release from the banks, the additional emissions after 2012 are projected to add 0.3–1.0 cumulative Gt CO_2-eq emissions between 2020 and 2060.

5.1 SCENARIOS IN PREVIOUS ASSESSMENT REPORTS

In the Scientific Assessment Panel reports (WMO, 1999, 2003, 2007, 2011, 2014, 2018), a one-box model is used to project ODS emissions and mixing ratios and EESC levels (Daniel et al., 2007, 2011; Velders and Daniel, 2014). See Appendix C for details of how scenarios are constructed. The same approach is applied here (see the equations in Box 3.1).

The data sets and parameters used in the scenarios have various confidence levels. A high confidence level (low uncertainty) can be assigned to observed mixing ratios. A medium confidence level can be assigned to reported production data and the atmospheric lifetime and consequently also to the emissions inferred from observed mixing ratios. A low confidence level is assigned to the emission factor and bank sizes. Since the emission factor and bank

sizes are anti-correlated because of how they are derived, there is a moderate level of confidence in emission projections. Potential unreported production and the rate of release from use and banks add to the low level of confidence of projections of emissions.

The specifics of the data used for CFC-11 emissions have varied in the past five ozone assessment reports (see Table 5.1). The estimated atmospheric lifetime of CFC-11 changed from 45 years (WMO, 2011) to 52 years (WMO, 2014), resulting in a lower inferred historical emission rate to the atmosphere. With the 2008 bank size unchanged, this affects (lowers) the derived emission factor. Through this emission factor, the projected emissions and banks after 2008 are affected as well, with the projected bank size increasing and the emissions initially decreasing strongly because of the lower emission factor, then decreasing more moderately because of the larger bank size. The importance of a good estimate of the bank size increased after production of CFC-11 was thought to have ceased.

The changes in parameters result in different projected CFC-11 emissions and mixing ratios in the past five ozone assessment reports (Figure 5.1). The black line, corresponding to the WMO (2018) assessment, shows the true historical emissions from 1980 to 2016, as inferred from observations. Clearly the other projections all underestimated the historical emissions in the period 2012–2016. The historical emissions are changed because they are inferred from new updates to observed mixing ratios in each assessment, as is clearly visible by the increased emissions for 2012–2016 in WMO (2018). The lowest projected emissions and mixing ratios are found in WMO (2003) and are associated with the shortest lifetime and largest emission factor. The sudden decrease in emissions in 2005 seen in WMO (2007), at the transition from historical to projected emissions, is caused by the small emission factor, which was estimated based on a reported bank in 2002 and a projected bank in 2015 in IPCC/TEAP (2005). The projected CFC-11 emissions of the last four ozone assessment reports are rather similar after 2020. The differences in emissions are directly reflected in different projected mixing ratios, which range from 131 to 169 ppt in 2040.

Table 5.1. Information and data used in the CFC-11 scenarios in past ozone assessment reports (WMO, 2003, 2007, 2011, 2014, 2018)

	Production	*Bank*	*Bank size 2018 (Gg)*	*Emission factor*	*Based on observations during these years*	*Lifetime (y)*
WMO (2003)	Emissions from AFEAS, McCulloch	AFEAS[a]	112	12.0%	1986–1999	45
WMO (2007)	1986–2004: UNEP[b] 2005–2009: MP phaseout from 2010: zero	2002: 1 687 Gg (IPCC/TEAP, 2005)	996	3.3%	1979–2005	45
WMO (2011)	1986–2008: UNEP 2009–2010: essential use exemptions only from 2011: zero	2008: 1 420 Gg (TEAP/UNEP, 2009)	847	5.0%	1979–2009	45
WMO (2014)	1986–2009: UNEP from 2010: zero	2008: 1 420 Gg (TEAP/UNEP, 2009)	912	4.2%	1980–2013	52
WMO (2018)	1986–2009: UNEP from 2010: zero	2008: 1 420 Gg (TEAP/UNEP, 2009)	788	6.0%	1980–2017	52

[a] AFEAS was the Alternative Fluorocarbons Environmental Acceptability Study, established in 1989.
[b] United Nations Environment Programme

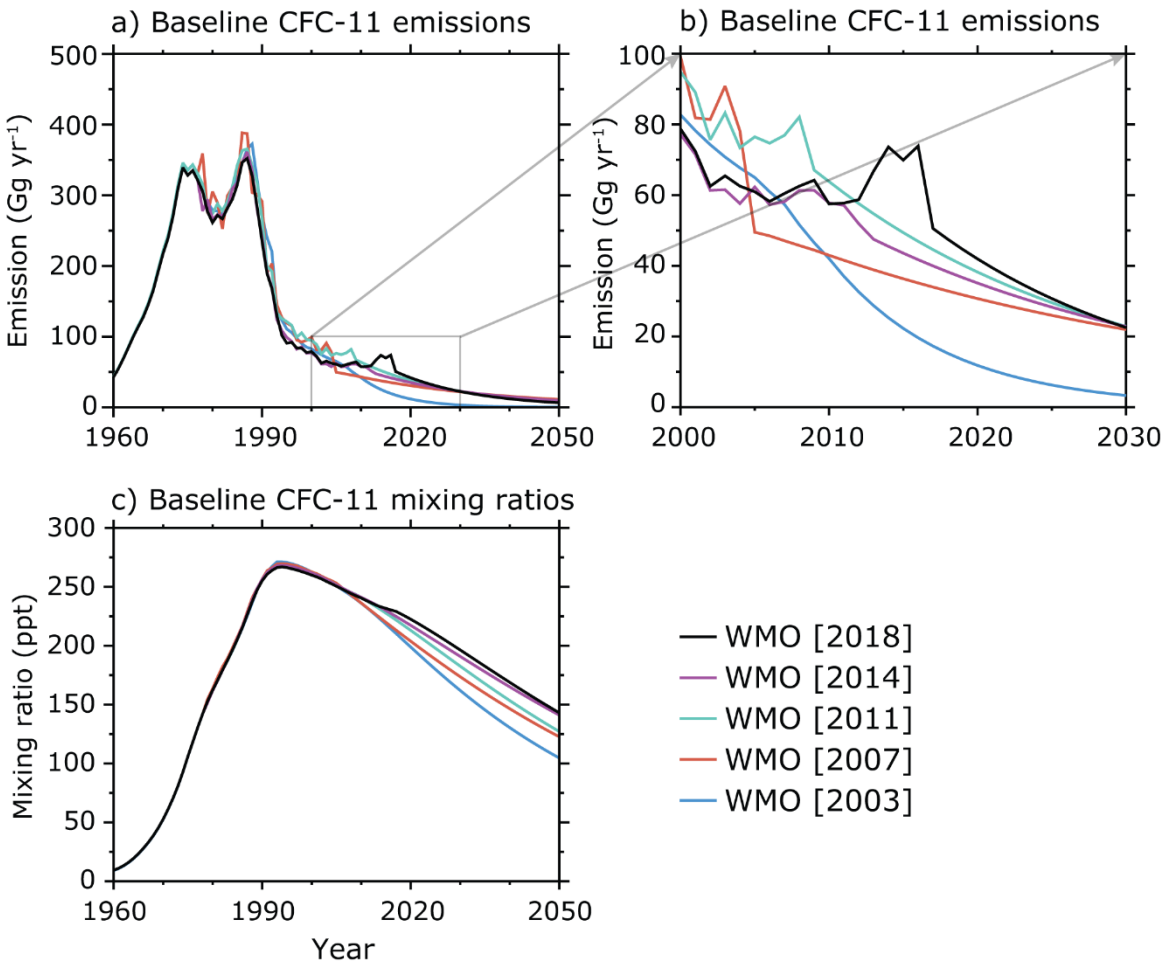

Figure 5.1. (a) Global CFC-11 emissions in the baseline scenario of past ozone assessments. (b) Detail for the period 2000–2030. The historical emissions were inferred from the available observed mixing ratios (section 2). This means that for the baseline scenario in WMO (2018), the emissions from 1980 to 2016 are inferred from observations from 1980 to 2017 (see Table 5.1). The emissions after 2016 are based on projections. The emissions of four of the five projections coincidentally converge in around 2030 and diverge again after that. Higher emissions before 2030 deplete the bank faster, resulting in lower emissions later on, and vice versa. (c) Corresponding global average mixing ratios.

In the reports of the Technology and Economic Assessment Panel/United Nations Environment Programme (TEAP/UNEP) CFC-Task Force, ODS emission scenarios and sensitivity analyses are constructed differently, using a bottom-up approach. TEAP/UNEP (2019*b*) scenarios use production and market-consumption data from industry reporting; country-specific production and consumption data reported to UNEP; estimates of sales of newly produced ODSs into multiple markets (use sectors); estimates of ODS release at different stages of the ODS lifecycle in various sectors; and projections of future demand, consumption and production for ODS. Total global emissions are emission sums from different sectors and regions. CFC-11 emission details from different sectors and for different products in different regions are

included in TEAP/UNEP (2019*b*).

The tasks carried out by the TEAP/UNEP Task Force (2019*b*) included:

- Considering a broad range of variables, including higher and lower emissions than found in the literature and higher and lower production rates than reported by the Alternative Fluorocarbons Environmental Acceptability Study (AFEAS) to the Ozone Secretariat.

- Exploring combinations of these variables as well as the use of CFC-11 in various product sectors. Although the task force eliminated a significant number of scenarios for specific technical and economic reasons, it retained four selected from the full range of scenario types that it evaluated (low, medium, high, and most likely). The low and high cases were outside the range of reasonableness based on technical and economic factors noted in the TEAP reports.

- Exploring lifetimes and banks for products and equipment that would have historically contained or used CFC-11. The task force found that the significant majority of the remaining bank was likely to be in closed cell foam, in situ, in accessible (foams in buildings) or inaccessible (foams in landfills) banks in North America and Europe, where the overwhelming majority of CFC-11 was sold and used.

- Estimating that 94% of the reported CFC-11 produced was used by non-Article 5 countries.

- Exploring possible uses of newly produced CFC-11 and concluded that it was probably for the manufacture of closed cell foams. It excluded all other product sectors as likely uses of newly produced CFC-11 based on specific technical and economic factors discussed in both of the 2019 TEAP/UNEP Task Force reports (TEAP/UNEP 2019*a*, 2019*b*). Even the fairly recent 2006 Foam Technical Options Committee (FTOC) Assessment report found that more than 70% of polyurethane closed cell foam was produced in the United States, Western Europe and Japan.

- Identifying a disparity between the bank emission rates derived from atmospheric concentrations (approximately 3%) and those reported in product literature from in situ closed cell foams (less than 1.5%), such as from the Intergovernmental Panel on Climate Change. These release rates are determined to a large extent by toxicity testing used to determine safe re-entry times into buildings using spray foams and based on the longevity of the devices (e.g., cooling equipment) or foam insulation in buildings. Emissions temporarily increase during the decommissioning and transition of foams from "in use" to a landfill.

5.2 CFC-11 SCENARIOS AND SENSITIVITY CASES

Projections of CFC-11 emissions in WMO ozone assessment reports have depended on projections of production, the historical bank size and the emission factor (see Figure C.1). The 2008 bank size – the most recent bank estimate – has played an important role in emissions projections of the ozone assessments, since CFC production allowed under the Montreal Protocol is very small and has been reduced to virtually zero since 2010, with only limited essential use exemptions for dispersive uses. The emission factor used in the projections also depends on the estimated bank, since it is derived from the top-down inferred emissions and the size of the bank (see section 5.1). The 2008 bank has been used as constraint and the bank sizes for subsequent years have been derived from it.

As shown by Montzka et al. (2018) and in sections 3 and 4, the emission increases since 2012, as inferred from atmospheric observations, cannot be explained by the global production reported to UNEP and the bottom-up bank estimates, which are anchored in the 2008 bank estimate from TEAP/UNEP (2009). Sensitivity calculations have been performed here to test the effects on the emission projections of uncertainties in the projections of production, in the 2008 bank size, and in the rate of release from banks (emission factor) (TEAP/UNEP, 2019*b*). The same box model and atmospheric lifetime is used as in the 2018 ozone assessment (WMO, 2018). Two scenarios are used as a reference: 1) the A1 baseline scenario of WMO (2018) and 2) the "most likely" scenario of TEAP/UNEP (2019*b*), with specific emission factors for various applications and different stages in the life cycle (see Table 5.2 and Figure 5.2).

5.2.1 Effects on EESC return dates

In WMO (2018), the A1 baseline scenario EESC returns to the 1980 values in 2049 for mid-latitudes and 2076 for the Antarctic (see Table 5.2). In this scenario, the increased CFC-11 emissions until 2016 are taken into account, but beyond 2016 the emissions follow the projection and drop sharply following the projection (see section 5.1 and Appendix C). Montzka et al. (2021) reported that the increase in emissions ceased in 2018 then dropped sharply in 2019 to about 52 Gg yr^{-1}, a level similar to the 2008–2012 average. In the WMO (2018) "A1 baseline scenario", the 2019 emission was slightly lower than that, at 45 Gg yr^{-1}. A CFC-11 scenario taking into account the increased emissions until 2018 and the drop in 2019 yields similar results to those obtained with the WMO (2018) A1 baseline scenario. If, on the other hand, CFC-11 emissions had remained constant at 67 Gg yr^{-1} starting in 2017, the year at which EESC returns to its 1980 value would be delayed by 7 years for mid-latitudes and 20 years for the Antarctic (see Figure 5.3) (WMO, 2018). Section 6 addresses the impact of these EESC increases and other scenarios of cumulative CFC-11 emissions on ozone recovery.

Table 5.2. Comparison of CFC-11 scenarios for the year in which EESC drops below the 1980 value (mid-latitude and Antarctic conditions), difference in integrated EESC relative to a reference scenario from WMO (2018) or TEAP/UNEP (2019*b*), and changes in integrated ozone depletion potential-weighted emissions and global warming potential-weighted emissions

Scenario and cases	*Per cent difference in integrated EESC relative to the A1 baseline scenario: mid-latitude*		*Year when EESC is expected to drop below 1980 value*		*Change in cumulative ODP-weighted emission: 2020–2060*	*Change in cumulative GWP-weighted emission: 2020–2060*
	$\sqrt{\int_{1980}^{x} EESC \ dt}$	$\sqrt{\int_{2020}^{x} EESC \ dt}$	*Mid-latitude*	*Antarctic vortex*	*million tons CFC-11-eq*	*billion tons CO_2-eq*
WMO (2018) Scenarios						
A1 baseline scenario[a]	0.0	0.0	2049.4	2076	0.00	0.0
CFC-11 emissions (Montzka et al., 2021)[b]	0.1	0.6	2049.4	2076	−0.05	−0.3
Constant 67 Gg yr^{-1}	4.0	17.1	2056.7	2097	2.04	10.5
No unexpected CFC-11 emissions[c]	−1.7	−6.5	2048.7	2076	0.06	0.3
Larger bank[d]	−0.6 to 2.4	−2.8 to 10.2	2049.0 to 2052.4	2076 to 2080	−0.05 to 0.82	−0.3 to 4.2
TEAP/UNEP [2019*b*] Scenarios [e]						
Most likely scenario[f]	0.0	0.0	2047.9	2075	0.00	0.0
High-low range	−0.5 to 0.1	−2.4 to 0.3	2047.3 to 2048.0	2074 to 2075	−0.23 to 0.03	−1.2 to 0.1
Additional CFC-11 production[g]	0.6	2.7	2048.7	2076	0.20	1.0
Destruction of active bank in 2020	−0.2	−0.7	2047.8	2075	−0.05	−0.3
Destruction of inactive bank in 2020	−0.5	−2.2	2047.3	2074	−0.25	−1.3

[a] The WMO (2018) scenarios below are compared with the WMO (2018) A1 baseline scenario, which includes emissions from additional 2012–2016 production. Cumulative 2020–2060 emissions are 0.64 Mt CFC-11-eq and 3.3 Gt CO_2-eq. The EESC is calculated using the same method as in WMO (2018).

[b] Scenario based on the A1 baseline scenario, but with 2017–2019 emissions reported by Montzka et al. (2021).

[c] Scenario starting in 2008 with a bank of 1 420 Gg, as in the A1 baseline scenario, a constant emission factor of 3.2% yr^{-1} (Montzka et al., 2018), and no additional production or emissions after 2007.

[d] The larger 2008 bank of 1 417–2 666 Gg (95% confidence range) from Lickley et al. (2020) is used, with an emission factor of 3.8% derived as the ratio of the top-down emission over the bank, averaged over 2010–2016. This emission factor is somewhat larger than the 2.85% derived by Lickley et al. (2020).

[e] In the EESC calculations, the emissions of the TEAP/UNEP (2019*b*) scenario are used only for the projection for 2017–2100. The WMO (2018) A1 baseline scenario emissions are used for 1950–2016.

[f] The TEAP/UNEP (2019*b*) scenarios below are compared with the TEAP/UNEP (2019*b*) "most likely" scenario. Cumulative 2020–2060 emissions are 0.30 Mt CFC-11-eq and 1.6 Gt CO_2-eq.

[g] Additional production of 30 Gg yr^{-1} for 2007–2011 and 100 Gg yr^{-1} for 2012–2016, on top of the TEAP/UNEP (2019*b*) "most likely" scenario, to match the top-down derived emissions.

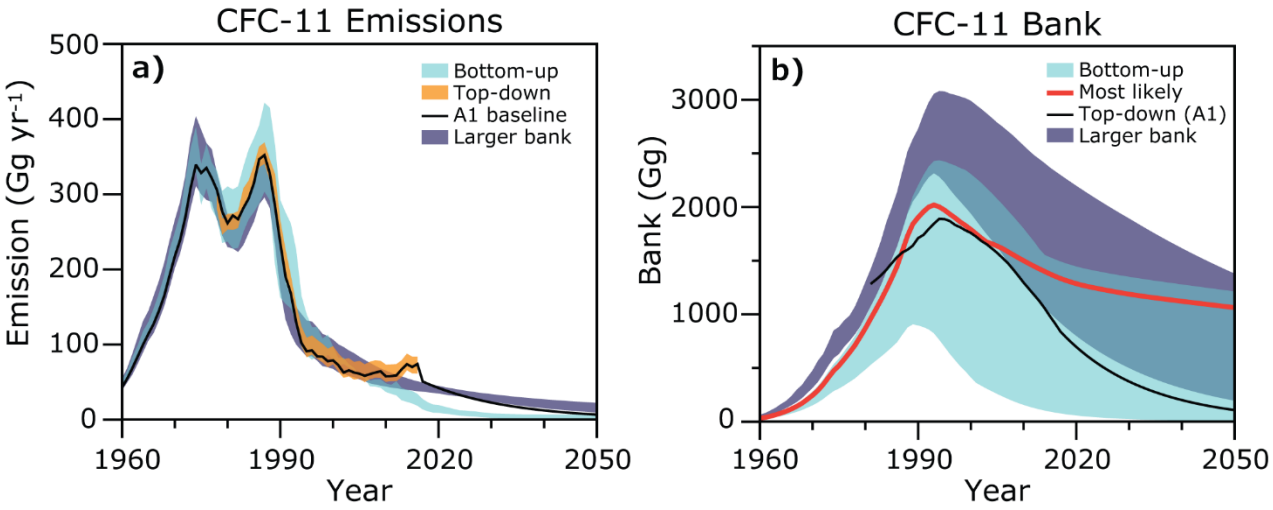

Figure 5.2. Range of global average CFC-11 emissions (a) and bank size (b) from the TEAP/UNEP (2019*b*) bottom-up model (cyan), with emissions derived top-down from atmospheric observations (orange) (WMO, 2018), and emissions based on analyses of the "larger bank" from Lickley et al. (2020) (purple). Also shown are the values from the A1 baseline scenario (black lines) (WMO, 2018).

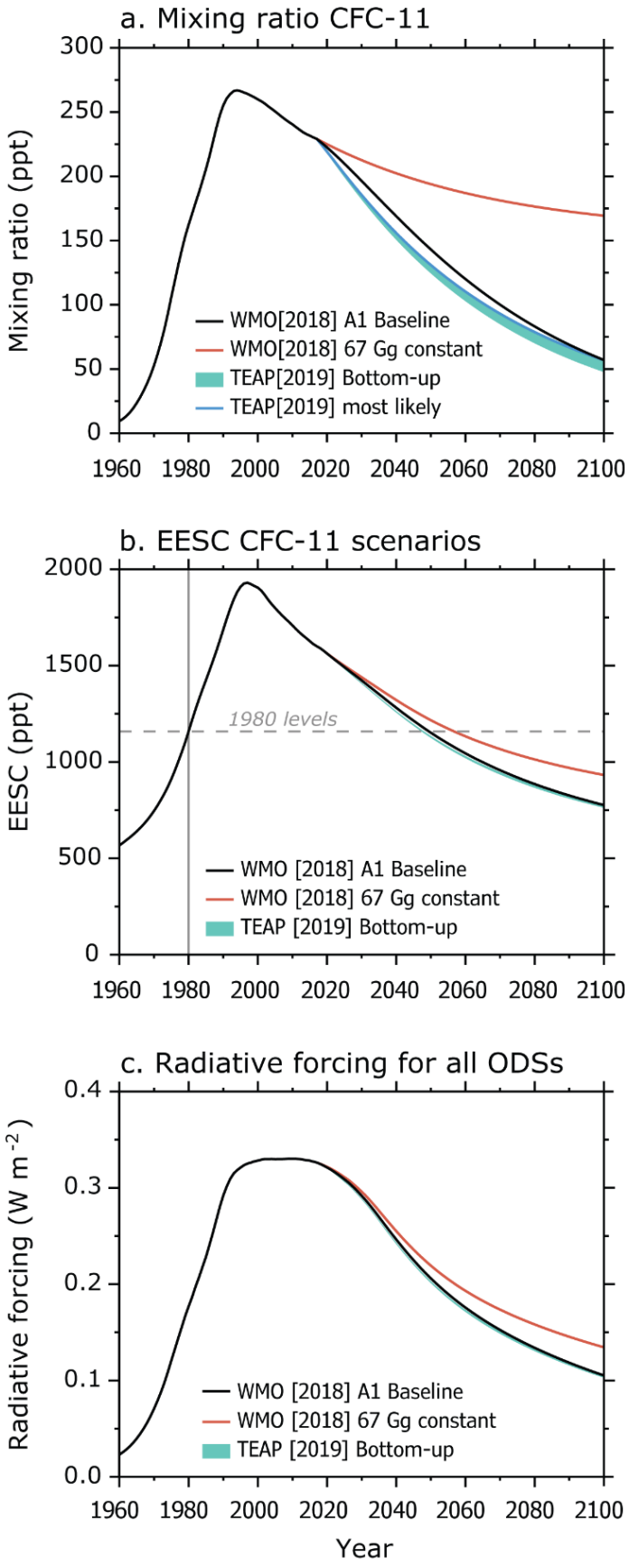

Figure 5.3. (a) Projected CFC-11 mixing ratios, (b) EESC, and (c) radiative forcing for the range of scenarios described in the text. In the EESC panel, the 1980 value is shown as a dashed line.

To estimate the effect of only the additional unexpected emissions needed to explain the top-down inferred emissions (Montzka et al., 2018), the A1 baseline scenario containing these emissions from 2008 to 2016 is compared with a scenario without these additional emissions (the "No unexpected CFC–11 emissions" scenario in Table 5.2). The latter scenario starts in 2008 with a bank of 1 420 Gg, as is the case in the A1 baseline scenario, and it uses a constant emission factor of 3.2% yr^{-1}, as derived by Montzka et al. (2018) for 2002–2006, as opposed to the 6.0% yr^{-1} factor in the original A1 baseline scenario. This yields a bank of 1 028 Gg in 2018, 240 Gg above the A1 baseline scenario bank, while cumulative emissions until 2017 are reduced by the same amount (240 Gg). As a result of the additional emissions needed to match the top-down inferred emissions, the year at which EESC returns to 1980 values is delayed by 0.7 years for mid-latitudes. This scenario only includes the extra emissions from 2008 to 2017 and does not take into account the larger bank and associated emissions after 2017.

Lickley et al. (2020) estimate the CFC-11 bank using a Bayesian probabilistic model for the total banks and their emissions, applying a broad range of constraints. Their analysis uses both bottom-up and top-down information and estimates that total CFC-11 production is 13% larger than production reported through AFEAS and to the Ozone Secretariat, and that the resulting total CFC-11 bank sizes are larger than used in recent WMO ozone assessments. This bank accounts for much of current estimated CFC-11 emissions, but not for the observed unexpected CFC-11 emissions increase after 2012 (see Figures 5.2 and 3.2). The 2008 median bank size is 2 063 Gg (95% confidence interval from 1 417 to 2 666 Gg), compared with 1 420 Gg in WMO (2018). The estimated size of the 2018 bank is 878–2 264 Gg. Using this larger bank range, the return of EESC to its 1980 values changed by −0.4 to +3.0 years for mid-latitudes and by 0.0 to 4.2 years for the Antarctic compared with the A1 baseline scenario in WMO (2018) (the "larger bank" scenario in Table 5.2). They also found larger total bank sizes for CFC-12, but the underestimates were much smaller than for CFC-11 (see Appendix D). The effect of emissions from these larger estimated banks could delay Antarctic ozone-hole recovery by about 6 years (see section 6), assuming no additional production.

In TEAP/UNEP (2019*b*), a bottom-up model is used to derive a "most likely" scenario for CFC-11 emissions using specific emission factors for the average life cycle stages of CFC-11 products. Emissions are lower than those in the A1 baseline scenario and cannot explain the top-down inferred emissions past about 2007 (see Figures 5.2 and 3.2). TEAP/UNEP (2019*b*) presents a range of bottom-up scenarios with low, medium and high emission factors, with the emission factors used in the "most likely" scenario situated between the low and high scenarios. The emission range in these scenarios is limited, but the range in corresponding bank sizes in these scenarios is much larger. Low emission factors result in a large estimated bank size. The emissions themselves are not very sensitive to the emission factors, since the emissions are the product of the bank sizes and the emission factors. The TEAP/UNEP (2019*b*) CFC-11 bank ranges from 70 to 1 475 Gg for 2018, but the lower range was considered outside the range of realistic values. The 13% higher production modelled by Lickley et al. (2020) was also estimated as an unlikely scenario in TEAP/UNEP (2019*b*). See also section 3.1 for a discussion on the uncertainty of the bottom-up inventory.

Mixing ratios calculated using the TEAP/UNEP (2019*b*) emission scenarios, a box model and a fixed atmospheric lifetime of 52 years deviate significantly from observed mixing ratios. Since a useful projection of CFC-11 mixing ratios and EESC values requires the observed mixing ratios to be closely reproduced, the TEAP/UNEP (2019*b*) emission scenarios cannot be used directly. Instead, the WMO (2018) A1 baseline scenario is used for 1950–2016 and the TEAP/UNEP (2019*b*) emission scenarios are used for 2017–2100. The calculated mixing ratios up to 2016 then agree with the observed mixing ratios, as in the A1 baseline scenario (Figure 5.3). Using a box model, the TEAP/UNEP (2019*b*) scenario results in only a limited range in the year that EESC returns to 1980 values: about a 0.7-year range for mid-latitudes and about a 1.5-year range for the Antarctic ("high-low range" in Table 5.2).

The top-down inferred emissions can also be approximately met using the TEAP/UNEP (2019*b*) "most likely" scenario, with additional production of 30 Gg yr^{-1} for 2007–2011 and 100 Gg yr^{-1}

for 2012–2016. This yields additional cumulative emissions of 263 Gg for 2017–2100. Additional production of 100 Gg yr^{-1} is equal to about 25% of the peak CFC-11 global production at the end of the 1980s. In this scenario, with no unreported production after 2016, EESC returns to 1980 values about 0.8 years later for mid-latitudes compared with the TEAP/UNEP (2019*b*) "most likely" scenario. This scenario differs somewhat from the WMO (2018) A1 baseline scenario because of the much smaller emission factor, which is effectively less than 2%, compared with 6% in the A1 baseline scenario.

The TEAP/UNEP (2019*b*) banks and emissions in the bottom-up model are divided into active banks and inactive banks. Active banks are CFCs in situ during a product's lifetime, such as CFC-11 in use in foams or as refrigerant. Inactive banks are CFCs at the end of the product's lifetime, when the product is landfilled. Due to average lifetimes of appliances and buildings assumed in the simplified global inventory model, after around 2017 the total CFC-11 banks are dominated by inactive banks, i.e. closed cell foams in landfills[5] (see also the long tail in Figure 5.2). A hypothetical case with a complete recovery and destruction of the 2020 inactive banks would bring the year at which EESC returns to the 1980 value forward by about 0.7 years for mid-latitudes (Table 5.2). Similarly, a complete recovery and destruction of the 2020 active banks would bring the year at which EESC returns to the 1980 value forward by about 0.2 years for mid-latitudes. These values are based on the TEAP/UNEP (2019*b*) "most likely" scenario and do not include the extra CFC-11 production and emissions after 2012, as in the WMO (2018) A1 baseline scenario, or a much larger bank, as estimated by Lickley et al. (2020). The uncertainty in these numbers depends directly on the uncertainty in the bank estimates.

5.2.2 Effects on radiative forcing of climate

These new scenarios result in additional CFC-11 contributions to climate forcing. The CFC-11 effects on climate are expressed in terms of the GWP-weighted cumulative emissions and the radiative forcing (see Table 5.2 and Figure 5.3). The CFC-11 contribution to radiative forcing in 2100 is about 0.015 W m^{-2}. In the hypothetical scenario that emissions are constant at 67 Gg yr^{-1} starting in 2017, the contribution will increase to 0.029 W m^{-2} by 2100. For all other scenarios, the change in radiative forcing is 0.0024 W m^{-2} or less in 2100. This can be compared with the total hydrofluorocarbon (HFC) radiative forcing of about 0.08 W m^{-2} in 2100, assuming full compliance with the Kigali Amendment (WMO, 2018).

CFC-11 contributes up to 3–4 cumulative Gt CO_2-eq emissions between 2020 and 2060 in the absence of the unexpected emission increase. Depending on the assumed release rate from the banks, the additional 2012–2016 emissions from the increased banks are projected to add 0.3–1.0 cumulative Gt CO_2-eq emissions between 2020 and 2060. Constant CFC-11 emissions at 67 Gg yr^{-1} will yield an additional cumulative emission of 11 Gt CO_2-eq between 2020 and 2060 and 24 Gt CO_2-eq between 2020 and 2100. In comparison, cumulative HFC emissions under the Kigali Amendment (excluding HFC-23 (fluoroform)) are calculated to be 62–63 Gt CO_2-eq between 2020 and 2060 and 88–90 Gt CO_2-eq between 2020 and 2100 (WMO, 2018).

The recovery and destruction of CFC-11 banks would not only accelerate the ozone layer recovery, but also yield climate benefits. Based on the TEAP/UNEP (2019*b*) scenario, recovery and destruction of the active and inactive banks would reduce emissions by 1.6 Gt CO_2-eq between 2020 and 2060 and by 2.6 Gt CO_2-eq between 2020 and 2100 (see Table 5.2).Using their much larger banks, Lickley et al. (2020) estimated that recovery and destruction of the CFC-11 and CFC-12 banks would reduce emissions by 9 Gt CO_2-eq between 2020 and 2100.

---

[5] TEAP has also developed a regional build-up of CFC-11 in various types of foams with unique average lifetimes, but this more complex model was not used for the global estimate in 2019.

6. MODELLED IMPACT ON THE STRATOSPHERIC OZONE LAYER

Main points:

- The cumulative unexpected emission enhancements during 2012–2019, of between 120 and 440 Gg (see section 3), will have only a small impact on the ozone layer, consistent with the small perturbation to stratospheric chlorine loading of 15–57 ppt Cl. The emissions are estimated to lead to a decrease in mean global column ozone of less than 0.3 DU and an additional September Antarctic ozone loss of less than 2.5 DU. Ozone recovery will be delayed and 1980 return dates extended by up to 0.4–1.3 years globally and 0.5–3.1 years for the Antarctic ozone hole.

- A return to emissions of CFC-11 at the elevated 2014–2017 level would cause additional depletion of stratospheric ozone and lead to a delay in its recovery. The magnitude of the impact varies with region and scales with the total additional emissions. Globally, column ozone is decreased by 0.4–0.7 DU and 1980 return dates are delayed by 3 years under the large scenario of 1 000 Gg of cumulative emissions (see also section 5). For the Antarctic, models show a near-linear decrease of 5 DU in springtime column ozone and a delay of 4–7 years for September 1980 return dates per 1 000 Gg of cumulative CFC-11 emissions.

- In addition, co-production and emissions of other Cl-containing gases (e.g., CFC-12, CCl_4, CFC-113 ($C_2Cl_3F_3$) (Lickley et al., 2020), HCFCs (Vollmer et al., 2020); see also previous sections) would increase the delay in ozone recovery. The impact will roughly scale with the amount of Cl released from any source, so results shown here for CFC-11 can provide a guideline.

- Atmospheric models are tools to understand and quantify the past, current and future response of stratospheric ozone to changes in atmospheric ODS concentrations. ODSs cause ozone depletion by releasing chlorine and bromine into the stratosphere. In particular, chlorine plays a major role in catalysing ozone depletion in the upper stratosphere and the springtime polar lower stratosphere, e.g., the Antarctic ozone hole. It is therefore in these regions that additional CFC-11 emissions would be expected to enhance ozone depletion and delay recovery most significantly. Additional emissions of other ODSs that release chlorine would have similar impacts to CFC-11 on the ozone layer; the overall effect of any such co-emitted gas is most simply analysed by considering the impact on total chlorine loading.

Any model projection of the future state of the ozone layer, and of ozone recovery in particular, using new CFC-11 emission estimates also depends on the assumed scenarios of the major greenhouse gases (GHGs) carbon dioxide (CO_2), methane (CH_4) and nitrous oxide (N_2O). Nevertheless, for any particular GHG scenario, additional CFC-11 production and consumption above controls will lead to larger chlorine concentrations in the atmosphere, depletion of ozone, and a delay in ozone return dates (see Figure 6.2, below). Furthermore, given that CFC-11 is also a GHG, an increase in radiative forcing with respect to the projections without these additional emissions will contribute to climate change. Since stratospheric chlorine–ozone chemistry is well established, the main uncertainty in modelling the future impact of additional CFC-11 emissions is probably the realism of the CFC-11 scenarios used in the simulations (see section 5).

This section summarizes the currently available knowledge of potential impacts that higher CFC-11 emissions would have on the ozone layer and quantifies the delay in recovery due to these emissions based mainly on recently published model results. As such, the scenarios used do not correspond necessarily to the most realistic estimates of current emissions or the most likely future scenarios (see section 5). Nevertheless, the model results can be scaled accordingly for other scenarios. Section 6.1 describes the models used. Section 6.2 discusses

the impact that the additional unexpected CFC-11 emissions identified so far may have already had. Sections 6.3 and 6.4 address the possible future impact of a range of CFC-11 emission scenarios on the ozone layer and its recovery timescale, taking into account that these projections now represent potential impacts that have been avoided due to the recent emission reductions described in sections 3 and 4.

6.1 MODELS AND SIMULATIONS

Chemistry climate models (CCMs) represent dynamical, radiative, and chemical processes in the Earth's atmosphere in three dimensions (3-D; longitude, latitude, altitude) in a self-consistent way, thus allowing the study of the physical climate and its coupling to chemistry (e.g., Morgenstern et al., 2017). Since internal climate variability in such CCM simulations is considerable, large multi-model ensembles are needed to be able to detect and quantify a small, externally forced signal. Chemical transport models (CTMs) (e.g., Chipperfield, 1999) use offline meteorological fields obtained from reanalyses to drive the model, rather than calculating the winds and temperature online. One advantage of this approach is that a signal resulting from, for example, a chemical perturbation can be easily isolated; the disadvantage is that it does not allow for interactions between the chemistry and a changing climate. A useful simplification of the full 3-D CCM is the two-dimensional (2-D; latitude, altitude) radiative–dynamical–chemical model. These models use a simpler method to deal with dynamics, but they allow many computationally inexpensive simulations aimed at exploring sensitivities to different coupled forcings, such as ODS and GHG emissions, volcanic aerosol and solar forcing.

A number of recent studies based on such models (the EMAC (ECHAM/MESSy Atmospheric Chemistry), UMUKCA-UCAM (University of Cambridge – United Kingdom Chemistry and Aerosol), and GEOSCCM (Goddard chemistry climate model) CCMs; the TOMCAT (Toulouse Off-line Model of Chemistry And Transport) CTM; and the GSFC (NASA Goddard Space Flight Center) 2-D model) have assessed different aspects of the impacts of increased CFC-11 emissions on stratospheric ozone in the current and future atmosphere under various assumed scenarios. These published studies used different assumptions for the CFC-11 emissions and also different future GHG scenarios. Therefore, while their simulations are not necessarily directly comparable or linked to scenarios developed in section 5, their results can be synthesized to derive some overall conclusions.

6.2 IMPACT OF INCREASED CFC-11 EMISSIONS ON CURRENT OZONE LEVELS

Dhomse et al. (2019) investigated the impact of the inferred recent additional CFC-11 emissions on ozone levels in the recent past. They used TOMCAT 3-D CTM simulations from 2000 onwards with and without additional CFC-11 emissions based on observations up to 2017 (Montzka et al., 2018). The two assumed scenarios resulted in additional CFC-11 emissions of around 230 Gg by 2017 (in line with the 2012–2019 estimate of 120-440 Gg over the 2012–2019 period in section 3.2). These emissions yielded atmospheric CFC-11 concentrations that differed by around 10 ppt (30 ppt Cl) (see Box 3.1), which is larger than the <10 ppt Cl implied by the additional emissions of 10-13 Gg yr^{-1} for 2014–2017. Nevertheless, the impact from these modelled increased levels of CFC-11 in the atmosphere on Antarctic and Arctic total ozone was found to be very small (and only discernible because of the specified circulation in the CTM, see section 6.1). As the additional CFC-11 emissions will have smaller effects outside the polar regions, it can be inferred that additional emissions of around 230 Gg or less over the past few years have not been responsible for a detectable decrease in global stratospheric ozone, based on the small impact on stratospheric chlorine loading (see Box 3.1). In particular, the additional CFC-11 emissions do not explain the reported lower-stratospheric decreases in ozone between 1998 and 2019 of up to 5%, especially in the equatorial region (Ball et al., 2018, 2019; Chipperfield et al., 2018).

In the following sections the results from available model simulations are used to derive the impact of a cumulative additional CFC-11 emission of 120–440 Gg over the 2012–2019 period, which is the current best estimate (see section 3.2).

6.3 IMPACT OF INCREASED FUTURE CFC-11 EMISSIONS ON OZONE LEVELS

Continued unexpected CFC-11 emissions would have the potential to increase stratospheric ozone depletion, with the impact varying in different atmospheric regions. In section 5, the impact of increased CFC-11 emissions on EESC was quantified for a range of possible emission scenarios. Using the available model studies that take into account potential chemical and dynamical feedback mechanisms (section 6.1), section 5 assessed the impact of additional chlorine on ozone globally, as well as in the two regions where chlorine-catalysed ozone loss is most important: the global upper stratosphere and the springtime polar lower stratosphere.

The impact on mean global column ozone has been estimated to be a depletion of between 0.4 and 0.7 DU per 1 000 Gg cumulative CFC-11 emissions, following a near-linear relationship (Keeble et al., 2020; Fleming et al., 2021). Based upon the cumulative additional CFC-11 emissions of 120-440 Gg in the 2012–2019 period (see section 3.2), a decrease in mean global column ozone of less than 0.3 DU is derived, which confirms the finding of a small impact on ozone for this emission estimate, as discussed in section 6.2.

In the upper stratosphere (at around 40 km), chlorine is highly effective at destroying ozone through the ClO + O catalytic cycle. For this region, based on the GSFC 2-D simulations, Fleming et al. (2020) calculate a change in ozone of −0.3% to −0.4% per 1 000 Gg cumulative increase in CFC-11 between 2017 and 2041. Overall, this is the expected feedback based on the well-established gas-phase chemistry, which is represented in all models.

Chlorine also plays a dominant role in springtime ozone depletion in the polar lower stratosphere through the ClO + ClO and ClO + BrO catalytic cycles. These cycles are enabled by heterogeneous reactions on polar stratospheric clouds. Additional emissions of chlorine-containing species will therefore enhance polar ozone depletion (see Figure 6.2) and delay recovery (see section 6.4).

Dhomse et al. (2019) used the TOMCAT CTM to investigate the impact of unexpected CFC-11 emission increases on Antarctic ozone recovery. While simulating a significant delay in Antarctic recovery for large continued CFC-11 emissions (section 6.4), they also noted a compact and near-linear variation in the amount of additional ozone destroyed with cumulative additional CFC-11 emissions (see Figure 6.1(a)). This compact linear relationship was maintained even for simulations with co-emission of CFC-12, once converted to equivalent CFC-11 emissions based on chlorine content. The curvature in Figures 6.1(a) and 6.1(b) is due to removal from the atmosphere of chlorine released from earlier emissions of CFC-11 (lifetime ~52 years), which reduces the ozone decrease for a given amount of cumulative CFC emissions. In one experiment in Figure 6.1(a), the additional emissions stop completely.

Additional models generally confirm that the linear relationship between CFC-11 cumulative emissions and total column ozone depletion also holds true for the Antarctic springtime. Figure 6.1 includes panels for the same analysis using the GSFC 2-D model (Fleming et al., 2020; their Figure 3) and the GEOSCCM (Fleming et al., 2021), EMAC (Dameris et al., 2019) and UMUKCA (Keeble et al., 2020) 3-D CCMs. The regression slopes of the 3-D CCMs are not as well defined as those for the CTM and 2-D model due to the much larger internal meteorological variability in the 3-D CCMs. Based on the various model results, the best-guess estimate is around 5.25 DU of additional ozone loss per 1 000 Gg of cumulative added CFC-11 emissions. Based on the 120–440 Gg additional cumulative CFC-11 emission for 2012–2019 period, the additional September Antarctic ozone loss is less than 2.5 DU, based on the upper estimate of the emissions and the sensitivities shown in Figure 6.1.

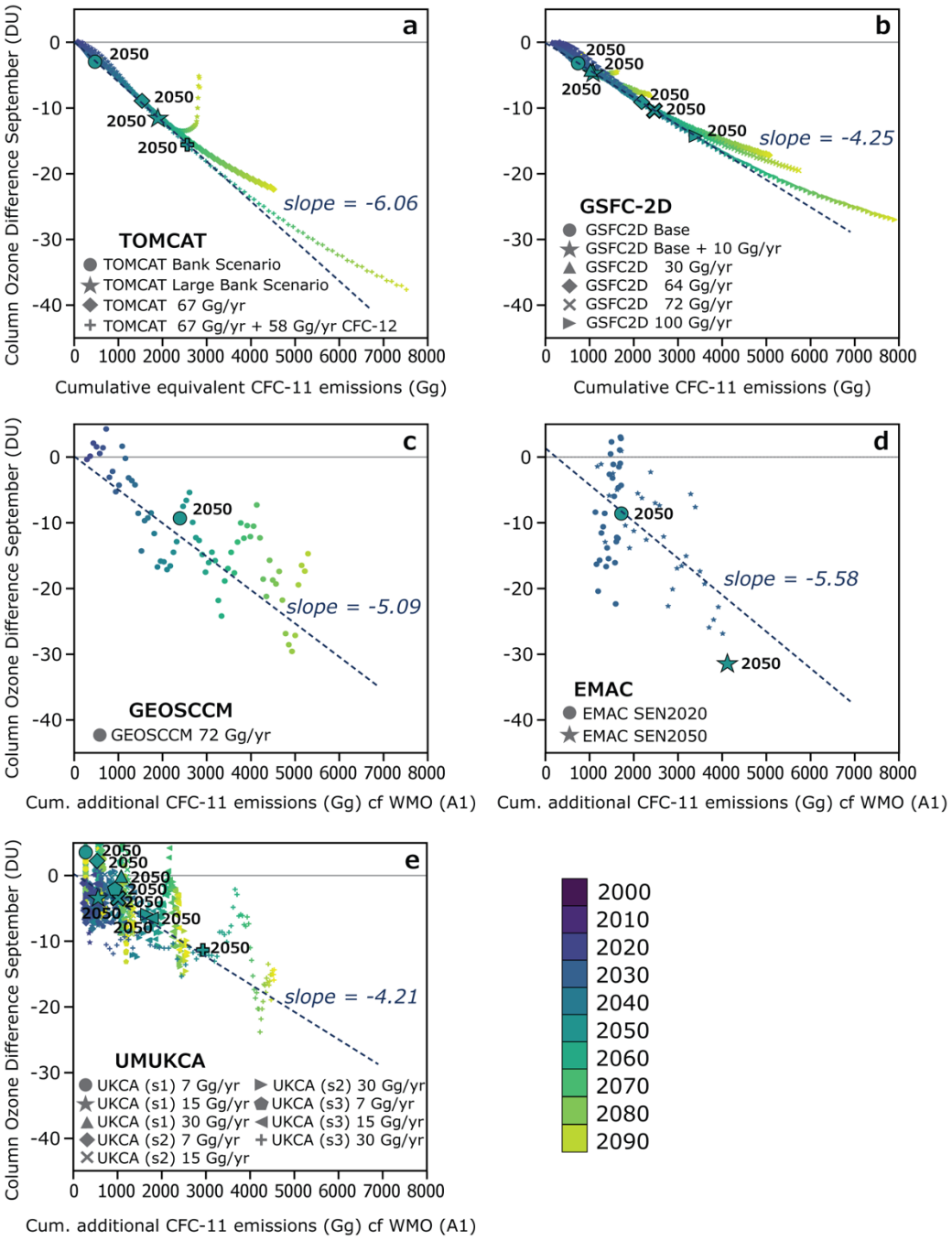

Figure 6.1. Decrease in the September mean Antarctic (65°S–90°S) column ozone (in DU) with cumulative additional (compared with the WMO (2018) A1 baseline) effective CFC-11 emissions (with different time variations denoted by the colours – see legend) as derived for five different models. For each simulation, the 2050 values are plotted with a larger symbol. The black dashed lines represent the linear best fit to the model data points in each panel (only the year 2050 points are used for TOMCAT and GSFC-2D), with numerical values of the slope in DU per 1 000 Gg. (Based on Figure 6(a) of Dhomse et al. (2019), with the addition of four other models.)

6.4 IMPLICATIONS FOR FUTURE OZONE RECOVERY

This section provides an assessment of the potential for additional future CFC-11 emissions to delay ozone recovery based on the available simulations, building on the preliminary estimates of WMO (2018) that were based solely on the GSFC-2D model. The results from the different

models are synthesized to deduce a more robust quantification of the CFC-11 impact, which can then be applied to other scenarios which may be developed (see section 5).

Ozone recovery, defined as a decrease in depletion from halogenated ODSs, is under way (Newchurch et al., 2003; Yang et al., 2006; Shepherd et al., 2014; Solomon et al., 2016; Chipperfield et al., 2017; WMO, 2018). A widely used recovery metric is the return of the ozone layer to 1980 values, the year when the ozone hole (defined as total column ozone values <220 DU) started appearing and global observations became routinely available. The concepts of ozone depletion, recovery and return dates are illustrated in Figure 6.2. Note that the rate and extent of ozone recovery will also depend on the future evolution of key GHGs such as CO_2, CH_4 and N_2O (WMO, 2018). In general, for a given GHG scenario, additional CFC-11 emissions lead to lower future ozone values relative to a scenario of compliance with the Montreal Protocol; this directly leads to a delay of the 1980 return date.

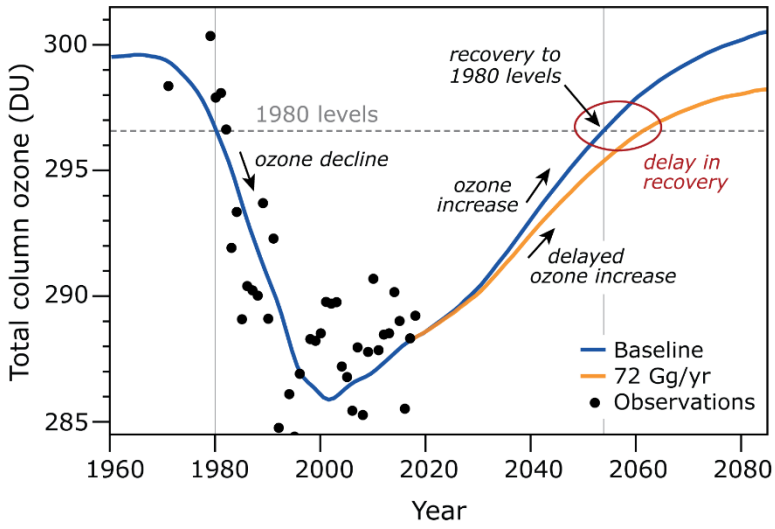

Figure 6.2. Schematic representation of ozone recovery and return dates based on global annual mean results from the GSFC 2-D model (Fleming et al., 2020). Black dots denote observations, illustrating large interannual variability, which complicates the definition of 1980 levels. The blue line shows results of a simulation using the WMO (2018) ODS scenario. Increased CFC-11 emissions at a constant 72 Gg yr^{-1} lead to cumulative additional CFC-11 emissions of around 2 600 Gg by 2060. The orange line shows the impact of these additional CFC-11 emissions: a delay in ozone recovery of around 7 years. See Figure 6.3 for quantification of this delay from a range of models.

Despite its wide use as a measure of ozone recovery from the effects of ODSs, the 1980 return date has a number of shortcomings, which must be borne in mind. First, significant depletion of the ozone layer occurred prior to 1980 (Shepherd et al., 2014; Langematz et al., 2016). Second, a change in the return date does not measure the overall integrated decrease in ozone prior to that date, which may be more relevant for the overall impact (e.g., changes in surface UV). Third, in certain atmospheric regions, ozone may not return to 1980 values before other factors (e.g., predicted circulation changes due to climate change) start to dominate changes in ozone levels, so it may not always be possible to define recovery by this measure. Finally, the ozone recovery curve shown in Figure 6.2 from the 2-D model is idealized and smooth. In practice (either in the real atmosphere or in more realistic 3-D CCMs) there is large inter-annual variability, which needs to be smoothed out to derive a return date in an averaged sense.

Simulations using the GSFC 2-D model reveal that recovery dates for different CFC-11 emission scenarios can vary substantially across different regions. Sustained emissions at 72 Gg yr^{-1} would, for example, shift the recovery date by 7 years for global ozone and 25 years for Antarctic ozone (Fleming et al., 2020). WMO (2018) reported that a similar scenario from this 2-D model (sustained emissions of 67 Gg yr^{-1}, see section 5) produced

similar delays. Using the UMUKCA CCM, Keeble et al. (2020) also note that the largest delay to recovery occurs in the Antarctic spring. This variation is likely due to the known impacts of climate change on ozone recovery, with the ozone return date diverging from the EESC return date (Shepherd, 2008) (section 5). This climate impact is small in the Antarctic spring but large (i.e. an earlier return date) in other regions.

Results from the available 2-D and 3-D models have been used to estimate the 1980 return dates for each separate simulation. This was done for the global annual mean ozone and for the Antarctic mean ozone in September, the month with the largest ozone loss rates. For the 3-D CCM simulations, for which there are no multi-member ensembles, the ozone time series needed significant smoothing in order for a mean return date to be extracted. These global and Antarctic return dates have been correlated against the cumulative additional CFC-11 emissions in each simulation compared with the WMO (2018) A1 reference ODS scenario (see Figure 6.3).

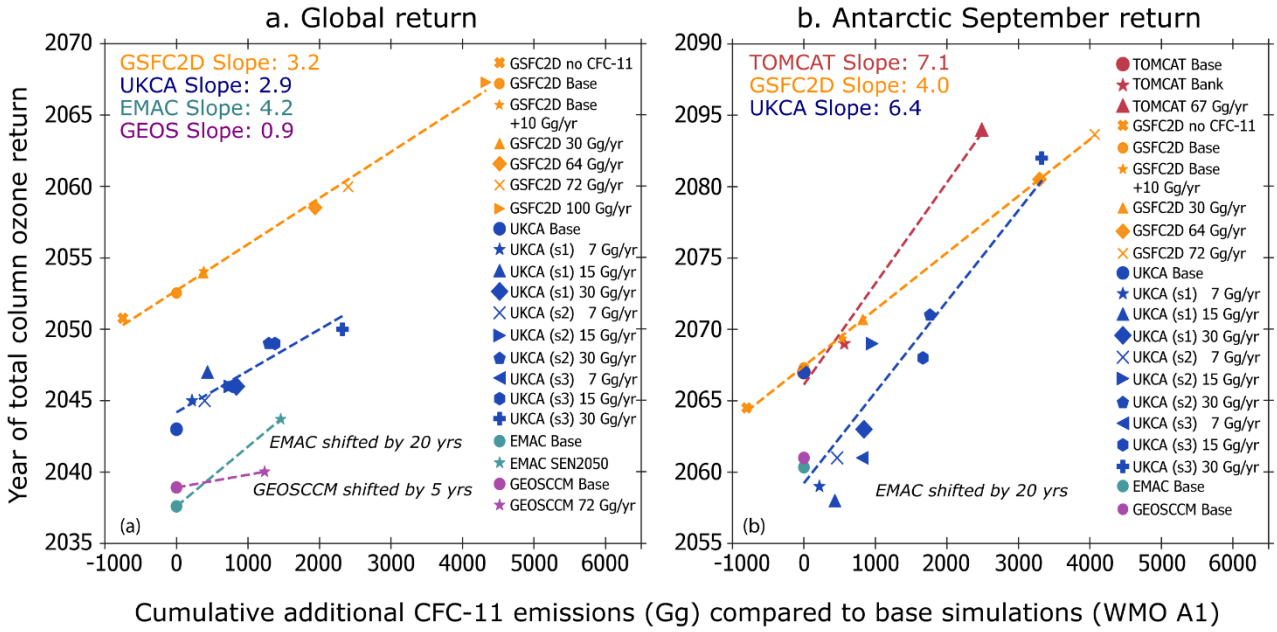

Figure 6.3. Dependence of 1980 return dates for (a) global (90°S–90°N) annual mean column ozone and (b) September mean Antarctic (90°S–65°S) column ozone on cumulative additional (compared with WMO A1) equivalent CFC-11 emissions (Gg) up to the return date for each simulation from various models. The colours indicate the model and the different symbols indicate different simulations. With each model, a base simulation has been performed using the WMO A1 baseline scenario and perturbation simulations have been performed using different assumptions of additional CFC-11 emissions (and in some cases CFC-12 emissions, which are converted to equivalent CFC-11), which are quantified by the x-axis. The lines (with numerical values for the slope in years per 1 000 Gg) show the best linear fits to the simulations for each model. For ease of plotting, the return dates have been shifted by 20 years in both panels for EMAC (which ignores some replacement chlorine compounds and produces early recovery) and by 5 years in panel (a) for GEOSCCM. The TOMCAT CTM is not used to calculate the global ozone return date as it does not consider important climate feedbacks.

Increased CFC-11 emissions cause a delay in ozone return dates both globally and for polar regions in the model simulations. It is worth emphasizing that there was no co-ordination between the different models in terms of CFC-11 or GHG scenarios, so the agreement between the results is encouraging and provides some indication of robustness. The most important information in Figure 6.3 is the relative delay in the ozone return date for a given amount of CFC-11 emitted. For the global case, individual models indicate a delay in the return date of between 0.9 years per 1 000 Gg and 4.2 years per 1 000 Gg. However, both the gentle slope of the GEOSCCM line and the somewhat steeper EMAC slope are based on only two simulations, and a more representative overall value is around 3 years per 1 000 Gg. For the

Antarctic in September, where ozone loss is strongly impacted by chlorine chemistry, the delay in the ozone return date is longer. Here, the TOMCAT CTM, which ignores climate feedbacks, gives the steepest slope, at 7.1 years per 1 000 Gg, and GSFC-2D gives the flattest slope. In the Antarctic, the 2-D model is likely to perform less well, as it cannot capture the full 3-D behaviour of the polar vortex. An objective estimate of the best value for the delay in the return date is therefore more difficult to obtain, but 4–7 years per 1 000 Gg is likely to be a representative range.

The results in Figure 6.3 therefore show a delay of a few years in ozone return for cumulative additional emissions of 1000 Gg of CFC-11. The linear fits to the Figure 6.3 data show that return dates can be scaled to different cumulative emission scenarios. The observations of changes in the CFC-11 atmospheric mixing ratio (see section 2) indicate that the additional, non-compliant CFC-11 emissions so far may have been around 10 Gg yr^{-1} (see sections 3 and 4). These emissions are therefore small compared with the cumulative emissions used in the model simulations, which give rise to delays of many years.

Based upon cumulative additional CFC-11 emissions of 120–440 Gg in the 2012–2019 period (see section 3.2), the global ozone recovery delay rises to 0.4–1.3 years, while the additional Antarctic ozone-hole recovery delay rises to 0.5–3.1 years using the sensitivities derived from Figure 6.3. It should be noted that the impact of recent emissions on future mid-century to late-century recovery dates will be mitigated by the removal of CFC-11 and its degradation products from the atmosphere in the intervening period based on its 52-year lifetime. While such a delay may not be detectable given the large uncertainty in expected recovery dates of ±6 years (1 sigma), as derived from a suite of model simulations that do not include these additional emissions (REF-C2; see Dhomse et al. (2018) for details), the projections still represent a clear shift in the mean to a later recovery.

_____

APPENDIX A. HISTORICAL EVOLUTION OF THE ATMOSPHERIC MIXING RATIO OF CFC-11

Tropospheric measurements of CFC-11 in the southern and northern hemispheres extend back to the 1930s, thanks to ambient air analysis and analysis of air trapped in firn. The tropospheric record of CFC-11 mixing ratios at remote stations is shown in Figure A.1. The first CFC-11 measurements were performed at Adrigole, Ireland, (52° N) in 1970 and 1971 (Lovelock, 1971, 1972) using the recently invented electron capture detector (ECD) in combination with gas chromatography (GC). The mixing ratio during background conditions (oceanic air) was 70 ppt, with an increase to ~170 ppt when polluted air from the United Kingdom reached the station. These data were obtained from a purpose-built GC with a tritium (^{3}H) ECD operating as an absolute detector (coulometric mode). The absolute uncertainty in this method, based on comparison with measurements calibrated using standards, was estimated by Wilkniss et al. (1975) to be ±15%. Pack et al. (1977) provided further measurements at Adrigole between 1973 and 1975, with monthly average mixing ratios exceeding 200 ppt when impacted by CFC-11 emissions from the United Kingdom and continental Europe.

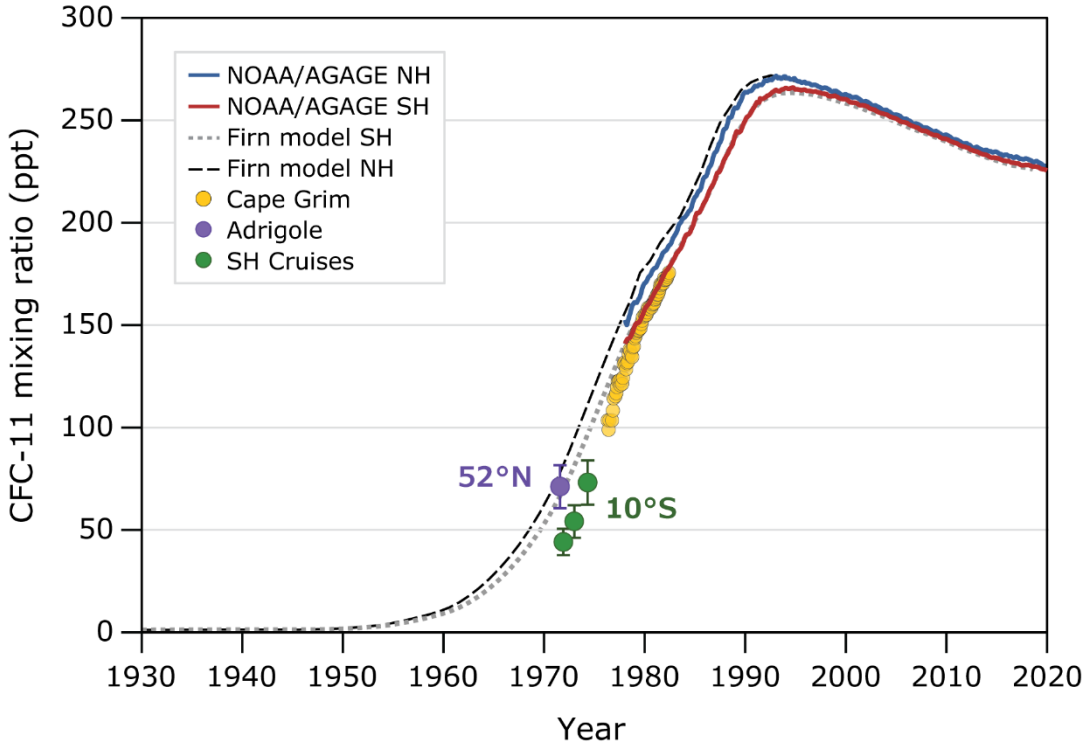

Figure A.1. Historic measurements and time series combined with modelled firn air mixing ratios. First measurement in the northern hemisphere at Adrigole (52° N): purple point. First measurements in the southern hemisphere from three ship cruises at 10°S: green points. First continuous CSIRO in situ measurements from Cape Grim, Tasmania, Australia: orange points. Time series of southern hemispheric (red) and northern hemispheric (blue) mean surface mixing ratios of CFC-11 shown as averages of the data independently derived by NOAA GMD (NOAA CFC-11 gravimetric scale) and AGAGE (SIO 2005 gravimetric scale) (Engel et al., 2018). In addition, results from the analysis of firn air samples are shown for both the southern hemisphere (dotted) and the northern hemisphere (dashed).

The first CFC-11 measurements in the southern hemisphere were taken on a ship cruise in 1972. The results from that cruise (Lovelock et al., 1973) and two later cruises (Wilkniss et al., 1973, 1975) were analysed in Wilkniss et al. (1975), who identified rising CFC-11 levels at 10° S: 41 ppt in November 1971 (Lovelock et al., 1973), 53 ppt in December 1972 (Wilkniss et al., 1973), and 72 ppt in April 1974 (Wilkniss et al., 1975).

Continuous CFC-11 measurements in the southern hemisphere started with an in situ CSIRO measurement programme at Cape Grim (Australia) in October 1976 (Fraser et al., 1983). These data (open orange circles in Figure A.1) have been adjusted to the current AGAGE CFC-11 scale (SIO 2005). CFC-11 flask measurements started at the end of the 1970s in the NOAA programme (1977 until the present, Elkins et al., 1993) and continuous, in situ measurements commenced in the ALE/GAGE/AGAGE programme in mid-1978 and have continued to the present (Prinn et al., 1983, 2018).

The earliest published NOAA CFC-11 flask data from the southern hemisphere are for 1977 (South Pole, January 1977; Cape Matatula, January 1977) and these data are incorporated into the NOAA southern hemisphere average CFC-11 data (see Figure 2.2).

The earliest published AGAGE CFC-11 data from the southern hemisphere are for 1978 (Cape Matatula and Cape Grim, July to December 1978), and these data are incorporated into the AGAGE southern hemisphere average CFC-11 data (see Figure 2.2).

Firn observations extend the CFC-11 time series from the early 1970s back to 1930. The analysis of firn air samples is shown in Figure A.1 for both hemispheres (C. Trudinger, CSIRO, pers. comm.; update of Sturrock et al., 2002). The firn air model-derived data are a combination of measured firn air concentration and age distribution and they use the AFEAS emission data as prior information.

There are obvious differences between the earliest measurements in the southern hemisphere troposphere and the derived mixing ratios from firn air samples. These differences are difficult to reconcile, as there are significant calibration uncertainties in the very early measurements, as well as uncertainties in calculating age in firn air. Mixing ratios found in firn air samples before anthropogenic production/emissions of CFC-11 started are not statistically different from zero. This largely excludes a significant natural source of CFC-11 before the onset of the anthropogenic emissions. Nevertheless, volcanoes were discussed as a potentially relevant natural source after Isidorov et al. (1990) found mixing ratios up to 80 ppb (parts per billion, 10^{-9} mol mol^{-1}) in volcanic outflows in Russia. Later, these high values were not confirmed by Jordan et al. (2000), who found maximum mixing ratios of ~1 ppb from the outflow of volcanoes in Italy and Japan, or by Schwandner et al. (2004), who measured a maximum of 3.7 ppb from fumaroles from a volcano in Italy. These studies estimated global CFC-11 emissions due to volcanoes of between <0.3 t yr^{-1} and 8.6 t yr^{-1}, which would result in very small mixing ratios in the range of parts per quadrillion (10^{-15} mol mol^{-1}). More recently, CFC concentrations below those in ambient air were found in volcanic outflows in Nicaragua (Frische et al., 2006) and Italy (Tassi et al., 2012). It is therefore concluded that volcanoes are, if at all, only a negligible source of CFC-11 in ambient air.

APPENDIX B. CFC-11 DATA FROM CAMPAIGNS

B.1 CAMPAIGNS IN SPECIFIC REGIONS AND HIGHER PARTS OF THE ATMOSPHERE

In addition to the continuous measurements by the global NOAA and AGAGE networks, measurements in important source regions have been made during intensive field campaigns. The first measurement campaign, which covered both hemispheres, was performed by Lovelock et al., (1973) (see Appendix A). The most important campaigns were in Russia, the United States, Canada (Hurst et al., 2004, 2006), and offshore in East Asia (Palmer et al., 2003). Several other campaigns have been performed in recent decades within the East Asian source region. These are discussed further in section B2 below.

The earliest (1974) vertical profile measurements of CFC-11 in the northern hemisphere were obtained by Lovelock (1974) up to about 10 km altitude over the United Kingdom. This was quickly followed by the first measurements in the stratosphere over the United States, where the actual breakdown of CFC-11 was detected by Schmeltekopf et al. (1975), Hester et al. (1975) and Krey et al. (1976). The earliest vertical profile measurements of CFC-11 in the southern hemisphere were obtained in late 1976, up to 12 km over Cape Grim, Australia (Fraser and Pearman, 1978).

Many aeroplane campaigns and balloon flights have followed since then and are still ongoing. Major findings based on these campaigns have included the estimation of stratospheric lifetimes (Volk et al., 1997), the determination of the fractional release factors (Schauffler et al., 2003; Laube et al., 2013) and the changing stratospheric chlorine budget (Engel et al., 2002). The newest technology includes the use of airborne in situ GC-MS measurements (Keber et al., 2019) and reusable sampling lines (AirCore, Karion et al., 2010) for collecting stratospheric air (Laube et al., 2020).

B.2 OVERVIEW OF MEASUREMENT DATA FROM SOUTH ASIAN AND EAST ASIAN SOURCE REGIONS

Several intensive field campaigns between 2000 and 2019 (see Figure B.1) have collected observations of CFC-11 concentrations in South and East Asia. These campaigns are shown in comparison with the long-term data set of Gosan, Republic of Korea (Park et al., 2021). Generally, the mixing ratios observed at remote sites in East Asia are comparable and are similar to the northern hemisphere background concentrations (see Lee and Chiou, 2007; Ou-Yang et al., 2017). In cities and industrial areas, the mixing ratios are higher due to the proximity of the measurements to sources. However, differences between the campaigns are large. Biases and uncertainties associated with these observations are difficult to assess due to the use of different measurement methods and standards across the campaigns.

From 2000 to 2010, the averaged mixing ratios observed in industrial areas in East Asia, e.g., the Pearl River Delta and Northern China, ranged from ~280 ppt to ~360 ppt, i.e. up to >100 ppt higher than northern hemisphere background levels (Barletta et al., 2006; Chan et al., 2006; Chan and Chu, 2007; Qin, 2007; Chang et al., 2008; Shao et al., 2011; Zeng et al., 2020). From 2010 to 2012, following the total ban on CFC-11 production, CFC-11 mixing ratios decreased to ~250-270 ppt within Chinese cities and heavily populated areas (Wu et al., 2013, 2014; Yang et al., 2016; Zhang et al., 2017). However, from 2014 to 2017, mixing ratios ranging from 270 ppt to more than 400 ppt, which are comparable to the observed mixing ratios before CFC-11 was banned, were reported in Northern China and the Pearl River Delta (Yang et al., 2017; Lin et al., 2019; Zheng et al., 2019; Yang et al., 2021).

There are also a few observational studies in South-East Asia and South Asia, where CFC-11 concentrations were measured to be only slightly higher than the global background values (e.g., Sarkar et al., 2018). In 2016, CFC-11 mixing ratios were measured as ~230 ppt during an airborne campaign over India (Say et al., 2019), only a few ppt higher than the northern hemisphere background.

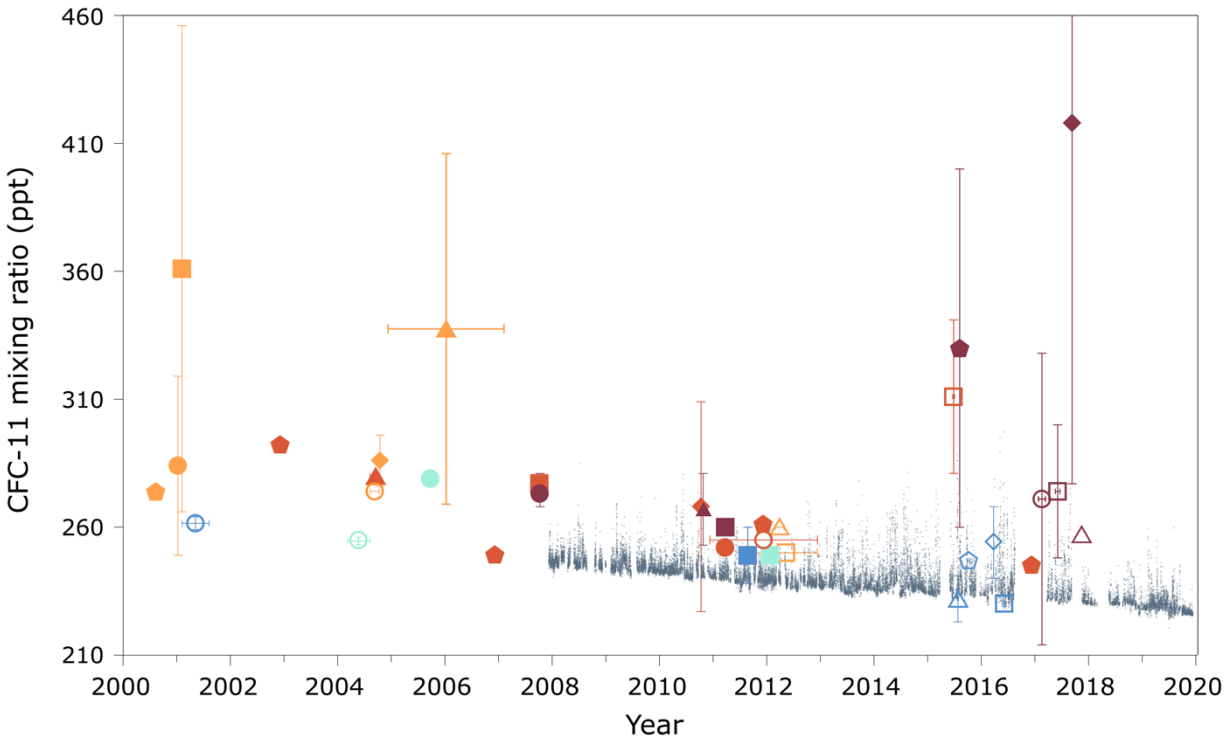

In-situ since 2008
- Park et al. 2021 (Gosan, Korea)

From 2000 - 2009
- Palmer et al. 2003 (Eastern Asian)
- Barletta et al. 2006 (45 Chinese cities)
- Chan et al. 2006 (Guangzhou, Guangdong, China)
- Qin 2007 (Beinjing, China)
- Chan and Chu 2007 (Pearl River Delta, China)
- Lee and Chiou 2007 (Lukang, Taiwan, China)
- Chang et al. 2008 (Taipei, Taiwan, China)
- Chang et al. 2008 (Guangzhou, Guangdong, China)
- Zhang YL et al. 2010 (Hongkong, China)
- Zhang YL et al. 2010 (Guangzhou, Guangdong, China)
- Shao et al. 2011 (Guangzhou, Guangdong, China)
- Shao et al. 2011 (Xinkeng, Guangdong, China)
- Zent et al. 2020 (Pearl River Delta, China)

From 2010 - 2012
- Fang et al. 2012 (46 Chinese cities)
- Wu et al. 2013 (Guangzhou, Guangdong, China)
- Wu et al. 2013 (Hangzhou, Zhejiang, China)
- Wu et al. 2014 (Pearl River Delta, China)
- Ou-Yang et al. 2015 (Taipei, Taiwan, China)
- Wu et al. 2016 (Mt. Changbai, Jilin, China)
- Yang et al. 2016 (Mt. Lu, Jiangxi, China)
- Zhang et al. 2017 (Lin'an, Zhejiang, China)
- Sarkar et al. 2018 (Singapore)
- Zent et al. 2020 (Pearl River Delta, China)

From 2014 - 2017
- Li et al. 2016 (Beijing, China)
- Ou-Yang et al. 2017 (Mt. Fuji, Japan)
- Yang et al. 2017 (Mt. Tai, Shandong, China)
- Li et al. 2017 (East China Sea)
- Zheng et al. 2019 (Yellow River Delta, Shandong, China)
- Zheng et al. 2019 (Yellow River Delta, Shandong, China)
- Lin et al. 2019 (Nanlin, Guangdong, China)
- Say et al. 2019 (India)
- Zent et al. 2020 (Pearl River Delta, China)
- Yang et al. 2021 (Mt. Tai, Shandong, China)
- Simpson et al. 2020 (East China Sea & Rep. of Korea)

Figure B.1. CFC-11 mixing ratios from atmospheric measurement campaigns in South and East Asia since 2000. Solid points represent measurements in urban areas or in pollution plumes, and unfilled symbols represent measurements at background or rural sites. The blue symbols represent observations in Japan, Singapore, India and the East China Sea; the turquoise symbols represent observations in Taiwan Province of China; other symbols represent observations in China's mainland.

APPENDIX C. CONSTRUCTING SCENARIOS

Figure C.1 shows the general flow chart of how the projections are constructed:

1. Global average observed mixing ratios are used in combination with the atmospheric lifetime of the ODS to infer global average historical emissions. The atmospheric lifetime used (52 years for CFC-11) is from the latest quadrennial ozone assessment (WMO, 2018).

2. In IPCC/TEAP (2005) and TEAP/UNEP (2009), the sizes of global ODS banks were derived from inventories of consumption data (i.e. a bottom-up approach). The bottom-up CFC-11 bank size is estimated at 1 687 Gg for 2002, and is projected (extrapolated) at 1 125 Gg for 2015. The 2008 bank (1 420 Gg) is based on an interpolation of these two bank estimates. All WMO ozone assessments since 2010 have relied on the 2008 bank estimate, since no more recent estimate had been made until the TEAP/UNEP (2019*b*) report.

3. Production and consumption data reported to UNEP for A5 (developed) and non-A5 (developing) Parties are obtained from UNEP for the individual ODSs. Together, these data, the inferred emissions, and the bank amount for 2008 are used to derive a time series of the bank amount from 1986 to the latest year for which inferred emissions are available. (In some cases, large discrepancies between bottom-up and inferred emissions and/or inconsistencies in calculated banks have been found. In those cases, it was assumed that additional production had taken place and the bank was adjusted to obtain a better agreement between calculated bottom-up emissions and the inferred emissions.)

4. Emission factors from banks are derived as the ratio of the emission rate over the total bank amount, taking into account emissions during production (see Figure C.1 caption). An average bank emission factor for the ODS is calculated as the average of the ratio derived for the most recent 5–10 years. This bank emission factor is an effective factor combining all different types of applications. Since banks of different applications are depleted at different rates, the obtained average emission factor will likely change over time, but this is not taken into account in the future scenarios in past WMO ozone assessment reports or in the present report.

5. The inferred global average historical emissions, the calculated historical banks, the reported production/consumption and the derived average emission factor are used as a starting point and constraint for projections.

6. The Montreal Protocol phaseout schedules are applied to the reported consumption data to construct projections of ODSs for A5 and non-A5 Parties separately. Allowed essential use exemptions are taken into account.

7. Banks and emissions are then calculated from the projected consumption rate and the derived emission factor.

8. Mixing ratios are calculated based on the emissions and an adopted CFC-11 atmospheric lifetime, which is assumed to be constant over time.

9. Complete time series are obtained this way for consumption, bank, emissions and mixing ratios from which CFC-11-eq emissions, CO_2-eq emission, EESC and radiative forcing are calculated. These time series are then used as inputs for global CCMs to assess the impact of ODSs on the ozone layer.

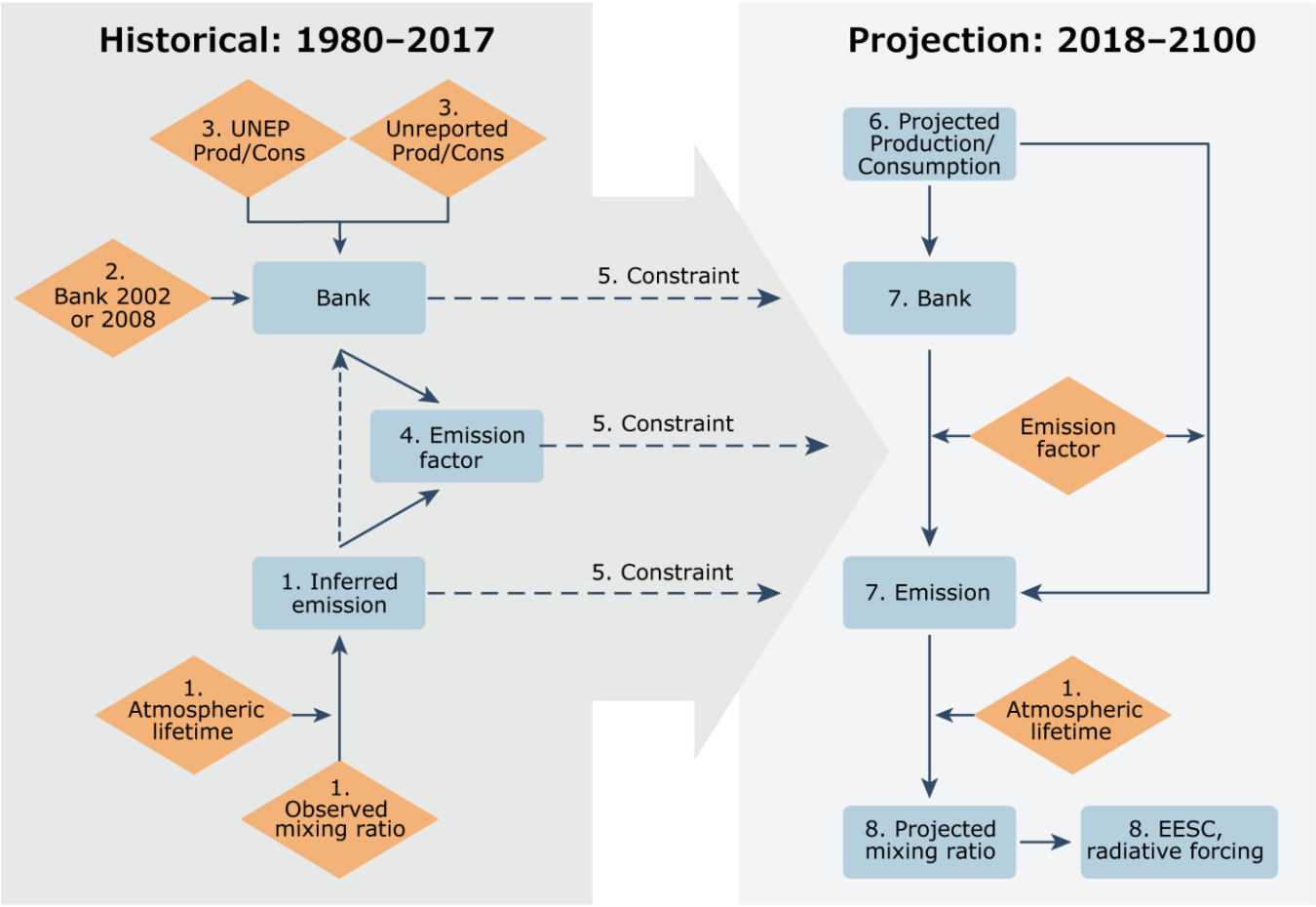

Figure C.1. General flow chart of the construction of ODS scenarios for WMO ozone assessment reports (WMO, 1999, 2003, 2007, 2011, 2014, 2018) and those given here. The left-hand side shows how observed mixing ratios and reported bank data for 2008 and UNEP production/consumption are used to infer historical emissions and an emission factor. The right-hand side shows how these are used as inputs (constraints) for projections of emissions and mixing ratios. Blue rectangles are calculated parameters and tan diamonds are input parameters and observed mixing ratios. The numbers refer to the steps in the text above. Global production is assumed to be equal to consumption. The bank in year y is calculated using the formula bank(y) = bank(y−1) + production(y−1) − emission(y-1). The year y emission is calculated as emission(y) = emission factor × (bank(y) + production(y)).

APPENDIX D. CFC-12 EMISSIONS

Emissions of CFC-12 decrease faster than those of CFC-11, because of their use patterns (see Figure D.1(a)). For example, CFC-12 was seldom used in closed cell foam; instead, it was used in air conditioning and refrigeration, in which the lifetime of the equipment is relatively short compared to the lifetime of building insulation. Like CFC-11 emissions, CFC-12 emissions in the baseline scenario often increased in successive WMO ozone assessment reports, with the lowest projected emissions in WMO (2003) and the largest in WMO (2018). These increases in emissions, inferred from observed mixing ratios, show that the projections were often too low.

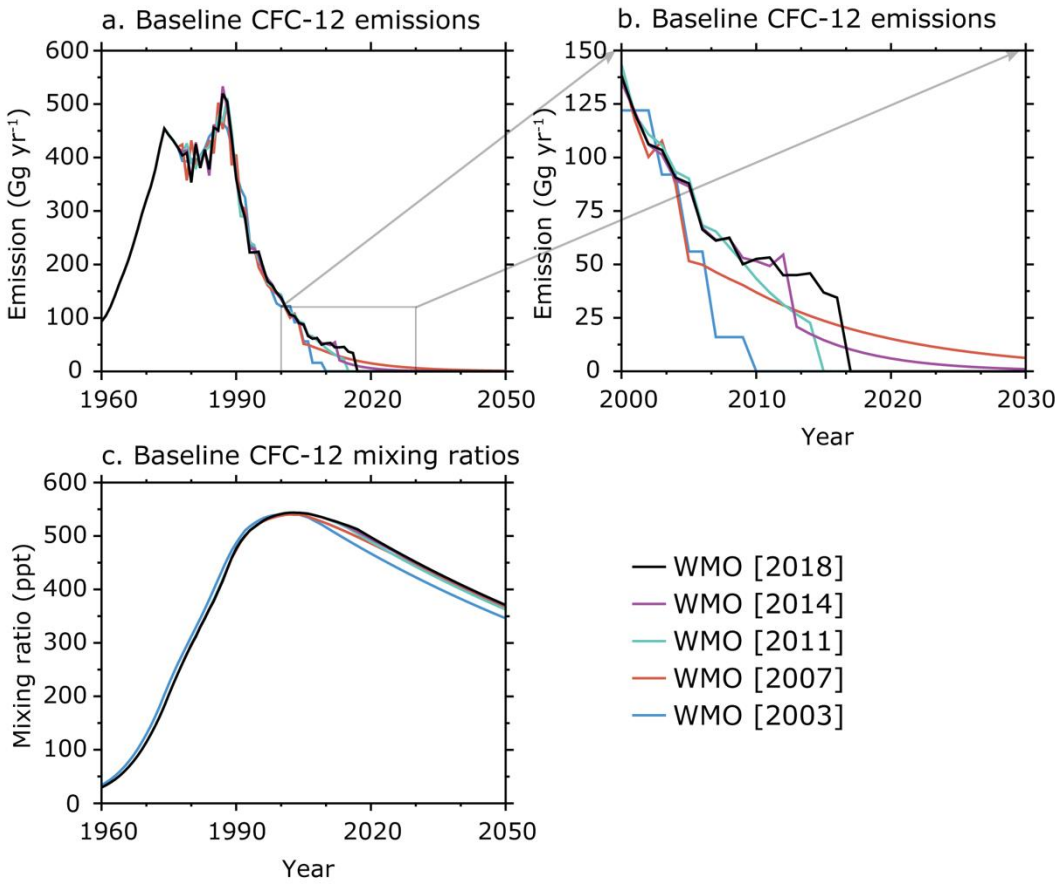

Figure D.1. (a) Global CFC-12 emissions in the baseline scenario of past WMO ozone assessment reports. (b) Inset of emissions for the period 2000–2030 only. (c) Corresponding mixing ratios from the emissions. The historical emissions have been inferred from the available observed mixing ratios. This means that, for the baseline scenario in WMO (2018), the emissions from 1980 to 2016 are inferred from observations from 1980 to 2017 (see Table 5.1). The emissions after 2016 are based on projections.

The 2008 bank of CFC-12 from IPCC/TEAP (2005) and TEAP/UNEP (2009) of 394 Gg is used in WMO (2011), WMO (2014) and WMO (2018). This is lower than the bank size of 562–1 464 Gg (95% confidence interval) estimated by Lickley et al. (2020). The CFC-12 bank in the scenarios decreases faster than the CFC-11 bank because of the larger emission factor related to its use as a refrigerant in equipment that was characterized by leaks, recovery, venting, etc. Consequently, the projected emissions of CFC-12 (based on Lickley et al., (2020)) decrease faster than those of CFC-11. These emission projections strongly contrast with the non-zero emissions observed in the 2015–2019 period (see Figure 3.3), suggesting large uncertainties in bank projections and possible unreported production. However, the inferred emissions of CFC-12 for 2012–2016 do not exhibit an increase, as is seen for CFC-11 emissions.

APPENDIX E. CHEMICAL FORMULAE AND NOMENCLATURE

BrO	bromine monoxide
CCl_4	carbon tetrachloride
CFC-11	trichlorofluoromethane, CCl_3F
CFC-12	dichlorodifluoromethane, CCl_2F_2
CFC-113	trichlorotrifluoroethane, $C_2Cl_3F_3$
CH_4	methane
Cl	atomic chlorine
ClO	chlorine monoxide
CO_2	carbon dioxide
CO_2-eq	CO_2-equivalent
HCFC-22	chlorodifluoromethane
HFC-23	fluoroform
N_2O	nitrous oxide
O	atomic oxygen
$O(^1D)$	atomic oxygen (first excited state)

APPENDIX F. ACRONYMS

2-D	two-dimensional – latitude, altitude
3-D	three-dimensional – longitude, latitude, altitude
ACE-FTS	Atmospheric Chemistry Experiment Fourier Transform Spectrometer
AFEAS	Alternative Fluorocarbons Environmental Acceptability Study
AGAGE	Advanced Global Atmospheric Gases Experiment
AIRS	Atmospheric Infrared Sounder satellite instrument
ALE	Atmospheric Lifetime Experiment
CCM	chemistry-climate model
CFC	chlorofluorocarbon
CSIRO	Commonwealth Scientific and Industrial Research Organisation (Australia)
CTM	chemical transport model
DU	Dobson units
ECD	electron capture detector
ECHAM	global climate model developed by the Max Planck Institute for Meteorology in Hamburg and by the University of Hamburg (Germany)
ECMWF	European Centre for Medium-Range Weather Forecasts
EESC	equivalent effective stratospheric chlorine
EMAC	ECHAM/MESSy Atmospheric Chemistry numerical global atmosphere-chemistry model
FTIR	Fourier transform infrared
FTOC	Foam Technical Options Committee
GAGE	Global Atmospheric Gases Experiment
GAW	Global Atmosphere Watch Programme of WMO
GC	gas chromatography
GC-ECD	gas chromatography-electron capture detection
GC-MS	gas chromatography-mass spectrometry
GEOSCCM	Goddard chemistry climate model
Gg	gigagram – 1 Gg = 1 kilotonne = 10^9 g
GHG	greenhouse gas
GR	growth rate
GSFC	NASA Goddard Space Flight Center (United States)
Gt	gigatonne – 1 Gt = 10^9 tonnes = 10^{15} g
GWP	global warming potential
HCFC	hydrochlorofluorocarbon
HFC	hydrofluorocarbon
IHD	interhemispheric difference
IPCC	Intergovernmental Panel on Climate Change
MESSy	Modular Earth Submodel System
MIPAS	Michelson Interferometer for Passive Atmospheric Sounding
NASA	National Aeronautics and Space Administration (United States)
NDACC	Network for the Detection of Atmospheric Composition Change
NIES	National Institute for Environmental Studies (Japan)
NOAA	National Oceanic and Atmospheric Administration (United States)
ODP	ozone depletion potential
ODS	ozone-depleting substance

ppb	parts per billion
ppt	parts per trillion
QBO	quasi-biennial oscillation
SIO	Scripps Institution of Oceanography
SPARC	Stratospheric Processes And their Role in Climate (project of WCRP)
TEAP	Technology and Economic Assessment Panel
TOMCAT	Toulouse Off-line Model of Chemistry And Transport
UMUKCA-UCAM	University of Cambridge – United Kingdom Chemistry and Aerosol model
UCI	University of California, Irvine
UNEP	United Nations Environment Programme
UV	ultraviolet
WACCM	Whole Atmosphere Community Climate Model
WCRP	World Climate Research Programme
WMO	World Meteorological Organization

_____

APPENDIX G. LIST OF AUTHORS, CONTRIBUTORS, AND REVIEWERS

SCIENTIFIC ASSESSMENT PANEL CO-CHAIRS

David W. Fahey (United States)
Paul A. Newman (United States)
John A. Pyle (United Kingdom)
Bonfils Safari (Rwanda)

ADVISORY GROUP

David W. Fahey (United States)
Paul J.B. Fraser (Australia)
Neil R.P. Harris (United Kingdom)
Jianxin Hu (China)
Paul A. Newman (United States)
John A. Pyle (United Kingdom)
Bonfils Safari (Rwanda)
Michelle L. Santee (United States)

AUTHORS

Martyn P. Chipperfield (United Kingdom)
Michaela I. Hegglin (United Kingdom)
Stephen A. Montzka (United States)
Paul A. Newman (United States)
Sunyoung Park (Republic of Korea)
Stefan Reimann (Switzerland)
Matthew Rigby (United Kingdom)
Andreas Stohl (Norway)
Guus J.M. Velders (Netherlands)
Helen Walter-Terrinoni (United States)
Bo Yao (China)

REPORT COORDINATOR

Sarah J. Doherty (United States)

CONTRIBUTORS

Peter F. Bernath (United States)
Martin Dameris (Germany)
Sandip S. Dhomse (United Kingdom)
Geoffrey S. Dutton (United States)
Eric L. Fleming (United States)
Paul J.B. Fraser (Australia)
Bradley D. Hall (United States)
Lei Hu (United States)
Patrick Jöckel (Germany)
James Keeble (United Kingdom)
Megan Lickley (United States)
Emmanuel Mahieu (Belgium)
Alistair J. Manning (United Kingdom)
J. David Nance (United States)
Matthias Nützel (Germany)
Eric A. Ray (United States)
Helen K. Tope (Australia)
Cathy M. Trudinger (Australia)
Isaac Vimont (United States)
Luke M. Western (United Kingdom)

REVIEWERS

Tina Birmpili (Kenya)
Martin Dameris (Germany)
Andreas Engel (Germany)
Sophie Godin-Beekman (France)
Lambert Kuijpers (Netherlands)
Prabir Patra (Japan)
David Plummer (Canada)
A.R. Ravishankara (United States)
Takuya Saito (Japan)
Susan Solomon (United States)
Darryn W. Waugh (United States)
Ray F. Weiss (United States)

EDITORIAL, GRAPHICS, AND REFERENCE SUPPORT

Susan K. McFadden (United States)
Amy K. Moran (United States)
Chelsea R. Thompson (United States)
Kathy A. Thompson (United States)

REFERENCES

Adcock, K.E., M.J. Ashfold, C. C-K. Chou, L.J. Gooch, N. Mohd Hanif, J.C. Laube, D.E. Oram, C-F. Ou-Yang, M. Panagi, W.T. Sturges and C.E. Reeves, 2020: Investigation of East Asian emissions of CFC-11 using atmospheric observations in Taiwan, *Environmental Science & Technology*, 54(7), 3814–3822, doi:10.1021/acs.est.9b06433.

Arnold, T., J. Mühle, P.K. Salameh, C.M. Harth, D.J. Ivy and R.F. Weiss, 2012: Automated measurement of nitrogen trifluoride in ambient air, *Analytical Chemistry*, 84(11), 13305–13320, doi:10.1021/ac300373e.

Arnold, T., A.J. Manning, J. Kim, S. Li, H. Webster, D. Thomson, J. Mühle, R.F. Weiss, S. Park and S. O'Doherty, 2018: Inverse modelling of CF_4 and NF_3 emissions in East Asia, *Atmospheric Chemistry and Physics*, 18(18), 4798–4804, doi:10.5194/acp-18-13305-2018.

Ball, W.T., J. Alsing, D.J. Mortlock, J. Staehelin, J.D. Haigh, T. Peter, F. Tummon, R. Stübi, A. Stenke, J. Anderson, A. Bourassa, S.M. Davis, D. Degenstein, S. Frith, L. Froidevaux, C. Roth, V. Sofieva, R. Wang, J. Wild, P. Yu, J.R. Ziemke and E.V. Rozanov, 2018: Evidence for a continuous decline in lower stratospheric ozone offsetting ozone layer recovery, *Atmospheric Chemistry and Physics*, 18(2), 1379–1394, doi:10.5194/acp-18-1379-2018.

Ball, W.T., J. Alsing, J. Staehelin, S.M. Davis, L. Froidevaux and T. Peter, 2019: Stratospheric ozone trends for 1985–2018: Sensitivity to recent large variability, *Atmospheric Chemistry and Physics*, 19(19), 12731–12748, doi:10.5194/acp-19-12731-2019.

Barletta, B., S. Meinardi, I.J. Simpson, F. Sherwood Rowland, C.Y. Chan, X. Wang, S. Zou, L.Y. Chan and D.R. Blake, 2006: Ambient halocarbon mixing ratios in 45 Chinese cities, *Atmospheric Environment*, 40(40), 7706–7719, doi:10.1016/j.atmosenv.2006.08.039.

Bernath, P.F., J. Steffen, J. Crouse and C.D. Boone, 2020: Sixteen-year trends in atmospheric trace gases from orbit, *Journal of Quantitative Spectroscopy & Radiative Transfer*, 253, 107178, doi: 10.1016/j.jqsrt.2020.107178.

Bönisch, H., A. Engel, T. Birner, P. Hoor, D.W. Tarasick and E.A. Ray, 2011: On the structural changes in the Brewer-Dobson circulation after 2000, *Atmospheric Chemistry and Physics*, 11(8), 3937–3948, doi:10.5194/acp-11-3937-2011.

Burkholder, J.B. and W. Mellouki, 2013: Evaluation of Atmospheric Loss Processes, Chapter 3 in *SPARC Report on the Lifetimes of Stratospheric Ozone-Depleting Substances, Their Replacements, and Related Species*, M.K.W. Ko, P.A. Newman, S. Reimann, and S.E. Strahan (Eds.), SPARC Report No. 6, WCRP-15/2013.

Butchart, N., The Brewer-Dobson circulation, 2014: *Reviews of Geophysics*, 52(2), 157–184, doi:10.1002/2013RG000448.

Carpenter, L.J., J.S. Daniel, E.L. Fleming, T. Hanaoka, J. Hu, A.R. Ravishankara, M.N. Ross, S. Tilmes, T.J. Wallington and D.J. Wuebbles, 2018: Scenarios and Information for Policymakers. In: *Scientific Assessment of Ozone Depletion: 2018*, Global Ozone Research and Monitoring Project – Report No. 58, World Meteorological Organization, Geneva.

Chan, C.Y., J.H. Tang, Y.S. Li and L.Y. Chan, 2006: Mixing ratios and sources of halocarbons in urban, semi-urban and rural sites of the Pearl River Delta, South China, *Atmospheric Environment*, 40(38), 7331–7345, doi:10.1016/j.atmosenv.2006.06.041.

Chan, L.Y. and K.W. Chu, 2007: Halocarbons in the atmosphere of the industrial-related Pearl River Delta region of China, *Journal of Geophysical Research*, 112(4), doi:10.1029/2006JD007097.

Chang, C.C., C.H. Lai, C.H. Wang, Y. Liu, M. Shao, Y. Zhang and J.L. Wang, 2008: Variability of ozone depleting substances as an indication of emissions in the Pearl River Delta, China, *Atmospheric Environment*, 42(29), 6973–6981, doi:10.1016/j.atmosenv.2008.04.051.

Chen, X., X. Huang and L.L. Strow, 2020: Near-global CFC-11 trends as observed by atmospheric infrared sounder from 2003 to 2018, *Journal of Geophysical Research*, 125(22), doi:10.1029/2020JD033051.

Chipperfield, M.P., 1999: Multiannual simulations with a three-dimensional chemical transport model, *Journal of Geophysical Research*, 104(D1), 1781–1805, doi:10.1029/98JD02597.

Chipperfield, M.P., Q. Liang, S.E. Strahan, O. Morgenstern, S. Dhomse, N.L. Abraham, A.T. Archibald, S. Bekki, P. Braesicke and G. Di Genova, 2014: Multimodel estimates of atmospheric lifetimes of long-lived ozone-depleting substances: Present and future, *Journal of Geophysical Research*, 119(5), 2555–2573, doi:10.1002/2013JD021097.

Chipperfield, M.P., S. Bekki, S. Dhomse, N.R.P. Harris, B. Hassler, R. Hossaini, W. Steinbrecht, R. Thiéblemont and M. Weber, 2017: Detecting recovery of the stratospheric ozone layer, *Nature*, 549(7671), 211–218, doi:10.1038/nature23681.

Chipperfield, M.P., S. Dhomse, R. Hossaini, W. Feng, M.L. Santee, M. Weber, J.P. Burrows, J.D. Wild, D. Loyola and M. Coldewey-Egbers, 2018: On the cause of recent variations in lower stratospheric ozone, *Geophysical Research Letters*, 45(11), 5718–5726, doi:10.1029/2018GL078071.

Cunnold, D.M., R.F. Weiss, R.G. Prinn, D. Hartley, P.G. Simmonds, P.J. Fraser, B. Miller, F.N. Alyea and L. Porter, 1997: GAGE/AGAGE measurements indicating reductions in global emissions of $CC1_3F$ and $CC1_2F_2$ in 1992–1994, *Journal of Geophysical Research*, 102(D1), 1259–1269, doi:10.1029/96JD02973.

Dameris, M., P. Jöckel and M. Nützel, 2019: Possible implications of enhanced chlorofluorocarbon-11 concentrations on ozone, *Atmospheric Chemistry and Physics*, 19(22), 13759–13771, doi:10.5194/acp-19-13759-2019.

Daniel, J.S., G.J.M. Velders, A.R. Douglass, P.M.D. Forster, D.A. Hauglustaine, I.S.A. Isaksen, L.J.M. Kuijpers, A. McCulloch and T.J. Wallington, 2007: Halocarbon Scenarios, Ozone Depletion Potentials, and Global Warming Potentials. In: *Scientific Assessment of Ozone Depletion: 2006*, Global Ozone Monitoring Project – Report No. 50, World Meteorological Organization, Geneva.

Daniel, J.S., G.J.M. Velders, O. Morgenstern, D.W. Toohey, T.J. Wallington and D.J. Wuebbles, 2011: A Focus on Options and Information for Policymakers. In: *Scientific Assessment of Ozone Depletion: 2010*, Global Ozone Monitoring Project – Report No. 52, World Meteorological Organization, Geneva.

Dhomse, S.S., W. Feng, S.A. Montzka, R. Hossaini, J. Keeble, J.A. Pyle, J.S. Daniel and M.P. Chipperfield, 2019: Delay in recovery of the Antarctic ozone hole from unexpected CFC-11 emissions, *Nature Communications*, 10(1), 5781, doi:10.1038/s41467-019-13717-x.

Eckert, E., A. Laeng, S. Lossow, S. Kellmann, G. Stiller, T. Von Clarmann, N. Glatthor, M. Höpfner, M. Kiefer, H. Oelhaf, J. Orphal, B. Funke, U. Grabowski, F. Haenel, A. Linden, G. Wetzel, W. Woiwode, P.F. Bernath, C. Boone, G.S. Dutton, J.W. Elkins, A. Engel, J.C. Gille, F. Kolonjari, T. Sugita, G.C. Toon and K.A. Walker, 2016: MIPAS IMK/IAA CFC-11 (CCl_3F) and CFC-12 (CCl_2F_2) measurements: Accuracy, precision, and long-term stability, *Atmospheric Measurement Techniques*, 9(7), 3355–3389, doi:10.5194/amt-9-3355-2016.

Elkins, J.W., T.M. Thompson, T.H. Swanson, J.H. Butler, B.D. Hall, S.O. Cummings, D.A. Fishers and A.G. Raffo, 1993: Decrease in the growth rates of atmospheric chlorofluorocarbons 11 and 12, *Nature*, 364(6440), 780, doi:10.1038/364780a0.

Engel, A., M. Rigby, J.B. Burkholder, R.P. Fernandez, L. Froidevaux, B.D. Hall, R. Hossaini, T. Saito, M.K. Vollmer and B. Yao, 2018: Update on Ozone-Depleting Substances (ODSs) and Other Gases of Interest to the Montreal Protocol, Chapter 1 in *Scientific Assessment of Ozone Depletion: 2018*, Global Ozone Research and Monitoring Project – Report No. 58, World Meteorological Organization, Geneva.

Engel, A., M. Strunk, M. Müller, H.P. Haase, C. Poss, I. Levin and U. Schmidt, 2002: Temporal development of total chlorine in the high-latitude stratosphere based on reference distributions of mean age derived from CO_2 and SF_6, *Journal of Geophysical Research*, 107(12), doi:10.1029/2001jd000584.

Engel, A., T. Möbius, H. Bönisch, U. Schmidt, R. Heinz, I. Levin, E. Atlas, S. Aoki, T. Nakazawa, S. Sugawara, F. Moore, D. Hurst, J. Elkins, S. Schauffler, A. Andrews and K. Boering, 2009: Age of stratospheric air unchanged within uncertainties over the past 30 years, *Nature Geoscience*, 2(1), 28–31, doi:10.1038/ngeo388.

Fang, X., J. Wu, J. Xu, D. Huang, Y. Shi, D. Wan, H. Wu, M. Shao and J. Hu, 2012: Ambient mixing ratios of chlorofluorocarbons, hydrochlorofluorocarbons, and hydrofluorocarbons in 46 Chinese cities, *Atmospheric Environment*, 54, 387−392, doi:10.1016/j.atmosenv.2012.02.070.

Fleming, E.L., P.A. Newman, Q. Liang and J.S. Daniel, 2020: The impact of continuing CFC-11 emissions on stratospheric ozone, *Journal of Geophysical Research*, 125(3), doi:10.1029/2019JD031849.

Fraser, P.J.B. and G.I. Pearman, 1978: Atmospheric halocarbons in the southern hemisphere, *Atmospheric Environment (1967)*, 12(4), 839–844, doi:10.1016/0004-6981(78)90021-5.

Fraser, P.J., P. Hyson, I.G. Enting and G.I. Pearman, 1983: Global distribution and southern hemispheric trends of atmospheric CCl_3F, *Nature*, 302, 692–695, doi:10.1038/302692a0.

Fraser, P.J., B.L. Dunse, P.B. Krummel, L.P. Steele, N. Derek, B. Mitrevski, C.E. Allison, Z. Loh, A.J. Manning, A. Redington and M. Rigby, 2020: Australian chlorofluorocarbon (CFC) emissions: 1960–2017, *Environmental Chemistry*, 17, 525–544, doi:10.1071/EN19322.

Frische, M., K. Garofalo, T.H. Hansteen, R. Borchers and J. Harnisch, 2006: The origin of stable halogenated compounds in volcanic gases, *Environmental Science and Pollution Research*, 13(6), 406–413, doi:10.1065/espr2006.01.291.

Graziosi, F., J. Arduini, P. Bonasoni, F. Furlani, U. Giostra, A.J. Manning, A. McCulloch, S. O'Doherty, P.G. Simmonds, S. Reimann, M.K. Vollmer and M. Maione, 2016: Emissions of carbon tetrachloride from Europe, *Atmospheric Chemistry and Physics*, 16(20), 12849–12859, doi:10.5194/acp-16-12849-2016.

Hall, B.D., A. Engel, J. Mühle, J.W. Elkins, F. Artuso, E. Atlas, M. Aydin, D. Blake, E.G. Brunke, S. Chiavarini, P.J. Fraser, J. Happell, P.B. Krummel, I. Levin, M. Loewenstein, M. Maione, S.A. Montzka, S. O'Doherty, S. Reimann, G. Rhoderick, E.S. Saltzman, H.E. Scheel, L.P. Steele, M.K. Vollmer, R.F. Weiss, D. Worthy and Y. Yokouchi, 2014: Results from the International Halocarbons in Air Comparison Experiment (IHALACE), *Atmospheric Measurement Techniques*, 7(2), 469–490, doi:10.5194/amt-7-469-2014.

Harris, N.R.P., D.J. Wuebbles, J.S. Daniel, J. Hu, L.J.M. Kuijpers, K.S. Law, M.J. Prather and R. Schofield, 2014: Scenarios and Information for Policymakers. In *Scientific Assessment of Ozone Depletion: 2014*, Global Ozone Research and Monitoring Project – Report No. 55, World Meteorological Organization, Geneva.

Henne, S., D. Brunner, B. Oney, M. Leuenberger, W. Eugster, I. Bamberger, F. Meinhardt, M. Steinbacher and L. Emmenegger, 2016: Validation of the Swiss methane emission inventory by atmospheric observations and inverse modelling, *Atmospheric Chemistry and Physics*, 16(6), 3683–3710, doi:10.5194/acp-16-3683-2016.

Hester, N.E., E.R. Stephens and O.C. Taylor, 1975: Fluorocarbon air pollutants measurements in lower stratosphere, *Environmental Science & Technology*, 9(9), 875–876, doi:10.1021/es60107a005.

Hodson, E.L., D. Martin and R.G. Prinn (2010). The municipal solid waste landfill as a source of ozone-depleting substances in the United States and United Kingdom. *Atmospheric Chemistry and Physics*, 10(4), 1899–1910, doi:10.5194/acp-10-1899-2010.

Hu, L., S.A. Montzka, B.R. Miller, A.E. Andrews, J.B. Miller, S.J. Lehman, C. Sweeney, S.M. Miller, K. Thoning, C. Siso, E.L. Atlas, D.R. Blake, J. De Gouw, J.B. Gilman, G. Dutton, J.W. Elkins, B. Hall, H. Chen, M.L. Fischer, M.E. Mountain, T. Nehrkorn, S.C. Biraud, F.L. Moore and P. Tans, 2016: *Continued emissions of carbon tetrachloride from the United States nearly two decades after its phaseout for dispersive uses*, *PNAS*, 113(11), doi:10.1073/pnas.1522284113.

Hu, L., S.A. Montzka, S.J. Lehman, D.S. Godwin, B.R. Miller, A.E. Andrews, K. Thoning, J.B. Miller, C. Sweeney, C. Siso, J.W. Elkins, B.D. Hall, D.J. Mondeel, D. Nance, T. Nehrkorn, M. Mountain, M.L. Fischer, S.C. Biraud, H. Chen and P.P. Tans, 2017: Considerable contribution of the Montreal Protocol to declining greenhouse gas emissions from the United States, *Geophysical Research Letters*, 44(15), 8075–8083, doi:10.1002/2017GL074388.

Hurst, D.F., P.A. Romashkin, J.W. Elkins, E.A. Oberländer, N.F. Elansky, I.B. Belikov, I.G. Granberg, G.S. Golitsyn, A.M. Grisenko, C.A.M. Brenninkmeijer and P.J. Crutzen, 2004: Emissions of ozone-depleting substances in Russia during 2001, *Journal of Geophysical Research*, 109(14), doi:10.1029/2004JD004633.

Hurst, D.F., J.C. Lin, P.A. Romashkin, B.C. Daube, C. Gerbig, D.M. Matross, S.C. Wofsy, B.D. Hall and J.W. Elkins, 2006: Continuing global significance of emissions of Montreal Protocol-restricted halocarbons in the United States and Canada, *Journal of Geophysical Research*, 111(D15302), doi:10.1029/2005JD006785.

Intergovernmental Panel on Climate Change / Technical and Economic Assessment Panel (IPCC/TEAP), 2005: *Special Report on Safeguarding the Ozone Layer and the Global Climate System: Issues Related to Hydrofluorocarbons and Perfluorocarbons*, Cambridge, Cambridge University Press, doi:10.13140/2.1.4337.2161 and https://www.ipcc.ch/report/safeguarding-the-ozone-layer-and-the-global-climate-system/.

Isidorov, V.A., I.G. Zenkevich and B.V. Ioffe, 1990: Volatile organic compounds in solfataric gases, *Journal of Atmospheric Chemistry*, 10(3), 329–340, doi:10.1007/BF00053867.

Jordan, A., J. Harnisch, R. Borchers, F. Le Guern and H. Shinohara, 2000: Volcanogenic halocarbons, *Environmental Science & Technology*, 34(6), 1122–1124, doi:10.1021/es990838q.

Karion, A., C. Sweeney, P. Tans and T. Newberger, 2010: AirCore: An innovative atmospheric sampling system, *Journal of Atmospheric and Oceanic Technology*, 27(11), 1839–1853, doi:10.1175/2010JTECHA1448.1.

Keber, T., H. Bönisch, C. Hartick, M. Hauck, F. Lefrancois, F. Obersteiner, A. Ringsdorf, N. Schohl, T. Schuck, R. Hossaini, P. Graf, P. Jöckel and A. Engel, 2020: Bromine from short-lived source gases in the extratropical northern hemispheric upper troposphere and

lower stratosphere (UTLS), *Atmospheric Chemistry and Physics*, 20(7), 1–36, doi:10.5194/acp-20-4105-2020.

Keeble, J., N. Luke Abraham, A.T. Archibald, M.P. Chipperfield, S. Dhomse, P.T. Griffiths and J.A. Pyle, 2020: Modelling the potential impacts of the recent, unexpected increase in CFC-11 emissions on total column ozone recovery, *Atmospheric Chemistry and Physics*, 20(12), doi:10.5194/acp-20-7153-2020.

Kellmann, S., T. Von Clarmann, G.P. Stiller, E. Eckert, N. Glatthor, M. Höpfner, M. Kiefer, J. Orphal, B. Funke, U. Grabowski, A. Linden, G.S. Dutton and J.W. Elkins, 2012: Global CFC-11 (CCl_3F) and CFC-12 (CCl_2F_2) measurements with the Michelson Interferometer for Passive Atmospheric Sounding (MIPAS): Retrieval, climatologies, and trends, *Atmospheric Chemistry and Physics*, 12(24), 11857–11875, doi:10.5194/acp-12-11857-2012.

Krey, P.W., R.J. Lagomarsino and J.J. Frey, 1976: Stratospheric concentrations of CCl_3F in 1974, *Journal of Geophysical Research*, 81(9), 1557–1560, doi:10.1029/jc081i009p01557.

Langematz, U., F. Schmidt, M. Kunze, G.E. Bodeker and P. Braesicke, 2016: Antarctic ozone depletion between 1960 and 1980 in observations and chemistry-climate model simulations, *Atmospheric Chemistry and Physics*, 16(24), 15619–15627, doi:10.5194/acp-16-15619-2016.

Laube, J.C., A. Keil, H. Bönisch, A. Engel, T. Röckmann, C.M. Volk and W.T. Sturges, 2013: Observation-based assessment of stratospheric fractional release, lifetimes, and ozone depletion potentials of ten important source gases, *Atmospheric Chemistry and Physics*, 13(5), 2779–2791, doi:10.5194/acp-13-2779-2013.

Laube, J.C., E.C.L. Elvidge, K.E. Adcock, B. Baier, C.A.M. Brenninkmeijer, H. Chen, E.S. Droste, J.U. Grooß, P. Heikkinen, A.J. Hind, R. Kivi, A. Lojko, S.A. Montzka, D.E. Oram, S. Randall, T. Röckmann, W.T. Sturges, C. Sweeney, M. Thomas, E. Tuffnell and F. Ploeger, 2020: Investigating stratospheric changes between 2009 and 2018 with halogenated trace gas data from aircraft, AirCores, and a global model focusing on CFC-11, *Atmospheric Chemistry and Physics*, 20(16), 1–19, doi:10.5194/acp-20-9771-2020.

Lee, B.S. and C.B. Chiou, 2007: The use of CFC-12, CFC-11, and CH_3CCl_3 to trace terrestrial airborne pollutant transport by land-sea breezes, *Atmospheric Environment*, 41(16), 3360–3372, doi:10.1016/j.atmosenv.2006.12.025.

Li, G.L., Z. He, G.P. Yang and D. Yuan, 2017: Distribution characteristics and sea-to-air fluxes of volatile halocarbons in the East China Sea in autumn, *Zhongguo Huanjing Kexue/China Environmental Science*, 37(5), 1724−1734.

Li, J., R. Wu, Y. Li, Y. Hao, S. Xie and L. Zeng, 2016: Effects of rigorous emission controls on reducing ambient volatile organic compounds in Beijing, China, *Science of the Total Environment*, 557–558, 531–541, doi:10.1016/j.scitotenv.2016.03.140.

Lickley, M., S. Solomon, S. Fletcher, G.J.M. Velders, J. Daniel, M. Rigby, S.A. Montzka, L.J.M. Kuijpers and K. Stone, 2020: Quantifying contributions of chlorofluorocarbon banks to emissions and impacts on the ozone layer and climate, *Nature Communications*, 11(1), doi:10.1038/s41467-020-15162-7.

Lin, Y., D. Gong, S. Lv, Y. Ding, G. Wu, H. Wang, Y. Li, Y. Wang, L. Zhou and B. Wang, 2019: Observations of high levels of ozone-depleting CFC-11 at a remote mountain-top site in Southern China, *Environmental Science & Technology Letters*, 6(3), 114–118, doi:10.1021/acs.estlett.9b00022.

Liu, Yanjun, W. Lu, W. Dastyar, Yanting Liu, H. Guo, X. Fu, H. Li, R. Meng, M. Zhao and H. Wang, 2017: Fugitive halocarbon emissions from working face of municipal solid waste

landfills in China. Waste Management, 70, 149–157, https://www.sciencedirect.com/science/article/pii/S0956053X17306207.

Lovelock, J.E., 1971: Atmospheric fluorine compounds as indicators of air movements, *Nature*, 230(5293), 379, doi:10.1038/230379a0.

———, 1972: Atmospheric turbidity and CCl_3F concentrations in rural Southern England and Southern Ireland, *Atmospheric Environment (1967)*, 6(12), 917–925, doi:10.1016/0004-6981(72)90100-X.

———, 1974: Atmospheric halocarbons and stratospheric ozone, *Nature*, 252, 292–294, doi:10.1038/252292a0.

Lovelock, J.E., R.J. Maggs and R.J. Wade, 1973: Halogenated hydrocarbons in and over the Atlantic, *Nature*, 241, 194–196, doi:10.1038/241194a0.

Lunt, M.F., M. Rigby, A.L. Ganesan and A.J. Manning, 2016: Estimation of trace gas fluxes with objectively determined basis functions using reversible-jump Markov chain Monte Carlo, *Geoscientific Model Development*, 9, 3213–3229, doi:10.5194/gmd-9-3213-2016.

Lunt, M.F., S. Park, S. Li, S. Henne, A.J. Manning, A.L. Ganesan, I.J. Simpson, D.R. Blake, Q. Liang, S. O'Doherty, C.M. Harth, J. Mühle, P.K. Salameh, R.F. Weiss, P.B. Krummel, P.J. Fraser, R.G. Prinn, S. Reimann and M. Rigby, 2018: Continued emissions of the ozone-depleting substance carbon tetrachloride from Eastern Asia, *Geophysical Research Letters*, 45(20), 11423–11430, doi:10.1029/2018GL079500.

Manning, A.J., S. O'Doherty, A.R. Jones, P.G. Simmonds and R.G. Derwent, 2011: Estimating UK methane and nitrous oxide emissions from 1990 to 2007 using an inversion modelling approach, *Journal of Geophysical Research*, 116(D2), doi:10.1029/2010JD014763.

Miller, B.R., R.F. Weiss, P.K. Salameh, T. Tanhua, B.R. Greally, J. Mühle and P.G. Simmonds, 2008: Medusa: A sample preconcentration and GC/MS detector system for in situ measurements of atmospheric trace halocarbons, hydrocarbons, and sulphur compounds, *Analytical Chemistry*, 80(5), 1536–1545, doi:10.1021/ac702084k.

Molina, M.J. and F.S. Rowland, 1974: Stratospheric sink for chlorofluoromethanes: Chlorine atom-catalysed destruction of ozone, *Nature*, 249, 810–812, doi:10.1038/249810a0.

Montzka, S.A., J.H. Butler, R.C. Myers, T.M. Thompson, T.H. Swanson, A.D. Clarke, L.T. Lock and J.W. Elkins, 1996: Decline in the tropospheric abundance of halogen from halocarbons: Implications for stratospheric ozone depletion, *Science*, 272(5266), 1318–1322, doi:10.1126/science.272.5266.1318.

Montzka, S.A., G.S. Dutton, P. Yu, E. Ray, R.W. Portmann, J.S. Daniel, L. Kuijpers, B.D. Hall, D. Mondeel, C. Siso, J.D. Nance, M. Rigby, A.J. Manning, L. Hu, F. Moore, B.R. Miller and J.W. Elkins, 2018: An unexpected and persistent increase in global emissions of ozone-depleting CFC-11, *Nature*, 557, 413–417, doi:10.1038/s41586-018-0106-2.

Montzka, S. A, G.S. Dutton, R.W. Portmann, M.P. Chipperfield, S. Davis, W. Feng, A.J. Manning, E. Ray, M. Rigby, B. Hall, C. Siso, J.D. Nance, P.B. Krummel, J. Mühle, D. Young, S. O' Doherty, P.K. Salameh, C. Harth, R.G. Prinn, R.F. Weiss, J.W. Elkins, H. Walter-Terrinoni and C. Theodoridi: A sharp decline in global CFC-11 emissions during 2018–2019, *Nature*, 590, 428–432 (2021). https://doi.org/10.1038/s41586-021-03260-5.

Morgenstern, O., M.I. Hegglin, E. Rozanov, F.M. O'Connor, N.L. Abraham, H. Akiyoshi, A.T. Archibald, S. Bekki, N. Butchart, M.P. Chipperfield, M. Deushi, S.S. Dhomse, R.R. Garcia, S.C. Hardiman, L.W. Horowitz, P. Jöckel, B. Josse, D. Kinnison, M. Lin, E. Mancini, M.E. Manyin, M. Marchand, V. Marécal, M. Michou, L.D. Oman, G. Pitari, D.A. Plummer, L.E.

Revell, D. Saint-Martin, R. Schofield, A. Stenke, K. Stone, K. Sudo, T.Y. Tanaka, S. Tilmes, Y. Yamashita, K. Yoshida and G. Zeng, 2017: Review of the global models used within phase 1 of the Chemistry-Climate Model Initiative (CCMI), *Geoscientific Model Development*, 10(2), 639–671, doi:10.5194/gmd-10-639-2017.

Nevison, C. D, E. Dlugokencky, G. Dutton, J.W. Elkins, P. Fraser, B. Hall, P.B. Krummel, R.L. Langenfelds, S. O'Doherty and R.G. Prinn, 2011: Exploring causes of interannual variability in the seasonal cycles of tropospheric nitrous oxide, *Atmospheric Chemistry and Physics*, 11(8), 3713–3730, doi:10.5194/acp-11-3713-2011.

Newchurch, M.J., E.-S. Yang, D. Cunnold, G. Reinsel, J.M. Zawodny and J. Russell, 2003: Evidence for slowdown in stratospheric ozone loss: First stage of ozone recovery, *Journal of Geophysical Research*, 108, 4507.

Ou-Yang, C.-F., C.-C. Chang, S.-P. Chen, C. Chew, B.-R. Lee, C.-Y. Chang, S.A. Montzka, G.S. Dutton, J.H. Butler, J.W. Elkins and J.-L. Wang, 2015: Changes in the levels and variability of halocarbons and the compliance with the Montreal Protocol from an urban view, *Chemosphere*, 138, 438–446, doi:10.1016/j.chemosphere.2015.06.070.

Ou-Yang, C.-F., C.-C. Chang, J.-L. Wang, K. Shimada, S. Hatakeyama, S. Kato, J.-Y. Chiu, G.-R. Sheu and N.-H. Lin, 2017: Characteristics of summertime volatile organic compounds in the lower free troposphere: Background measurements at Mt. Fuji, *Aerosol and Air Quality Research*, 17, 3037–3051, doi:10.4209/aaqr.2017.04.0144.

Pack, D.H., J.E. Lovelock, G. Cotton and C. Curthoys, 1977: Halocarbon behaviour from a long time series, *Atmospheric Environment (1967)*, 11(4), 329–344, doi:10.1016/0004-6981(77)90161-5.

Palmer, P.I., D.J. Jacob, L.J. Mickley, D.R. Blake, G.W. Sachse, H.E. Fuelberg and C.M. Kiley, 2003: Eastern Asian emissions of anthropogenic halocarbons deduced from aircraft concentration data, *Journal of Geophysical Research*, 108(D24), doi:10.1029/2003JD003591.

Park, S., L.M. Western, T. Saito, A.L. Redington, S. Henne, X. Fang, R.G. Prinn, A.J. Manning, S.A. Montzka, P.J. Fraser, A.L. Ganesan, C.M. Harth, J. Kim, P.B. Krummel, Q. Liang, J. Mühle, S. O'Doherty, H. Park, M.K. Park, S. Reimann, P.K. Salameh, R.F. Weiss and M. Rigby: Significant recent reductions in the emissions of CFC-11 and related ozone depleting substances from Eastern China, Nature 590, 433–437 (2021). https://doi.org/10.1038/s41586-021-03277-w.

Polyakov, A.V, Y.M. Timofeyev, Y.A. Virolainen, M. V Makarova, A.V Poberovskii and H.K. Imhasin, 2018: Ground-based measurements of the total column of freons in the atmosphere near St. Petersburg (2009–2017), *Izvestiya, Atmospheric and Oceanic Physics*, 54, 487–494, doi:10.1134/S0001433818050109.

Prinn, R.G., P.G. Simmonds, R.A. Rasmussen, R.D. Rosen, F.N. Alyea, C.A. Cardelino, A.J. Crawford, D.M. Cunnold, P.J. Fraser and J.E. Lovelock, 1983: The Atmospheric Lifetime Experiment: 1. Introduction, instrumentation, and overview, *Journal of Geophysical Research*, 88(C13), 8353–8367, doi:10.1029/JC088iC13p08353.

Prinn, R.G., R.F. Weiss, J. Arduini, T. Arnold, H. Langley Dewitt, P.J. Fraser, A.L. Ganesan, J. Gasore, C.M. Harth, O. Hermansen, J. Kim, P.B. Krummel, S. Li, Z.M. Loh, C.R. Lunder, M. Maione, A.J. Manning, B.R. Miller, B. Mitrevski, J. Mühle, S. O'Doherty, S. Park, S. Reimann, M. Rigby, T. Saito, P.K. Salameh, R. Schmidt, P.G. Simmonds, L. Paul Steele, M.K. Vollmer, R.H. Wang, B. Yao, Y. Yokouchi, D. Young and L. Zhou, 2018: History of chemically and radiatively important atmospheric gases from the Advanced Global Atmospheric Gases Experiment (AGAGE), *Earth System Science Data*, 10(2), 985–1018, doi:10.5194/essd-10-985-2018.

Qin, D., Decline in the concentrations of chlorofluorocarbons (CFC-11, 2007: CFC-12, and CFC-113) in an urban area of Beijing, China, *Atmospheric Environment*, 41(38), 8424–8430, doi:10.1016/j.atmosenv.2007.07.005.

Randel, W.J., F. Wu, H. Vömel, G.E. Nedoluha and P. Forster, 2006: Decreases in stratospheric water vapor after 2001: Links to changes in the tropical tropopause and the Brewer-Dobson circulation, *Journal of Geophysical Research*, 111(D12), doi:10.1029/2005JD006744.

Ray, E.A., F.L. Moore, K.H. Rosenlof, S.M. Davis, C. Sweeney, P. Tans, T. Wang, J.W. Elkins, H. Bönisch, A. Engel, S. Sugawara, T. Nakazawa and S. Aoki, 2014: Improving stratospheric transport trend analysis based on SF_6 and CO_2 measurements, *Journal of Geophysical Research*, 119(22), doi:10.1002/2014JD021802.

Ray, E.A., R.W. Portmann, P. Yu, J. Daniel, S.A. Montzka, G.S. Dutton, B.D. Hall, F.L. Moore and K.H. Rosenlof, 2020: The influence of the stratospheric Quasi-Biennial Oscillation on trace gas levels at the Earth's surface, *Nature Geoscience*, 13(1), doi:10.1038/s41561-019-0507-3.

Rigby, M., S. Park, T. Saito, L.M. Western, A.L. Redington, X. Fang, S. Henne, A.J. Manning, R.G. Prinn, G.S. Dutton, P.J. Fraser, A.L. Ganesan, B.D. Hall, C.M. Harth, J. Kim, K.R. Kim, P.B. Krummel, T. Lee, S. Li, Q. Liang, M.F. Lunt, S.A. Montzka, J. Mühle, S. O'Doherty, M.K. Park, S. Reimann, P.K. Salameh, P. Simmonds, R.L. Tunnicliffe, R.F. Weiss, Y. Yokouchi and D. Young, 2019: Increase in CFC-11 emissions from Eastern China based on atmospheric observations, *Nature*, 569, 546–550, doi:10.1038/s41586-019-1193-4.

Rosenlof, K.H. and G.C. Reid, 2008: Trends in the temperature and water vapor content of the tropical lower stratosphere: Sea surface connection, *Journal of Geophysical Research*, 113(D6), doi:10.1029/2007JD009109.

Sarkar, S., W.H. Fan, S. Jia, D.R. Blake, J.S. Reid, P. Lestari and L.E. Yu, 2018: A quantitative assessment of distributions and sources of tropospheric halocarbons measured in Singapore, *Science of the Total Environment*, 619–620, 528–544, doi:10.1016/j.scitotenv.2017.11.087.

Say, D., A.L. Ganesan, M.F. Lunt, M. Rigby, S. O'Doherty, C. Harth, A.J. Manning, P.B. Krummel and S. Bauguitte, 2019: Emissions of halocarbons from India inferred through atmospheric measurements, *Atmospheric Chemistry and Physics*, 19(15), 9865–9885, doi:10.5194/acp-19-9865-2019.

Schauffler, S.M., E.L. Atlas, S.G. Donnelly, A. Andrews, S.A. Montzka, J.W. Elkins, D.F. Hurst, P.A. Romashkin, G.S. Dutton and V. Stroud, 2003: Chlorine budget and partitioning during the Stratospheric Aerosol and Gas Experiment (SAGE) III Ozone Loss and Validation Experiment (SOLVE), *Journal of Geophysical Research*, 108(5), doi:10.1029/2001jd002040.

Scheutz, C., A.M. Fredenslund, J. Nedenskov and P. Kjeldsen (2010). Release and fate of fluorocarbons in a shredder residue landfill cell: 1. Laboratory experiments. Waste Management, 30(11), 2153–2162, doi:10.1016/j.wasman.2010.03.035 and https://www.sciencedirect.com/science/article/pii/S0956053X10002060.

Schmeltekopf, A.L., P.D. Goldan, W.R. Henderson, W.J. Harrop, T.L. Thompson, F.C. Fehsenfeld, H.I. Schiff, P.J. Crutzen, I.S.A. Isaksen and E.E. Ferguson, 1975: Measurements of stratospheric $CFCl_3$, CF_2Cl_2, and N_2O, *Geophysical Research Letters*, 2(9), 393–396, doi:10.1029/GL002i009p00393.

Schwandner, F.M., T.M. Seward, A.P. Gize, P.A. Hall and V.J. Dietrich, 2004: Diffuse emission of organic trace gases from the flank and crater of a quiescent active volcano (Vulcano,

Aeolian Islands, Italy), *Journal of Geophysical Research*, 109(D4), doi:10.1029/2003jd003890.

Shao, M., D. Huang, D. Gu, S. Lu, C. Chang and J. Wang, 2011: Estimate of anthropogenic halocarbon emission based on measured ratio relative to CO in the Pearl River Delta region, China, *Atmospheric Chemistry and Physics*, 11(10), 5011–5025, doi:10.5194/acp-11-5011-2011.

Shepherd, T.G., 2008: Dynamics, stratospheric ozone, and climate change, *Atmosphere-Ocean*, 46(1), 117–138, doi:10.3137/ao.460106.

Shepherd, T.G., D.A. Plummer, J.F. Scinocca, M.I. Hegglin, V.E. Fioletov, M.C. Reader, E. Remsberg, T. Von Clarmann and H.J. Wang, 2014: Reconciliation of halogen-induced ozone loss with the total-column ozone record, *Nature Geoscience*, 7, 443–449, doi:10.1038/ngeo2155.

Sherry, D., A. McCulloch, Q. Liang, S. Reimann and P.A. Newman, 2018: Current sources of carbon tetrachloride (CCl_4) in our atmosphere, *Environmental Research Letters*, 13(2), doi:10.1088/1748-9326/aa9c87.

Seibert, P. and A. Frank, 2004: Source-receptor matrix calculation with a Lagrangian particle dispersion model in backward mode, *Atmospheric Chemistry and Physics*, 4, 51–63, doi:10.5194/acp-4-51-2004.

Simmonds, P.G., R.G. Derwent, A. McCulloch, S. O'Doherty and A. Gaudry, 1996: Long-term trends in concentrations of halocarbons and radiatively active trace gases in Atlantic and European air masses monitored at Mace Head, Ireland from 1987–1994, *Atmospheric Environment*, 30(23), 4041–4063, doi:10.1016/1352-2310(96)00055-6.

Simpson, I.J., D.R. Blake, N.J. Blake, S. Meinardi, B. Barletta, S.C. Hughes, L.T. Fleming, J.H. Crawford, G.S. Diskin, L.K. Emmons, A. Fried, H. Guo, D.A. Peterson, A. Wisthaler, J.-H. Woo, J. Barré, B. Gaubert, J. Kim, M.J. Kim, Y. Kim, C. Knote, T. Mikoviny, S.E. Pusede, J.R. Schroeder, Y. Wang, P.O. Wennberg and L. Zeng, 2020: Characterization, sources and reactivity of volatile organic compounds (VOCs) in Seoul and surrounding regions during KORUS-AQ, *Elementa: Science of the Anthropocene*, 8(37), doi:10.1525/elementa.434.

Solomon, S., D.J. Ivy, D. Kinnison, M.J. Mills, R.R. Neely and A. Schmidt, 2016: Emergence of healing in the Antarctic ozone layer, *Science*, 353(6296), 269–274, doi:10.1126/science.aae0061.

SPARC (Stratosphere-troposphere Processes And their Role in Climate), 2013: *SPARC Report on the Lifetimes of Stratospheric Ozone-Depleting Substances, Their Replacements, and Related Species*, M.K.W. Ko, P.A. Newman, S. Reimann, and S.E. Strahan (Eds.), SPARC Report No. 6, WCRP-15/2013, http://www.sparc-climate.org/publications/sparc-reports/.

———, 2016: *SPARC Report on the Mystery of Carbon Tetrachloride* (Q. Liang, P.A. Newman and S. Reimann, eds.), SPARC Report No. 7, WCRP-13/2016, doi:10.3929/ethz-a-010690647 and http://www.sparc-climate.org/publications/sparc-reports/.

Steffen, J., P.F. Bernath and C.D. Boone, 2019: Trends in halogen-containing molecules measured by the Atmospheric Chemistry Experiment (ACE) satellite, *Journal of Quantitative Spectroscopy & Radiative Transfer*, 238, 106619, doi:10.1016/j.jqsrt.2019.106619.

Stohl, A., J. Kim, S. Li, S. O'Doherty, J. Mühle, P.K. Salameh, T. Saito, M.K. Vollmer, D. Wan, R.F. Weiss, B. Yao, Y. Yokouchi and L.X. Zhou, 2010: Hydrochlorofluorocarbon and hydrofluorocarbon emissions in East Asia determined by inverse modelling, *Atmospheric Chemistry and Physics*, 10(8), 3545–3560, doi:10.5194/acp-10-3545-2010.

Sturrock, G.A., D.M. Etheridge, C.M. Trudinger, P.J. Fraser and A.M. Smith, 2002: Atmospheric histories of halocarbons from analysis of Antarctic firn air: Major Montreal Protocol species, *Journal of Geophysical Research*, 107(24), ACH 12-1-ACH 12–14, doi:10.1029/2002JD002548.

Tassi, F., F. Capecchiacci, J. Cabassi, S. Calabrese, O. Vaselli, D. Rouwet, G. Pecoraino and G. Chiodini, 2012: Geogenic and atmospheric sources for volatile organic compounds in fumarolic emissions from Mt. Etna and Vulcano Island (Sicily, Italy), *Journal of Geophysical Research*, 117(17), doi:10.1029/2012JD017642.

Thompson, R.L. and A. Stohl, 2014: FLEXINVERT: An atmospheric Bayesian inversion framework for determining surface fluxes of trace species using an optimized grid, *Geoscientific Model Development*, 7(5), 2223–2242, doi:10.5194/gmd-7-2223-2014.

Technology and Economic Assessment Panel/United Nations Environment Programme (TEAP/UNEP), 2009: *Task Force Decision XX/8 Report: Assessment of Alternatives to HCFCs and HFCs and Update of the TEAP 2005 Supplement Report Data*. Nairobi.

———, 2019*a*: *Volume 3: Decision XXX/3 TEAP Task Force Report on Unexpected Emissions of Trichlorofluoromethane (CFC-11)* (May). Nairobi. https://ozone.unep.org/science/assessment/teap/.

———, 2019*b*: *Volume 1: Decision XXX/3 TEAP Task Force Report on Unexpected Emissions of Trichlorofluoromethane (CFC-11)* (September). Nairobi. https://ozone.unep.org/science/assessment/teap/.

U.S. Environmental Protection Agency, 2016: *Inventory of U.S. Greenhouse Gas Emissions and Sinks: 1990–2014*. Washington, D.C.

Velders, G.J.M. and J.S. Daniel, 2014: Uncertainty analysis of projections of ozone-depleting substances: Mixing ratios, EESC, ODPs, and GWPs, *Atmospheric Chemistry and Physics*, 14(6), 2757–2776, doi:10.5194/acp-14-2757-2014.

Volk, C.M., J.W. Elkins, D.W. Fahey, G.S. Dutton, J.M. Gilligan, M. Loewenstein, J.R. Podolske, K.R. Chan and M.R. Gunson, 1997: Evaluation of source gas lifetimes from stratospheric observations, *Journal of Geophysical Research*, 102(21), 25543–25564, doi:10.1029/97jd02215.

Vollmer, M.K., J. Mühle, S, Henne, D. Young, M. Rigby, B. Mitrevski, S. Park, C.R. Lunder, T.S. Rhee, C.M. Harth and M. Hill, 2021: *Unexpected nascent atmospheric emissions of three ozone-depleting hydrochlorofluorocarbons*. *PNAS*, 118(5). doi: 10.1073/pnas.2010914118.

Wilkniss, P.E., R.A. Lamontagne, R.E. Larson, J.W. Swinnerton, C.R. Dickson and T. Thompson, 1973: Atmospheric trace gases in the southern hemisphere, *Nature Physical Science*, 245(142), 45–47, doi:10.1038/physci245045a0.

Wilkniss, P.E., J.W. Swinnerton, R.A. Lamontagne and D.J. Bressan, 1975: Trichlorofluoromethane in the troposphere, distribution and increase, 1971 to 1974, *Science*, 187(4179), 832–834, doi:10.1126/science.1114326.

World Meteorological Organization (WMO), 1999: *Scientific Assessment of Ozone Depletion: 1998*, Global Ozone Research and Monitoring Project – Report No. 44, Geneva.

_____, 2003: *Scientific Assessment of Ozone Depletion: 2002*, Global Ozone Research and Monitoring Project – Report No. 47, Geneva.

_____, 2007: *Scientific Assessment of Ozone Depletion: 2006*, Global Ozone Research and Monitoring Project – Report No. 50, Geneva.

_____, 2011: *Scientific Assessment of Ozone Depletion: 2010*, Global Ozone Research and Monitoring Project – Report No. 52, Geneva.

_____, 2014: *Scientific Assessment of Ozone Depletion: 2014*, Global Ozone Research and Monitoring Project – Report No. 55, Geneva.

_____, 2018: *Scientific Assessment of Ozone Depletion: 2018*, Global Ozone Research and Monitoring Project – Report No. 58, Geneva.

Wu, F.K., J. Sun, Y. Yu, G.Q. Tang and Y.S. Wang, 2016: Variation characteristics and sources analysis of atmospheric volatile organic compounds in Changbai Mountain Station, *Huanjing Kexue/Environmental Science*, 37(9), 3308–3314, doi:10.13227/j.hjkx.2016.09.008.

Wu, J., X. Fang, W. Xu, D. Wan, Y. Shi, S. Su, J. Hu and J. Zhang, 2013: Chlorofluorocarbons, hydrochlorofluorocarbons, and hydrofluorocarbons in the atmosphere of four Chinese cities, *Atmospheric Environment*, 75, 83–91, doi:10.1016/j.atmosenv.2013.04.031.

Wu, J., X. Fang, J.W. Martin, Z. Zhai, S. Su, X. Hu, J. Han, S. Lu, C. Wang, J. Zhang and J. Hu, 2014: Estimated emissions of chlorofluorocarbons, hydrochlorofluorocarbons, and hydrofluorocarbons based on an interspecies correlation method in the Pearl River Delta region, China, *Science of the Total Environment*, 470–471, 829–834, doi:10.1016/j.scitotenv.2013.09.071.

Yang, E.S., D.M. Cunnold, R.J. Salawitch, M.P. McCormick, J. Russell, J.M. Zawodny, S. Oltmans and M.J. Newchurch, 2006: Attribution of recovery in lower-stratospheric ozone, *Journal of Geophysical Research*, 111(17), D17309, doi:10.1029/2005JD006371.

Yang, F., Y. Wang, H. Li, M. Yang, T. Li, F. Cao, J. Chen and Z. Wang, 2017: Influence of cloud/fog on atmospheric VOCs in the free troposphere: A case study at Mount Tai in Eastern China, *Aerosol and Air Quality Research*, 17(10), 2401–2412, doi:10.4209/aaqr.2016.12.0536.

Yang, M., Y. Wang, J. Chen, H. Li and Y. Li, 2016: Aromatic hydrocarbons and halocarbons at a mountaintop in Southern China, *Aerosol and Air Quality Research*, 16(3), 478–491, doi:10.4209/aaqr.2015.03.0197.

Yang, M., F. Yang, H. Li, T. Li, F. Cao, X. Nie, J. Zhen, P. Li and Y. Wang, 2021: CFCs measurements at high altitudes in Northern China during 2017–2018: Concentrations and potential emission source regions, *Science of the Total Environment*, 754, 142290, doi:10.1016/j.scitotenv.2020.142290.

Zander, R., E. Mahieu, P. Demoulin, P. Duchatelet, C. Servais, G. Roland, L. DelBouille, M. De Mazière and C.P. Rinsland, 2005: Evolution of a dozen non-CO_2 greenhouse gases above central Europe since the mid-1980s, *Environmental Sciences*, 2(2-3), 295–303, doi:10.1080/15693430500397152.

Zeng, L., J. Dang, H. Guo, X. Lyu, I.J. Simpson, S. Meinardi, Y. Wang, L. Zhana and D.R. Blake, 2020. Long-term temporal variations and source changes of halocarbons in the Greater Pearl River Delta region, China, *Atmospheric Environment*, 234, 117550, doi:10.1016/j.atmosenv.2020.117550.

Zhang, F., L. Zhou, B. Yao, M.K. Vollmer, B.R. Greally, P.G. Simmonds, S. Reimann, F. Stordal, M. Maione, L. Xu and X. Zhang, 2010: Analysis of 3-year observations of CFC-11, CFC-12, and CFC-113 from a semi-rural site in China, *Atmospheric Environment*, 44(35), 4454–4462, doi:10.1016/j.atmosenv.2010.07.041.

Zhang, G., B. Yao, M.K. Vollmer, S.A. Montzka, J. Mühle, R.F. Weiss, S. O'Doherty, Y. Li, S. Fang and S. Reimann, 2017: Ambient mixing ratios of atmospheric halogenated

compounds at five background stations in China, *Atmospheric Environment*, 160, 55–69, doi:10.1016/j.atmosenv.2017.04.017.

Zhang, Y.L., H. Guo, X.M. Wang, I.J. Simpson, B. Barletta, D.R. Blake, S. Meinardi, F.S. Rowland, H.R. Cheng, S.M. Saunders and S.H.M. Lam, 2010: Emission patterns and spatiotemporal variations of halocarbons in the Pearl River Delta region, Southern China, *Journal of Geophysical Research*, 115(D15), doi:10.1029/2009JD013726.

Zheng, P., T. Chen, C. Dong, Y. Liu, H. Li, G. Han, J. Sun, L. Wu, X. Gao, X. Wang, Y. Qi, Q. Zhang, W. Wang and L. Xue, 2019: Characteristics and sources of halogenated hydrocarbons in the Yellow River Delta region, northern China, *Atmospheric Research*, 225, 70–80, doi:10.1016/j.atmosres.2019.03.039.

Zhou, M., C. Vigouroux, B. Langerock, P. Wang, G. Dutton, C. Hermans, N. Kumps, G. Toon and M. De Mazière, 2016: CFC-11, CFC-12, and HCFC-22 ground-based remote sensing FTIR measurements at Réunion Island and comparisons with MIPAS/ENVISAT data, *Atmospheric Measurement Techniques*, 9(11), 5621–5636, doi:10.5194/amt-9-5621-2016.

———————

For more information, please contact:

World Meteorological Organization

7 bis, avenue de la Paix – P.O. Box 2300 – CH 1211 Geneva 2 – Switzerland

Strategic Communications Office

Tel: +41 (0) 22 730 83 14 – Fax: +41 (0) 22 730 80 27

Email: communications@wmo.int

public.wmo.int

JN 21573